Birte Everts

Evaluation of drying processes for biomass co-firing in coal fired steam power plants

Cuvillier Verlag Göttingen
Internationaler wissenschaftlicher Fachverlag

Evaluation of drying processes for biomass co-firing in coal fired steam power plants

Dieses Werk ist copyrightgeschützt und darf in keiner Form vervielfältigt werden noch an Dritte weitergegeben werden.
Es gilt nur für den persönlichen Gebrauch.

Dieses Werk ist copyrightgeschützt und darf in keiner Form vervielfältigt werden noch an Dritte weitergegeben werden.
Es gilt nur für den persönlichen Gebrauch.

Evaluation of drying processes for biomass co-firing in coal fired steam power plants

Vom Promotionsausschuss der
Technischen Universität Hamburg
zur Erlangung des akademischen Grades

Doktor-Ingenieurin (Dr.-Ing.)

genehmigte Dissertation

von
Birte Mareile Everts

aus
Hamburg

2016

Dieses Werk ist copyrightgeschützt und darf in keiner Form vervielfältigt werden noch an Dritte weitergegeben werden.
Es gilt nur für den persönlichen Gebrauch.

Bibliografische Information der Deutschen Nationalbibliothek
Die Deutsche Nationalbibliothek verzeichnet diese Publikation in der Deutschen Nationalbibliografie; detaillierte bibliografische Daten sind im Internet über http://dnb.d-nb.de abrufbar.
1. Aufl. - Göttingen: Cuvillier, 2016
Zugl.: (TU) Hamburg-Harburg, Univ., Diss., 2016

Gutachter: 1. Prof. Dr.-Ing. Alfons Kather
2. Prof. Dr.-Ing. Joachim Werther

Datum der mündlichen Prüfung: 22. November 2016

© CUVILLIER VERLAG, Göttingen 2016
Nonnenstieg 8, 37075 Göttingen
Telefon: 0551-54724-0
Telefax: 0551-54724-21
www.cuvillier.de

Alle Rechte vorbehalten. Ohne ausdrückliche Genehmigung des Verlages ist es nicht gestattet, das Buch oder Teile daraus auf fotomechanischem Weg (Fotokopie, Mikrokopie) zu vervielfältigen.
1. Auflage, 2016
Gedruckt auf umweltfreundlichem, säurefreiem Papier aus nachhaltiger Forstwirtschaft.

ISBN 978-3-7369-9441-6
eISBN 978-3-7369-8441-7

Dieses Werk ist copyrightgeschützt und darf in keiner Form vervielfältigt werden noch an Dritte weitergegeben werden.
Es gilt nur für den persönlichen Gebrauch.

Danksagung

Die vorliegende Arbeit entstand während meiner Tätigkeit als wissenschaftliche Mitarbeiterin am Institut für Energietechnik der Technischen Universität Hamburg.

An erster Stelle möchte ich mich bei Professor Dr.-Ing. A. Kather für die Möglichkeit zur Promotion und die unvergessliche Zeit an diesem unvergleichlichen Institut bedanken. Besonders bedanke ich mich für das entgegengebrachte Vertrauen und die hervorragende fachliche Unterstützung. Für die Übernahme des Koreferats gilt mein herzlicher Dank Professor Dr.-Ing. J. Werther. Professor Dr.-Ing. G. Ackermann sei für die Übernahme des Prüfungsvorsitzes gedankt.

Allen Kolleginnen und Kollegen am Institut danke ich dafür, dass sie mich nicht nur durch fachliche Diskussionen in meiner Arbeit unterstützt haben, sondern auch den alltäglichen Wahnsinn mit viel guter Laune versehen haben. Ich hoffe darauf mit vielen von euch auch nach der legendären IET Zeit in Kontakt zu bleiben. Der größte Dank für fachliche Unterstützung und viele produktive Diskussionen im Rahmen von nahezu vier Jahren Biomasseforschung gebührt natürlich Tobias. Auch Volker möchte ich an dieser Stelle für seine umfassende Unterstützung danken.

Ich danke allen studentischen Hilfskräften, die zum Erstellen dieser Arbeit beigetragen haben. Insbesondere Anna-Lena für ihre Fähigkeit zu erkennen, wann eine Problemstellung nur noch unter Zuhilfenahme von Süßwaren zu bewältigen ist.

Meinen Freunden danke ich für die großartige Unterstützung und die notwendige Ablenkung in anstrengenden Zeiten. Meiner Familie möchte ich besonders für den bedingungslosen und verlässlichen Rückhalt in allen Situationen und die stetige Motivation neue Herausforderungen anzugehen danken.

Hamburg, im Dezember 2016

Birte Everts

Dieses Werk ist copyrightgeschützt und darf in keiner Form vervielfältigt werden noch an Dritte weitergegeben werden.
Es gilt nur für den persönlichen Gebrauch.

Dieses Werk ist copyrightgeschützt und darf in keiner Form vervielfältigt werden noch an Dritte weitergegeben werden.
Es gilt nur für den persönlichen Gebrauch.

CONTENTS

Contents ..... **I**

List of Figures ..... **III**

List of Tables ..... **IX**

Abbreviations and symbols ..... **X**

1 Introduction **1**

1.1 Background 1
1.2 Aim and scope 2
1.3 Methodology 3

2 Co-firing biomass with coal **5**

2.1 Current Co-firing activities in power generation 6
2.2 Biomass fuel characteristics and resulting effects in the combustion system 8
2.3 Fuel supply and environmental aspects of biomass co-firing 13

3 Drying technologies **17**

3.1 Requirements of the drying material and dryer selection 18
3.2 Indirect steam-tube dryer 20
3.3 Direct rotary dryer 22

4 Introduction of Considered drying scenarios **25**

4.1 Definition of energy utilisation efficiency 26

5 Model development **31**

5.1 Steam power plant for biomass co-firing 31
5.1.1 Power plant overall process modelling 31
5.1.2 Boiler modelling 35
5.2 Indirect steam-tube dryer 36
5.2.1 Dryer modelling 36
5.2.2 Integration into the power plant process 38
5.3 Direct rotary dryer 44
5.3.1 Dryer modelling 44
5.3.2 Stand-alone dryer 46

Dieses Werk ist copyrightgeschützt und darf in keiner Form vervielfältigt werden noch an Dritte weitergegeben werden.
Es gilt nur für den persönlichen Gebrauch.

5.3.3 Integration of a direct rotary dryer into the power plant.....47
6 Effects of biomass co-firing on the power generation process 49
6.1 Effects on the boiler.....49
6.2 Effects on the overall process.....55
7 Analysis of Drying scenarios 61
7.1 Scenario 1 – integrated on-site drying by an indirect steam-tube dryer 61
7.1.1 Scenario 1_a – drying steam extracted from IP/LP crossover pipe 61
7.1.2 Scenario 1_b – drying steam extracted from IP/LP crossover pipe and LP turbine.....73
7.2 Scenario 2 – stand-alone drying by a direct rotary dryer.....79
7.3 Scenario 3 – integrated on-site drying by a direct rotary dryer.....84
7.4 Comparison of scenarios.....90
7.4.1 Transport related CO_2 emissions.....91
7.4.2 Total resulting CO_2 emissions.....92
7.4.3 Overall energy utilisation efficiency.....98
7.4.4 Alternative approach of comparison 100
7.4.5 Concluding evaluation of drying scenarios.....101
8 Summary and conclusions 103
References.....107

Dieses Werk ist copyrightgeschützt und darf in keiner Form vervielfältigt werden noch an Dritte weitergegeben werden.
Es gilt nur für den persönlichen Gebrauch.

LIST OF FIGURES

Figure 1: Lower heating values of biomass fuels for varying fuel moisture content 10

Figure 2: Global wood pellet production [40] 14

Figure 3: Global wood pellet consumption [40] 14

Figure 4: Diagram of an indirect steam tube dryer [44] 20

Figure 5: Steam tubes of an indirect dryer [56] 21

Figure 6: Diagram of a direct rotary dryer [44] 22

Figure 7: Flights and distribution of solids in the dryer [60] 23

Figure 8: Flights in a direct rotary dryer [60] 23

Figure 9: Scenarios of stand-alone drying and integrated on-site drying 25

Figure 10: Energy balance for Scenario 1_a 27

Figure 11: Energy balance for Scenario 1_b 28

Figure 12: Energy balance for Scenario 2_a 28

Figure 13: Energy balance for Scenario 2_b 29

Figure 14: Energy balance for Scenario 3 29

Figure 15: Simplified flowsheet of the modelled steam power plant 32

Figure 16: Simplified flowsheet of the boiler model 35

Figure 17: Considered feed and product mass flows of an indirect steam-tube dryer for drying biomass [49] 37

Figure 18: Indirect steam-tube dryer integrated into the power plant process – drying steam is extracted from the IP/LP crossover pipe 39

Figure 19: Indirect steam-tube dryer integrated in the power plant process – drying steam is extracted from the IP/LP crossover pipe and the LP turbine 41

Figure 20: Heat integration of ventilation air and exhaust vapours – theoretical evaluation of potential for low-pressure feedwater preheating 42

Dieses Werk ist copyrightgeschützt und darf in keiner Form vervielfältigt werden noch an Dritte weitergegeben werden.
Es gilt nur für den persönlichen Gebrauch.

Figure 21: Heat integration of ventilation air and exhaust vapours – Variation A 43

Figure 22: Heat integration of ventilation air and exhaust vapours – Variation B 44

Figure 23: Feed and product mass flows of a direct rotary dryer 45

Figure 24: Process flow sheet of the stand-alone direct rotary dryer 46

Figure 25: Process flow sheet of the integrated direct rotary dryer 48

Figure 26: Changes in adiabatic flame temperature and flue gas mass flow when co-firing poplar wood chips (10 % H_2O) with hard coal, in relation to the co-firing rate 50

Figure 27: Heat flow changes in all boiler heating surfaces when co-firing poplar wood chips with 10 % fuel moisture content, in relation to the co-firing rate 50

Figure 28: Changes in live and reheat steam heat output in relation to the co-firing rate 51

Figure 29: Relative changes of boiler parameters for co-firing wood chips with a moisture content of 10 %, in relation to the co-firing rate 52

Figure 30: Heat flow changes in all boiler heating surfaces when co-firing poplar wood chips with 20 % fuel moisture content, in relation to the co-firing rate 54

Figure 31: Net and gross efficiency and power output for direct co-firing of wood chips with moisture content of 10 % in relation to the co-firing rate... 55

Figure 32: Distribution of main shares in auxiliary power demand for direct co-firing of wood chips in relation to the co-firing rate 56

Figure 33: Air and flue gas temperatures and mass flows in the air preheater for direct co-firing of wood chips in relation to the co-firing rate . 57

Figure 34: Net and gross efficiency and power output for direct co-firing of poplar wood chips with a moisture content of 20 % in relation to the co-firing rate 58

Figure 35: Distribution of main shares in auxiliary power demand for direct co-firing of poplar wood chips with a moisture content of 20 % in relation to the co-firing rate 59

Dieses Werk ist copyrightgeschützt und darf in keiner Form vervielfältigt werden noch an Dritte weitergegeben werden.
Es gilt nur für den persönlichen Gebrauch.

Figure 36: Net and gross efficiency and power output for co-firing of wood chips (10 % H_2O) dried with a steam-tube dryer in relation to the co-firing rate, integrated Scenario 1_a 62

Figure 37: Steam pressure and mass flow decline upstream of the LP turbine due to drying steam extraction from IP/LP crossover pipe in relation to the co-firing rate 63

Figure 38: Development of drying steam pressure and resulting drying steam condensation temperature in Scenario 1_a in relation to the co-firing rate 64

Figure 39: Ventilation air heat integration potential in relation to the co-firing rate 66

Figure 40: Heat transfer for heat integration – air heat exchanger 1 67

Figure 41: Heat transfer for heat integration – air heat exchanger 2 68

Figure 42: Heat transfer for heat integration – air heat exchangers 1 and 2 68

Figure 43: Ventilation air heat integration - resulting ventilation air and dew point temperatures 69

Figure 44: Net efficiency improvement due to heat integration in relation to the co-firing rate 70

Figure 45: Ventilation air heat integration – Variation A: heat flow in additional LPFW preheater 71

Figure 46: Ventilation air heat integration – Variation B: heat flow in ventilation air preheater 72

Figure 47: Net and gross efficiency and power output for co-firing of wood chips dried with a steam tube dryer in relation to the co-firing rate, integrated Scenario 1_b 74

Figure 48: Development of drying steam pressure and drying steam condensation temperature in the first dryer half in relation to the co-firing rate, heated by steam extracted from the LP turbine 75

Figure 49: Development of drying steam pressure and drying steam condensation temperature in the second dryer half in relation to the co-firing

Dieses Werk ist copyrightgeschützt und darf in keiner Form vervielfältigt werden noch an Dritte weitergegeben werden.
Es gilt nur für den persönlichen Gebrauch.

rate, heated by steam extracted from the IP/LP crossover pipe, compared to the results of Scenario 1_a 76

Figure 50: Drying temperature over transferred drying heat flow for Scenario 1_a and the two drying stages of Scenario 1_b..... 77

Figure 51: Comparison of net efficiency for Scenario 1_a and Scenario 1_b in relation to the co-firing rate, including ventilation air preheating in both scenarios 78

Figure 52: Necessary fuel heat input for a stand-alone direct rotary dryer for drying wood chip mass flow corresponding to 10 % CFR 80

Figure 53: Electrical demand of a standalone direct rotary dryer 81

Figure 54: Sensitivity analysis of the air preheater's terminal temperature difference 82

Figure 55: Stand-alone direct rotary dryer - resulting air and flue gas temperatures for combustion air preheating 83

Figure 56: Flue gas mass flow shares for air preheater and dryer for a dryer outlet temperature of 160 °C, in relation to the co-firing rate 85

Figure 57: Flue gas and sulphuric acid dew point temperatures of an integrated rotary dryer for a dryer outlet temperature of 140 °C, in relation to the co-firing rate..... 86

Figure 58: Flue gas and sulphuric acid dew point temperatures of an integrated rotary dryer for a dryer outlet temperature of 150 °C, in relation to the co-firing rate..... 87

Figure 59: Flue gas and sulphuric acid dew point temperatures of an integrated rotary dryer for a dryer outlet temperature of 160 °C, in relation to the co-firing rate..... 87

Figure 60: Flue gas heat flow downstream of the air preheater, downstream of the dryer and upstream of the ESP for a dryer outlet temperature of 160 °C, in relation to the co-firing rate..... 89

Figure 61: Total resulting CO_2 emissions for all drying scenarios at 5 % CFR compared to coal-only..... 94

Figure 62: Total resulting CO_2 emissions for Scenarios 1 and 2 at 50 % CFR compared to coal-only power generation 95

Dieses Werk ist copyrightgeschützt und darf in keiner Form vervielfältigt werden noch an Dritte weitergegeben werden.
Es gilt nur für den persönlichen Gebrauch.

Figure 63: Total resulting CO_2 emissions for co-firing rates up to 50 % for all drying scenarios 97

Figure 64: Overall energy utilisation efficiency for co-firing rates up to 50 % for all drying scenarios, in relation to the co-firing rate 99

Dieses Werk ist copyrightgeschützt und darf in keiner Form vervielfältigt werden noch an Dritte weitergegeben werden.
Es gilt nur für den persönlichen Gebrauch.

Dieses Werk ist copyrightgeschützt und darf in keiner Form vervielfältigt werden noch an Dritte weitergegeben werden.
Es gilt nur für den persönlichen Gebrauch.

LIST OF TABLES

Table 1: Selection of large-scale European coal power plants with current biomass co-firing activities 7

Table 2: Composition of various biomass fuels and coals [2] 8

Table 3: Lower heating values of biomass fuels 9

Table 4: Composition of coal and biomass ashes 11

Table 5: Key parameters of the power plant process (coal-only at full load) . 33

Table 6: Modelling parameters for the indirect steam-tube dryer 38

Table 7: Modelling parameters and boundary conditions of a stand-alone direct rotary dryer 47

Table 8: Energy demand of a steam-tube dryer for 10 % CFR 65

Table 9: Net efficiency improvement by ventilation air heat integration in Scenario 1_a 73

Table 10: Energy demand of a steam-tube dryer for 10 % CFR in Scenario 1_b 77

Table 11: Drying gas results for a rotary dryer heated by an oil burner or a wet wood chips fired furnace ($T\text{dry, in} = 450\ °C, T\text{dry, out} = 105\ °C$) 83

Table 12: Net and gross efficiency and power output for Scenario 3 (dryer outlet temperature 150 °C) 90

Table 13: Specific CO_2 emissions for wood chip transport 92

Table 14: Electrical net power output, electrical demand for drying and thermal heat input for all drying scenarios for 5 % and 50 % CFR 98

Table 15: Total resulting CO_2 emissions and energy utilisation efficiency for Scenario 2_a and Scenario 1_b for 54 % CFR* 100

Dieses Werk ist copyrightgeschützt und darf in keiner Form vervielfältigt werden noch an Dritte weitergegeben werden.
Es gilt nur für den persönlichen Gebrauch.

ABBREVIATIONS AND SYMBOLS

Abreviations

DK	Denmark
NL	The Netherlands
B	Belgium
UK	United Kingdom
PM_1	particulate matter with a diameter of 1 µm or less
$PM_{2,5}$	particulate matter with a diameter of 2.5 µm or less
VOC	volatile organic carbon
HP	high pressure
IP	intermediate pressure
LP	low pressure
FGD	flue gas desulphurisation
ESP	electrostatic precipitator
G	generator
ECO	economiser
SCR	selective catalytic reduction
MT	main turbine
ST	second turbine
LPFW	low pressure feedwater
SH	superheater heating surface
RH	reheater heating surface
CFR	co-firing rate
CFR*	new co-firing rate
AHE	air heat exchanger
VAPH	ventilation air preheater

Chemical symbols

Dieses Werk ist copyrightgeschützt und darf in keiner Form vervielfältigt werden noch an Dritte weitergegeben werden.
Es gilt nur für den persönlichen Gebrauch.

Chemical symbols

C	carbon
H	hydrogen
O	oxygen
N	nitrogen
S	sulphur
Cl	chlorine
H_2O	water
SiO_2	silicon dioxide
CaO	calcium oxide
K_2O	potassium oxide
P_2O_5	phosphorus pentoxide
Al_2O_3	aluminium oxide
MgO	magnesium oxide
Fe_2O_3	iron oxide
SO_3	sulphur trioxide
Na_2O	sodium oxide
TiO_2	titanium dioxide
BaO	barium oxide
Mn_3O_4	manganese oxide
SO_2	sulphur dioxide
NO_x	nitrogen oxide
NH_3	ammonia
HCN	hydrogen cyanide
O_2	oxygen
H_2SO_4	sulphuric acid

Latin symbols

HHV	higher heating value	kJ/kg
LHV	lower heating value	kJ/kg
E	grinding energy	Wh/kg
M	material constant	-
H	moisture content in ground material	wt.-%

Dieses Werk ist copyrightgeschützt und darf in keiner Form vervielfältigt werden noch an Dritte weitergegeben werden.
Es gilt nur für den persönlichen Gebrauch.

z	particle size	mm
c	specific heat	kJ/kgK
T	temperature	°C
h	specific enthalpy	kJ/kg
u	water per dry matter	$kg_{H2O}/kg_{bm,db}$
$\dot{Q}$	heat flow	kW
x	mass concentration	-
R	recycle ratio	-
p	pressure	bar
p_i	partial pressure	mmHg
a	specific CO_2 emissions for biomass transport over 100km	$kg_{CO2}/(t_{bm}$ 100 km)
b	specific CO_2 emissions for biomass transport	g_{CO2}/kg_{bm}
E	specific CO_2 emissions	g_{CO2}/kWh_{el}
$\dot{m}$	mass flow	kg/s
P	electrical power	MW_{el}

Greek symbols

γ_i	mass concentration of component i	-
ϕ	ventilation ratio	kg_{air}/kg_{bm}
η	efficiency	%
ϑ	temperature	K
ζ	overall energy utilisation efficiency	%

Indices

air	air
b	boiler
bind	binding
bm	biomass
c	coal
crh	cold reheat

Dieses Werk ist copyrightgeschützt und darf in keiner Form vervielfältigt werden noch an Dritte weitergegeben werden.
Es gilt nur für den persönlichen Gebrauch.

Indices

D	drying
db	dry basis
dg	drying gas
DP	dew point
dry	dryer
el	electrical
evp	evaporated
f	fuel
fg	flue gas
fw	feedwater
gross	gross
hrh	hot reheat
ls	live steam
m	mean
net	net
oil	oil
PG	power generation
T	transport
th	thermal
tot	total
w	wood
ww	warm water

Dieses Werk ist copyrightgeschützt und darf in keiner Form vervielfältigt werden noch an Dritte weitergegeben werden.
Es gilt nur für den persönlichen Gebrauch.

Dieses Werk ist copyrightgeschützt und darf in keiner Form vervielfältigt werden noch an Dritte weitergegeben werden.
Es gilt nur für den persönlichen Gebrauch.

1 INTRODUCTION

A higher share of renewable energies in power generation is being striven for in many countries, especially in Europe. More sustainable forms of energy utilisation are desired in order to meet targets for greenhouse gas reduction designed to limit climate change.

In Germany, wind and solar energy are the main resources of renewable power generation [1]. However, one major disadvantage of these weather-dependent forms of power generation, compared to power generation from fossil fuels, is the impossibility of adjusting their power generation in response to variable needs. Using biomass as a fuel for a conventional steam power plant can provide adjustable power generation and simultaneously reduce greenhouse gas emissions. The CO_2 emissions caused by burning biomass are assumed to be balanced by the CO_2 absorbed in the growing process. Therefore, burning biomass is counted as carbon neutral.

Biomass in general includes all living or dead organic matter and its residues and products, unaltered or transformed by technical processes [2]. Of course, not all types of biomass are suitable for power generation, but solid biomasses with a high carbon content, such as wood or straw, can be used as fuel.

When co-firing biomass with coal, some of the fossil fuel in a conventional steam power plant is substituted by a renewable fuel.

1.1 Background

Today in Germany, power generation from solid biofuels is subsidised only for the use of 100 % biomass and up to 20 MW of electrical power generation [3]. As a result, there are many small, decentralised facilities dedicated to solely firing biomass. Co-firing biomass with coal in large-scale coal-fired steam power plants is not subsidised in Germany, even though this practice would have several benefits. Firstly, already existing infrastructure could be used. The construction of a new power plant and the necessary grid connection would not be required, which is economic and resource-saving at the same time. Secondly, large coal power plants are mostly very well designed and usually operate with far higher process efficiencies than small biomass-only facilities are able to achieve. The same amount of biomass energy can be converted into a larger amount of electricity through

Dieses Werk ist copyrightgeschützt und darf in keiner Form vervielfältigt werden noch an Dritte weitergegeben werden.
Es gilt nur für den persönlichen Gebrauch.

co-firing in a large-scale coal power plant compared to the use of a small biomass-only power plant.

Co-firing activities are currently carried out in the UK, the Netherlands and most Scandinavian countries. The most commonly used fuel for co-firing in these countries is white wood pellets. It is current practice to import these from North America, but the sustainability and carbon neutrality of power generation based on fuels imported from overseas is questionable. Therefore, the focus should be on using locally available biomasses for co-firing.

Short-rotation plantations offer the possibility of providing large amounts of woody biomass. Fast-growing species, such as poplar or willow, can be harvested in perennial cycles, and are generally high-rank biomass fuels. If cultivated in the vicinity of the power plant, the overall sustainability of co-firing could clearly be improved.

Probably the greatest obstacle in using wood chips from short-rotation plantations for co-firing in coal power plants is the high moisture content of freshly harvested wood, which is around 50 %. To upgrade the biomass fuel, and in doing so limit the problems that might arise from co-firing, drying the wood chips prior to co-firing is essential.

1.2 Aim and scope

This thesis aims to identify and analyse the effects of biomass co-firing in coal-fired steam power plants at high rates of up to 50 %, based on fuel heat input. Each power plant is usually designed for a certain fuel. If, like in co-firing, a fuel with different properties is fired, operation cannot be expected to match design operation. The limitations and impairments of co-firing coal with wood chips on the power generation process in a large-scale steam power plant will be highlighted below and, if possible, quantified.

As the poplar wood chips need to be dried prior to co-firing, several drying technologies will be considered in order to identify a suitable drying process. Large-scale steam power plants require a very high fuel heat input, so an efficient method for drying significant mass flows of wood chips would be required. The influence of several process parameters on each drying process's energy demand will be analysed. Also, the possibilities and limitations of using heat sources from the power generation process for drying will be investigated.

Dieses Werk ist copyrightgeschützt und darf in keiner Form vervielfältigt werden noch an Dritte weitergegeben werden.
Es gilt nur für den persönlichen Gebrauch.

Several scenarios for drying and power generation will be developed and analysed in order to identify the most favourable way of drying poplar wood chips for co-firing in a coal-fired steam power plant. Also, the effects on the power generation process of integrating drying processes into the water-steam cycle or the flue gas track will be considered. Again, the limitations and impairments of co-firing biomass with coal will be analysed and quantified. To complete the scenario analyses, CO_2 emissions caused by transporting the wood chips from a short-rotation plantation to the power plant will be included.

1.3 Methodology

All the thermal processes analysed in this thesis are modelled and simulated using EBSILON®*Professional*. This modelling tool was developed for designing and analysing thermodynamic cycle processes and provides a wide range of process compounds, as well as the possibility of creating additional compounds. The simulation results of all the analysed processes are the main resource for this study's conclusions.

Chapter 2 summarises current activities and experiences in biomass co-firing with coal. Different biomasses are compared with regard to their fuel characteristics. Also, the possible effects resulting from fuel composition while co-firing are considered. Additionally, several methods of fuel supply are introduced and evaluated.

Chapter 3 outlines the technical possibilities for drying large mass flows of poplar wood chips matching the requirements of co-firing with coal. Two different drying technologies, indirect steam-tube dryers and direct rotary dryers, are identified as suitable and their technical details and process characteristics are presented.

Chapter 4 describes the model developments of the boiler, the power generation process and the dryers. The power plant considered is modelled based on information provided by a German utility. The drying processes are modelled based on information gained through literature research and communication with dryer manufacturing companies.

Chapter 5 evaluates the effects of direct biomass co-firing on the power generation process. In the first stage, changes in heat transfer and the process parameters of the boiler are analysed. Afterwards, further effects on the overall process are demonstrated and interpreted.

Dieses Werk ist copyrightgeschützt und darf in keiner Form vervielfältigt werden noch an Dritte weitergegeben werden.
Es gilt nur für den persönlichen Gebrauch.

Chapter 6 develops three scenarios for drying and co-firing poplar wood chips in large-scale steam power plants. An indirect steam-tube dryer would need to be integrated into the power plant's water-steam cycle in order to be supplied with the necessary drying heat. A flue-gas-heated direct rotary dryer could function in a stand-alone version or be integrated into the power plant's flue-gas track. The heat demand of a stand-alone rotary dryer could be covered by burning biomass or fossil fuels.

The technical challenges in realising each scenario are discussed and, if technically feasible, the most favourable drying scenario would be the one with the lowest total resulting CO_2 emissions and highest overall energy utilisation efficiency. The total resulting CO_2 emissions are calculated by adding together the CO_2 emissions caused by power generation, drying and fuel transportation. To determine the overall energy utilisation efficiency, the additional energy input for drying in the non-integrated scenarios is included in an overall energy balance.

Dieses Werk ist copyrightgeschützt und darf in keiner Form vervielfältigt werden noch an Dritte weitergegeben werden.
Es gilt nur für den persönlichen Gebrauch.

2 CO-FIRING BIOMASS WITH COAL

There are multiple ways to realise power generation from biomasses. One of them is the co-firing of biomass with coal, which itself can be carried out in different ways. However, in this thesis, only the co-firing of solid biomass in pulverized hard-coal-fired large-scale steam power plants will be considered.

Three main concepts for biomass co-firing are generally distinguished [4]:

- direct co-firing
- indirect co-firing
- parallel co-firing

Technically, direct co-firing is the simplest approach. No significant modifications of the existing power plant are required for its realisation. The biomass fuel is fed directly into the coal mass flow or ground separately. In the first case, biomass is co-milled in vertical spindle mills. In the second case, the pulverized biomass can be injected into the pulverised coal mass flow upstream of the burners, although combustion by dedicated biomass burners is also possible. This concept is most commonly applied when co-firing biomass with coal.

For indirect co-firing, a fuel pre-treatment process is installed at the power plant site, which can also be integrated into the power generation process. This method of biomass co-firing requires greater investment and the operation of an additional complex process. However, it also allows the use of a broader range of biomasses, as the fuel properties can be adjusted to the power plant's requirements.

Parallel co-firing of biomass with coal requires a separate boiler for biomass combustion, since only the water-steam cycles are connected, with the biomass and the coal being combusted separately. Out of all three concepts, this requires the greatest number of necessary modifications to the existing power plant. However, it also enables the use of a wide variety of biomass fuels, as the biomass boiler is specially designed for biomass combustion only. This can help avoid the problems that typically occur in co-firing biomass with coal.

Dieses Werk ist copyrightgeschützt und darf in keiner Form vervielfältigt werden noch an Dritte weitergegeben werden.
Es gilt nur für den persönlichen Gebrauch.

2.1 Current Co-firing activities in power generation

Currently, biomass co-firing with coal is carried out in a small number of power plants in Europe. Along with many short term trials [5], [6], [7], [8], [9], [10], incentives have led to permanent co-firing activities, or even full conversion to biomass-only firing in countries like Denmark, the Netherlands and the UK. The co-firing of biomass with coal in large-scale steam power plants first started at the beginning of the new millennium.

Using biomass fuels for combined heat and power generation has a significantly longer tradition and is widely used in Austria and in all Scandinavian countries [11], [12], [13], [14]. Their local wood industry provides large amounts of wood residue that is often used in small-scale CHP plants.

The present thesis will only consider biomass co-firing in pulverised coal-fired, large-scale steam power plants. Table 1 lists a selection of such power plants currently co-firing biomass with coal in Europe.

Recently, the city of Copenhagen declared its intention of becoming the world's first capital city with a carbon neutral heat and electricity supply, by 2025 [15]. As a result, several units of the combined heat and power plants in Amager and Avedøre have already been fully converted to biomass combustion, and the conversion of further units is planned for future years [16]. Other power plants in Denmark use agricultural residue straw for co-firing. Studstrup power station, with a co-firing rate of 20 % based on fuel heat input, is just one example.

In the Netherlands, subsidy programmes have encouraged co-firing activities in various power plants. Co-firing rates do not exceed 10 % in most cases. The chosen biomass fuel is, once again, wood pellets. This is also the case for the fully converted Unit 4 at Rodenhuize power station in Belgium.

Several large facilities in the UK have been fully converted to power generation from biomass. In Drax power station, the third unit has been fired 100 % by wood pellets since 2015. Together with the biomass co-firing activities at Ferrybridge and other power plants, more than 600 MW_{el} of carbon neutral electricity is currently generated in the UK.

Dieses Werk ist copyrightgeschützt und darf in keiner Form vervielfältigt werden noch an Dritte weitergegeben werden.
Es gilt nur für den persönlichen Gebrauch.

Table 1: Selection of large-scale European coal power plants with current biomass co-firing activities

Power plant	Biomass	Co-firing rate	References
Amager (DK)			
Unit 1	Wood pellets	100 %	[17], [16]
Unit 2	Straw pellets	100 %	
Avedøre (DK)			
Unit 1	Wood pellets	100 %	[18],[19], [20]
Unit 2			
Studstrup (DK)			
Unit 1	Straw	20 %	[21], [4], [22]
Unit 4	Straw	20 %	
Amer (NL)			
Unit 9	Wood pellets	27 %	[23], [24]
Unit 8	Wood pellets	10-12 %	
Gelderland (NL)			
Unit 13	Wood, waste wood	5-8 %	[24]
Maasvlakte (NL)			
	Biomass pellets	6 %	[24]
Borselle (NL)			
	Kernels, paper sludge, shells, fibres	10-15 %	[24], [22]
Rodenhuize (B)			
Unit 4	Wood pellets	100 %	[25]
Drax (UK)			
Unit 1			
Unit 2	Wood pellets	100 %	[18],[25]
Unit 3			
Ferrybridge (UK)			
Unit 1	Wood pellets, palm kernels, olive stones, olive cake	20 %	[18]
Unit 2			

Dieses Werk ist copyrightgeschützt und darf in keiner Form vervielfältigt werden noch an Dritte weitergegeben werden.
Es gilt nur für den persönlichen Gebrauch.

2.2 Biomass fuel characteristics and resulting effects in the combustion system

Biomasses currently used as fuel for energy production are in most cases woody or herbaceous biomasses, either residues from various sources or energy plants cultivated for the purpose of energy production. Fast-growing woods like poplar or willow, for example, can be cultivated in short-rotation plantations. Spruce, on the other hand, is one of the most common tree species in the wood industry in Europe and North America. Another solid biomass fuel is straw, which represents a herbaceous biomass and is available as an agricultural residue.

Regarding their fuel characteristics, these biomass fuels can deviate significantly from fossil fuels. Typical elemental compositions for the dry matter of hard coal, lignite, poplar, willow and straw are listed in Table 2 [2]. Fossil fuels and biomass fuels differ most obviously in their oxygen content. While typical hard coals are characterised by an oxygen content of around 10 %, typical biomass fuels usually have an oxygen content of more than 40 %. As a result, the carbon content in biomasses is clearly lower.

Table 2: Composition of various biomass fuels and coals [2]

Fuel type	C	H	O	N	S	Cl	Ash
	in wt.-% of dry matter						
Hard coal	72.5	5.6	11.1	1.30	0.94	0.130	8.430
Lignite	65.9	4.9	23.0	0.70	0.39	0.100	5.010
Poplar	47.5	6.2	44.1	0.42	0.031	0.004	1.745
Willow	47.1	6.1	44.3	0.54	0.045	0.004	1.911
Spruce	49.8	6.3	43.2	0.13	0.015	0.005	0.550
Straw	45.6	5.8	42.4	0.48	0.082	0.190	5.448

The fuels' heating values depend on their elemental composition and moisture content. In this paper, the following equation (Eq. 2.1) from Boie [26], [27] is used to calculate the higher heating value HHV_{db} on dry basis:

$$HHV_{\mathrm{db}} = \left(151.2 \cdot \gamma_{\mathrm{C,db}} + 499.77 \cdot \gamma_{\mathrm{H,db}} - 47.7 \cdot \gamma_{\mathrm{O,db}} + 45 \cdot \gamma_{\mathrm{S,db}} - 27 \cdot \right. \qquad (2.1)$$

Dieses Werk ist copyrightgeschützt und darf in keiner Form vervielfältigt werden noch an Dritte weitergegeben werden.
Es gilt nur für den persönlichen Gebrauch.

$\gamma_{\mathrm{N,db}} - 189) \cdot 2326$ in kJ/kg.

With $\gamma_{\mathrm{C,db}}$, $\gamma_{\mathrm{H,db}}$, $\gamma_{\mathrm{O,db}}$, $\gamma_{\mathrm{S,db}}$ and $\gamma_{\mathrm{N,db}}$ being the mass shares of carbon, hydrogen, oxygen, sulphur and nitrogen on dry basis of the biomass fuel.

The higher heating value HHV_{db} can be converted into the lower heating value on dry basis LHV_{db} with Eq. 2.2 by subtracting the evaporation enthalpy of the water created by combusting the fuel hydrogen:

$$LHV_{\mathrm{db}} = HHV_{\mathrm{db}} - 2442 \cdot \left(8.936 \cdot \gamma_{\mathrm{H,db}}\right) \quad \text{in kJ/kg.} \tag{2.2}$$

The results for the lower heating values on dry basis for the biomasses poplar, willow, spruce and straw are shown in Table 3. Due to its comparatively high carbon content, the LHV_{db} of spruce is higher than those of the other fuels.

Table 3: Lower heating values of biomass fuels

	Poplar	**Willow**	**Spruce**	**Straw**
$\boldsymbol{LHV_{\mathrm{db}}}$ **(MJ/kg)**	17.20	16.94	18.22	16.35

With Eq. 2.3, the lower heating value of biofuels on wet basis LHV_{wet} can be calculated based on LHV_{db} and the fuel moisture content $\gamma_{\mathrm{H_2O}}$:

$$LHV_{\mathrm{wet}} = LHV_{\mathrm{db}} \cdot \left(1 - \gamma_{\mathrm{H_2O}}\right) - 2.442 \cdot \gamma_{\mathrm{H_2O}} \quad \text{in kJ/kg.} \tag{2.3}$$

The fuel moisture content has a substantial influence on the lower heating value LHV_{wet} of a fuel. Figure 1 shows the dependence of the lower heating values LHV_{wet} of spruce, poplar, willow and straw on fuel moisture content. Starting from lower heating values on dry basis of around 17 000 kJ/kg, the fuel energy content drops to lower heating values of around 9 000 kJ/kg for a fuel moisture content of 50 %.

Dieses Werk ist copyrightgeschützt und darf in keiner Form vervielfältigt werden noch an Dritte weitergegeben werden.
Es gilt nur für den persönlichen Gebrauch.

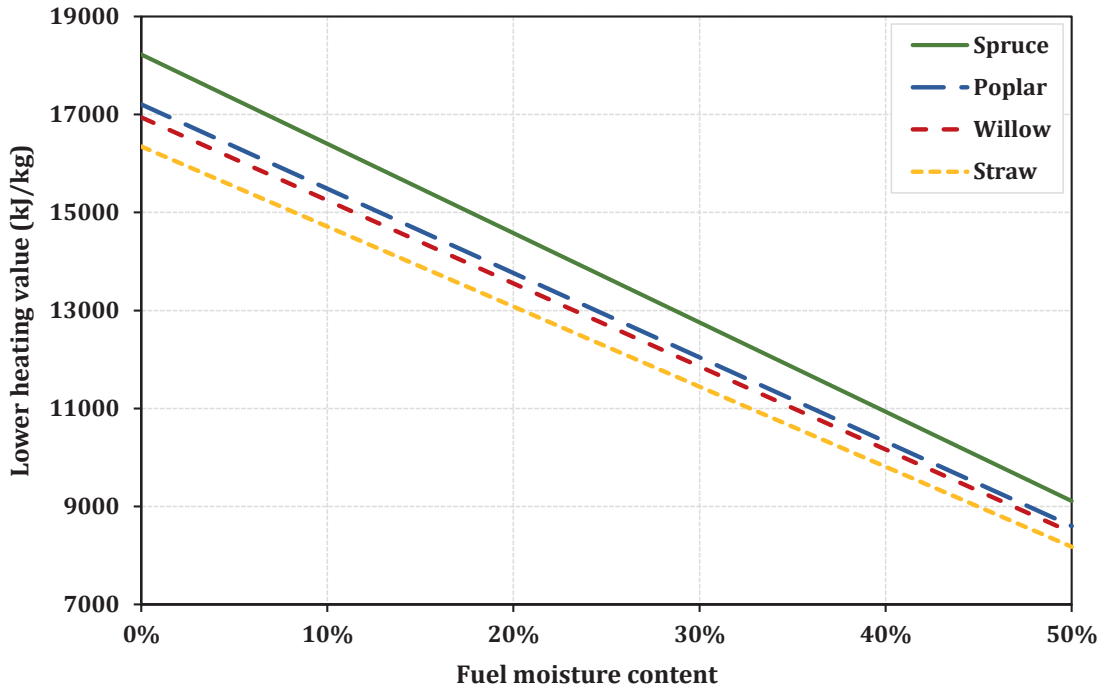

Figure 1: Lower heating values of biomass fuels for varying fuel moisture content

Table 2 also shows that woody and herbaceous biomass fuels generally have a lower ash content than hard coal. Nonetheless, the biomass ash might be problematic in co-firing, as the composition of biomass ash deviates from that of coal. VASSILIEV *et al.* [28], [29] analysed the composition of several biomass ashes, including beech wood, corn cobs, microalgae, plum pits, rice husks, switchgrass, sunflower shells and walnut shells. Table 4 shows the resulting mean value for each ash component, as well as the range of analysis results. Alongside biomasses, several hard coal ashes were also analysed. To gain a better picture of typical ash compositions, the results of poplar [30], eucalyptus and a second hard coal ash [31] are included in Table 4. Due to differing analysis methods, different elements are identified for ash composition.

The results show a very wide range in biomass ash composition, which underlines one of the most important characteristics of biomass fuels. Even within one biomass species, the fuel and ash composition can vary significantly. Coal ash composition can also vary. However, general differences between the ashes of woody biomass (here poplar and eucalyptus) and coal ashes can be specified. Coal ashes are richer in silicon and aluminium oxides, whereas most biomass ashes are richer in potassium and calcium oxides.

Dieses Werk ist copyrightgeschützt und darf in keiner Form vervielfältigt werden noch an Dritte weitergegeben werden.
Es gilt nur für den persönlichen Gebrauch.

Table 4: Composition of coal and biomass ashes

	Coal ash [28] (wt.% db)	Biomass ash [28] (wt.% db)	Poplar ash [30] (wt.% db)	Eucalyptus ash [31] (wt.% db)	Coal ash [31] (wt.% db)
SiO_2	54.06 (32.04-68.35)	29.14 (0.02-94.48)	14.0	26.50	44.80
CaO	6.57 (0.43-27.78)	25.99 (0.97-83.46)	34.0	21.80	23.10
K_2O	1.60 (0.29-4.15)	19.40 (2.19-63.90)	10.0	10.25	3.57
P_2O_5	0.50 (0.10-1.70)	5.92 (0.54-40.94)	3.0	2.88	1.13
Al_2O_3	23.18 (11.32-35.23)	4.49 (0.10-15.12)	1.7	7.60	6.21
MgO	1.83 (0.31-3.98)	5.60 (0.19-16.21)	4.8	5.88	2.55
Fe_2O_3	6.85 (0.79-16.44)	3.41 (0.22-36.27)	0.6	5.13	4.50
SO_3	3.54 (0.27-14.42)	3.27 (0.01-14.74)	-	2.53	3.53
Na_2O	0.82 (0.09-2.90)	2.54 (0.09-29.82)	0.9	2.52	1.52
TiO_2	1.05 (0.62-1.61)	0.24 (0.01-2.02)	-	0.33	4.07
BaO	-	-	-	0.22	0.49
Mn_3O_4	-	-	-	2.03	0.57

The following problems are commonly associated with biomass combustion, mainly occurring due to its lower ash-fusion temperature, caused by a high share of alkali components [4], [10]:

Dieses Werk ist copyrightgeschützt und darf in keiner Form vervielfältigt werden noch an Dritte weitergegeben werden.
Es gilt nur für den persönlichen Gebrauch.

- formation of fused or partly fused ash agglomerates and bonded ash deposits at high temperatures within furnaces and on heat exchanger surfaces
- accelerated metal wastage of boiler components due to gas-side corrosion and erosion
- formation and emission of sub-micron aerosols
- handling, utilisation and disposal of ash residues from biomass in coal-fired boilers

However, it is very likely that these problems will not arise in such severity when co-firing biomasses with coal. WU [32] and DAMOE [33] investigated the consequences for ash-deposit formation and aerosol formation during combustion when adding coal fly ash to a large-scale pulverised wood-fired boiler. The amount of coal ash added was about four times the amount of biomass ash. The shedding of ash deposits due to gravity and soot blowing increased as coal fly ash was added. Also, fewer PM_1 and $PM_{2.5}$ particles were formed. Therefore, it can be concluded that, due to the reaction of biomass-ash-associated alkali metals with coal-ash-associated aluminosilicates, some negative consequences of biomass co-firing, such as deposit formation, can be limited and thus corrosion rates reduced. Also, DeNOx catalyst degradation could be limited with coal fly ash dosing [34].

Due to the experience of using biomass in several large-scale power plants (see Table 1), some technical challenges can already be specified. So far, most of the technical problems are associated with fuel handling, storage and grinding. Wood pellets can be successfully milled in adjusted coal mills in Avedøre and Studstrup [34]. Nonetheless, the capacity of the roller mills used is questionable, and hammer mills or disc mills might perform better. According to the *UK Best Practice Brochure for Co-firing of Biomass* [35], co-grinding in spindle mills is save up to a biomass mass share of 15 %. However, mill capacity and performance are still adversely impacted and dedicated systems should be preferred.

Biomass moisture content should be limited, not just to ensure grinding performance, but also to limit problems with fuel handling and storage [35]. Hang ups and bridging in the mill bunkers can appear due to the bulk material properties, which can differ significantly from those of coal and make adjustment measures necessary. A more severe problem can be dust formation, which is mainly induced by wood pellet breakdown during handling. Dust spreading should be limited as much as possible to limit fire risks and the inhalation of fines by workers.

Dieses Werk ist copyrightgeschützt und darf in keiner Form vervielfältigt werden noch an Dritte weitergegeben werden.
Es gilt nur für den persönlichen Gebrauch.

Even though slight increases in particle emissions might occur [35], which can also accompany an increase in unburnt levels [34], [35], emissions are generally reduced with biomass co-firing. First of all, SO_x emissions are reduced due to the significantly lower sulphur content in biomass fuels (see Table 2) [35], [32], [36], [10]. NO_x emissions are also reduced. This is caused not only by a comparatively lower fuel nitrogen content but also by changed combustion characteristics due to increasing fuel volatility. The formation of NH_3 and HCN increases with increasing fuel volatility and so gas-phase combustion becomes predominant. Also, in the gas phase, the volatile biomass fuel nitrogen preferably forms NH_3, whereas HCN is more commonly formed by hard coal nitrogen [36]. These NH_3 molecules form NH_i radicals that then reduce the NO to molecular nitrogen [37], [36].

2.3 Fuel supply and environmental aspects of biomass co-firing

As can be seen in Table 1, the most commonly used biomass fuel for co-firing is wood in the form of untreated wood pellets as they cause few problems when co-fired and require only minor modification to the existing equipment. Large amounts of pellets are imported from North America to cover the demand.

Figure 2 and Figure 3 show global wood pellet production and consumption for 2010 and estimates for 2015 and 2020. It is obvious that, in Europe, demand for pellets largely exceeds production, whereas in North America, as well as in Eastern Europe and Russia, more pellets are produced than consumed. The Danish energy utility DONG Energy expects its total consumption of biomass to grow by up to 2.7 million tonnes per year, including 1.8 million tonnes of wood pellets, from 2016 on [34]. The cumulated European demand for wood pellets is estimated to reach 23.8 million tonnes per year in 2020 [25].

However, the CO_2 neutrality of biomass combustion has to be questioned if this fuel is transported over very long distances before being used for power generation. According to MAGELLI *et al.* [38], about 7.2 GJ of energy are consumed for each tonne of wood pellets produced in West Canada and transported to Europe, which represents approximately 39 % of the total energy content of the wood pellets. More than a third of this energy is associated with the long-distance sea transportation required. The *Industrial Wood Pellets Report* suggests that more pellets could be imported from Russia and, thus, the energy expense of crossing the Atlantic by ship could be avoided. However, in a paper considering trends and challenges in the wood pellets business in Russia, PROSKURINA *et al.* [39] concluded that, due to an

Dieses Werk ist copyrightgeschützt und darf in keiner Form vervielfältigt werden noch an Dritte weitergegeben werden.
Es gilt nur für den persönlichen Gebrauch.

oligopolistic market structure, inadequate infrastructure and a lack of foreign investment, it is unlikely that the Russian wood pellet market will develop significantly in the near future.

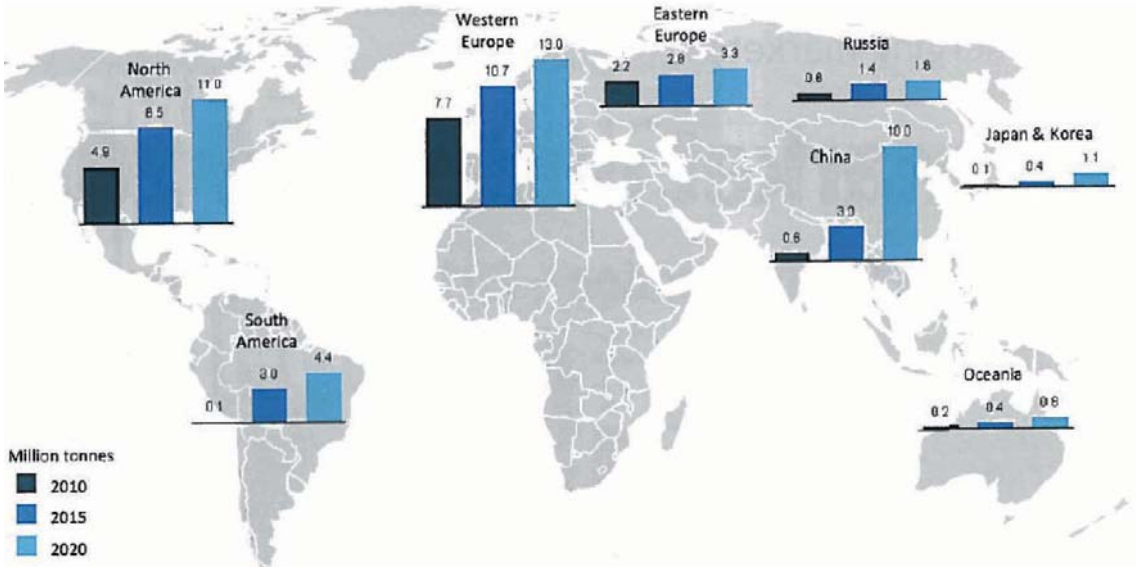

Figure 2: Global wood pellet production [40]

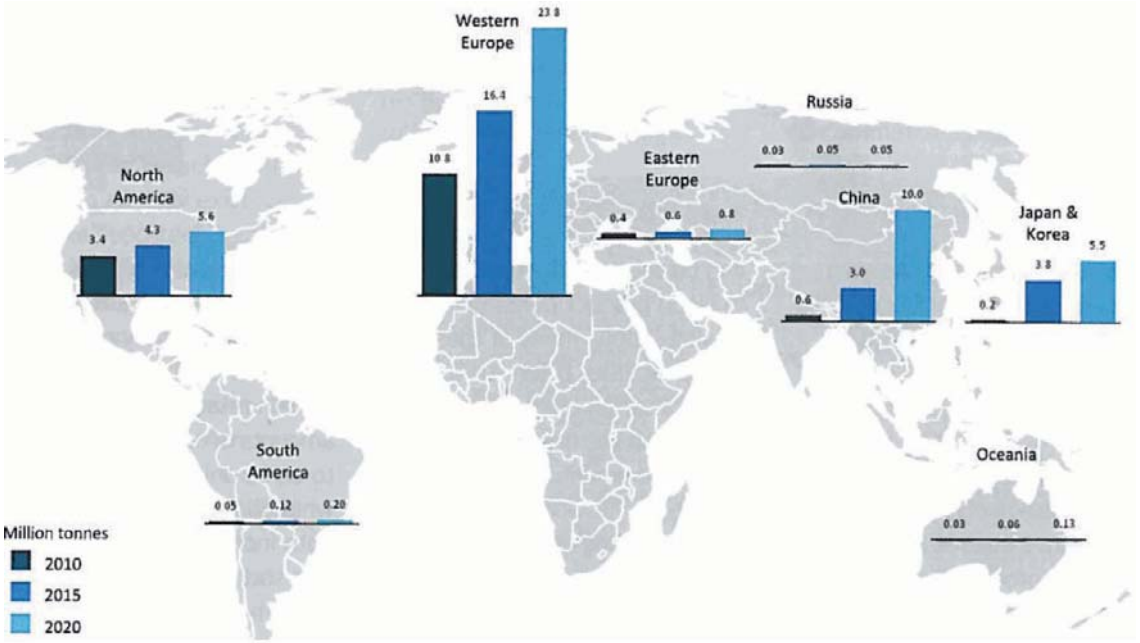

Figure 3: Global wood pellet consumption [40]

Dieses Werk ist copyrightgeschützt und darf in keiner Form vervielfältigt werden noch an Dritte weitergegeben werden.
Es gilt nur für den persönlichen Gebrauch.

Guidelines for sustainability requirements for biomass fuels have been published by the European Commission [41], [42] and include criteria for soil, water and air protection. Sustainability certification schemes are still not standardized and depend on each member state's regulations and subsidy schemes. However, only sustainably grown biomass can be counted as a CO_2-neutral fuel. And even then, the CO_2 neutrality is reduced due to transport-related emissions.

Using locally grown energy plants as fuel would make sustainability controls easier, and transportation distances could be reduced significantly. Therefore, poplar wood chips cultivated in a short-rotation plantation will be considered for biomass co-firing in this thesis.

Dieses Werk ist copyrightgeschützt und darf in keiner Form vervielfältigt werden noch an Dritte weitergegeben werden.
Es gilt nur für den persönlichen Gebrauch.

Dieses Werk ist copyrightgeschützt und darf in keiner Form vervielfältigt werden noch an Dritte weitergegeben werden.
Es gilt nur für den persönlichen Gebrauch.

3 DRYING TECHNOLOGIES

Freshly cut wood has a moisture content of around 50 % [2] and is thus not suitable for co-firing at high rates in large-scale pulverised coal power plants. The fuel needs to be dried. Of course, wood chips also dry naturally during storage, but the achievable final moisture content is limited to around 15 % [2]. Long storage times can also be accompanied by natural wood degradation processes. To reduce requirements for storage space and reach a reliable moisture content, a technical drying process is necessary.

The technical drying of goods is a long-proven technology and is commercially available in many variations. A very broad range of drying processes for all kinds of applications have been developed so far. Drying technologies can be classified according to the applied heating method, temperature and pressure of operation, and the method of material conveying in the dryer [43], [44]. Dryers are divided into three categories of heating method:

- convection (or direct dryers)
- conduction (or indirect dryers)
- radiation

In direct dryers, material is dried by a hot drying medium flowing over the material surface. The heat for evaporation is supplied by convection, and the evaporated moisture is carried away by the drying medium, which can be air, inert gas, combustion flue gases or superheated steam [44], [43].

In indirect dryers, the material comes into direct contact with a heated surface and the heat of evaporation is supplied by conduction. The evaporated moisture needs to be carried away by vacuum operation or a spill gas stream, which serves primarily as a carrier of moisture [43], [44].

Some types of dryers use electromagnetic radiation to supply the energy for evaporation. The wavelength used can range from the solar spectrum to microwaves and determines the intensity of drying, which can range from surface drying to heating and drying of the full material volume. These dryers are associated with very high capital and operation costs [44].

Most dryers operate at ambient air pressure. Both vacuum and overpressure applications are rare. The chosen drying temperature depends on many variables.

Dieses Werk ist copyrightgeschützt und darf in keiner Form vervielfältigt werden noch an Dritte weitergegeben werden.
Es gilt nur für den persönlichen Gebrauch.

Any drying process can be completed faster at higher temperatures, but as the dried material usually changes its characteristics during the process, the desired quality of the end product usually sets limits on drying temperature, temperature profile and residence time. Also, heating costs and the type and quality of available heat sources determine the drying temperature. If dried in an oxygen-rich atmosphere, an upper limit for the drying temperature is naturally formed by the self-ignition temperature of the product.

The method of conveying material through a dryer largely depends on the characteristics of the drying material, which can range from solids (free flowing or not free flowing), sludges and pastes to liquid slurries or solutions. MUJUMDAR [44] suggests eight categories for material transport in a dryer:

- not conveyed
- falling by gravity
- mechanically conveyed
- transported on trucks
- sheet-form materials can be supported on rolls
- conveying on bands
- suspending in air
- atomising in air

In general, a suitable dryer has to be chosen mainly based on the requirements of the drying material. Additionally, the context of co-firing in a large-scale pulverised coal power plant needs to be considered for dryer selection.

3.1 Requirements of the drying material and dryer selection

As explained in Chapter 2, woody biomass is most commonly used for co-firing in coal power plants. One possibility for providing large amounts of woody biomass for energy use is the use of short-rotation plantations, where fast-growing species, such as poplar, can be harvested with a chipper in a 2–6-year cycle [45], [46]. Poplar wood chips are being considered as fuel for biomass co-firing in this paper and, therefore, the material for which a suitable dryer has to be chosen.

Dieses Werk ist copyrightgeschützt und darf in keiner Form vervielfältigt werden noch an Dritte weitergegeben werden.
Es gilt nur für den persönlichen Gebrauch.

Their particle size typically ranges from 3 to 200 mm [47]. The product in general is quite robust, is usually free-flowing in transport and surface damage is not an issue. The production of very fine wood dust should be avoided, as this is highly inflammable [48]. The fresh wood has a moisture content of 50 % and has to be dried to a final moisture content of 10 % in order to significantly reduce the energy requirement of the biomass mills [49]. Moreover, further drying cannot be recommended, as the formation of volatile organic carbons (VOCs) is unwelcome [50].

For co-firing with coal, high mass flows of biomass fuel will be required, especially for co-firing rates of up to 50 %, based on fuel heat input. Therefore, a high evaporation capacity is desirable for an associated dryer to enable a high throughput rate. Also, a high drying temperature is beneficial in keeping the dryer's dimensions small.

Solar dryers can be a cost-efficient option for biomass drying [51] but are not an option for locations in Germany due to typically poor solar radiation. Belt dryers or conveyor dryers are quite commonly used for the drying of sawdust and wood chips [52], [53], [54]. However, due to drying temperatures in the range of 80–150 °C, the retention time in these dryers is usually quite long [44]. Even though the low drying temperatures seem attractive, as they can allow the use of waste heat flows in many process configurations, conveyor dryers will not be considered for biomass drying for co-firing in this paper. Substituting up to 50 % of the fuel input of coal with biomass requires considerable fuel mass flows. The space that conveyor dryers would require to cover the associated drying demand is deemed to be unreasonably high. Fluidized bed dryers, which offer a significantly higher volumetric heat transfer coefficient and can therefore be built in a more compact design, are not suitable in this case either. A fluidized bed would require a smaller and probably more homogeneous particle size than the poplar wood chips under consideration here. Grinding the wood chips prior to drying would cancel out the desired energy-saving effect of drying the wood chips prior to grinding.

Consequently, only two types of dryers can be considered for the large-scale drying of wood chips:

- indirect steam-tube dryers
- direct rotary dryers

Both dryers can offer a comparatively low retention time due to high drying temperatures in the range of 140–400 °C [44], [55]. Additionally, the method of

Dieses Werk ist copyrightgeschützt und darf in keiner Form vervielfältigt werden noch an Dritte weitergegeben werden.
Es gilt nur für den persönlichen Gebrauch.

material transport (falling by gravity) results in a high volumetric heating coefficient that enables a compact dryer design and thus a comparatively small space requirement. Both dryer types will be described in more detail in the following sections.

3.2 Indirect steam-tube dryer

An indirect steam-tube dryer usually has a drum-formed shell, which is slightly inclined (1° to 5° to the horizontal) [44], [43]. The inclination allows the transport of wood chips through the dryer by gravity. The dryer shell is filled with several rows of symmetrical steam tubes. A diagram of the dryer can be seen in Figure 4 and a photograph of the steam tubes in Figure 5.

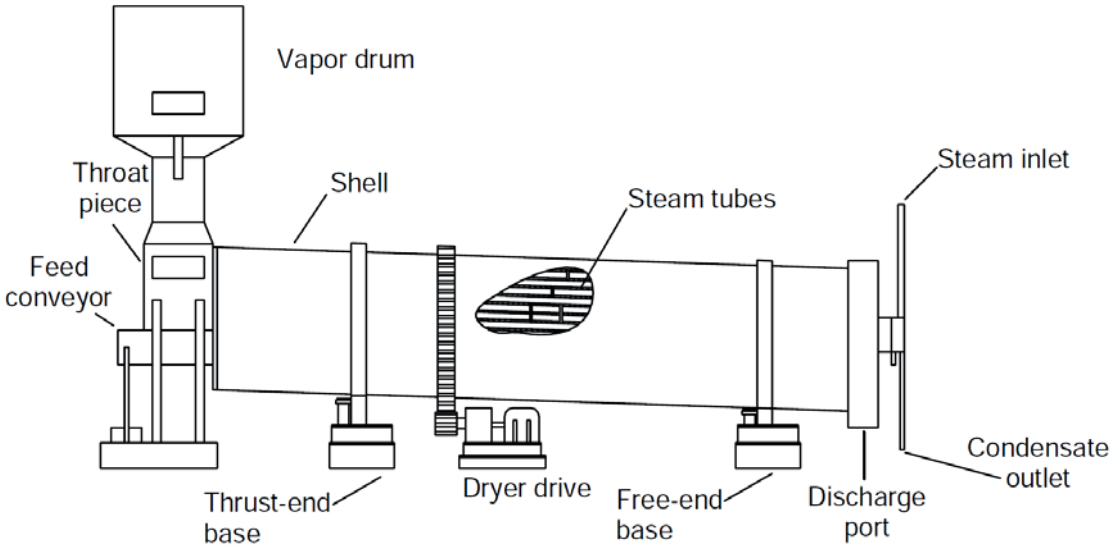

Figure 4: Diagram of an indirect steam tube dryer [44]

Dieses Werk ist copyrightgeschützt und darf in keiner Form vervielfältigt werden noch an Dritte weitergegeben werden.
Es gilt nur für den persönlichen Gebrauch.

Figure 5: Steam tubes of an indirect dryer [56]

The biomass is fed into the shell by the feed conveyor. The dryer operates continuously, not in a batch mode. The wood chips are heated up by conduction on contact with the steam tubes. Both the dryer shell and the steam tubes rotate to ensure an equal heat transfer to all wood chips. Figure 5 also shows small flights fixed onto the steam tubes, which help to improve the product mass flow in the dryer. The dried product leaves the dryer via the discharge point.

Typically, steam in a pressure range of 4–10 bar is used for heating [44]. The steam condenses in the tubes, which is why rotating the steam tubes is crucial for a homogeneous heat transfer. The drying temperature corresponds to the condensing temperature associated with the steam pressure and thus ranges from 140 °C to 180 °C. Heat transfer coefficients in steam-tube dryers may range from 30 to 85 $W/(m^2K)$ [44].

The evaporated moisture can be removed from the dryer by vacuum operation, but it is more common and less cost intensive to use a small air mass flow to ventilate the dryer [44]. The resulting hot stream of almost saturated air can provide a heat source for other process steps.

Dieses Werk ist copyrightgeschützt und darf in keiner Form vervielfältigt werden noch an Dritte weitergegeben werden.
Es gilt nur für den persönlichen Gebrauch.

3.3 Direct rotary dryer

According to FAGERNÄS [55], rotating drum dryers are currently the most common technology for biomass drying. A diagram of a direct rotary dryer is shown in Figure 6.

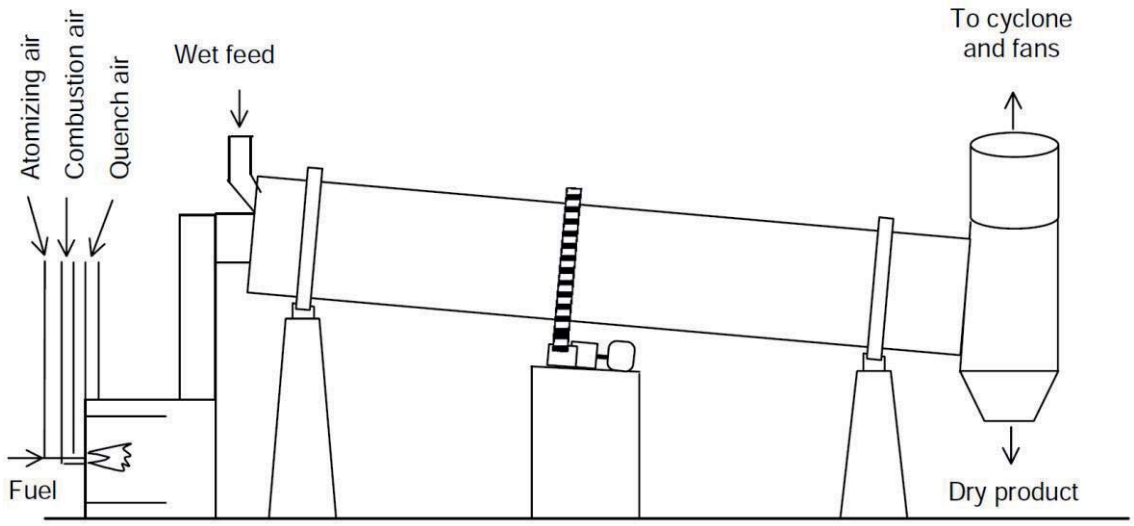

Figure 6: Diagram of a direct rotary dryer [44]

Here the drying medium is hot combustion gas from a small furnace, which only serves to cover the dryer's heat demand. However, in other applications, various heat sources like flue gases from small gas turbines or combined heat and power plants can be used as well [57]. Also, hot water or steam could be used as a heat source if an air preheater were to be used to warm up the drying-medium air [58]. However, this last process variation is not considered further in this paper, as it would be less efficient than a steam-tube dryer.

The wet feed enters the dryer and typically moves through it in co-current flow with the drying medium. As in the steam-tube dryer, the drum shell is slightly inclined to the horizontal so that the particles are transported by gravity, tumbling at the lower part of the shell but mostly due to lifting and showering [59].

Figure 7 shows how the solids in a direct rotary dryer are distributed through lifting by flights and showering. As most of the heat of evaporation is transferred to the particles during showering, while they are in direct contact with hot gas [59], their distribution is crucial for the dryer's efficiency.

Dieses Werk ist copyrightgeschützt und darf in keiner Form vervielfältigt werden noch an Dritte weitergegeben werden.
Es gilt nur für den persönlichen Gebrauch.

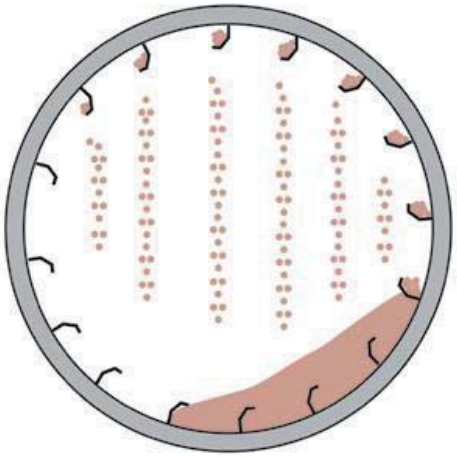

Figure 7: Flights and distribution of solids in the dryer [60]

The flights are usually offset every 0.6–2 m and their shape, which depends upon the characteristics of the solids, typically changes along the dryer's length [44]. Figure 8 shows an example of how flights are formed and distributed in a direct rotary dryer. The amount of solids that can be transported by the flights is limited, so overloading the dryer must be avoided to limit kiln action [44]. Particles that only roll through the lower part of the dryer without being lifted will not be dried to the desired moisture content at the dryer outlet.

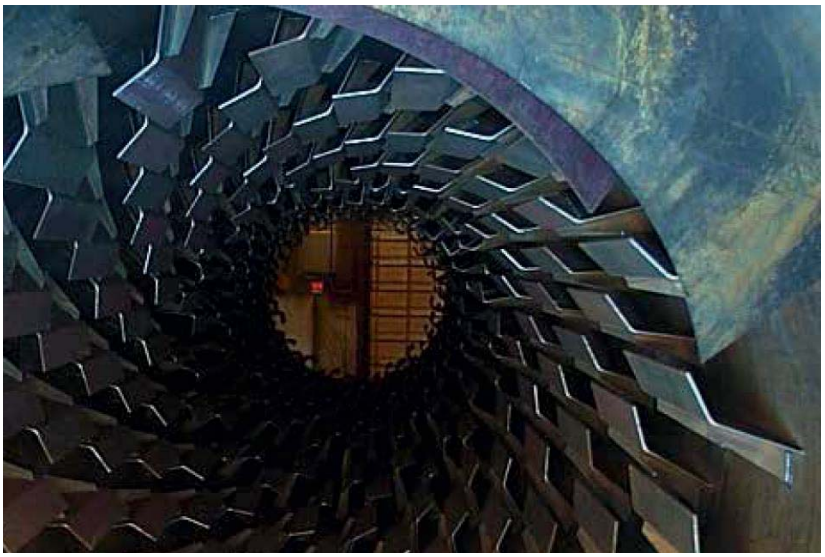

Figure 8: Flights in a direct rotary dryer [60]

When leaving the dryer, the drying gases have to pass through a cyclone. Fine particles that could be carried away by the drying gas are separated and fed into the

Dieses Werk ist copyrightgeschützt und darf in keiner Form vervielfältigt werden noch an Dritte weitergegeben werden.
Es gilt nur für den persönlichen Gebrauch.

mass flow of dried solids. Further treatment of the drying gases is optional and usually dependent on local regulations.

In industrial applications, evaporation rates of up to 60 t/h can be achieved with material throughput rates of up to 70 t/h [56]. Experience in wood drying originates mainly from the wood processing industry, where wood chips or sawdust need to be dried for purposes such as chipboard production.

Dieses Werk ist copyrightgeschützt und darf in keiner Form vervielfältigt werden noch an Dritte weitergegeben werden.
Es gilt nur für den persönlichen Gebrauch.

4 INTRODUCTION OF CONSIDERED DRYING SCENARIOS

The poplar wood chips used for co-firing can be dried by either a stand-alone dryer located at the short-rotation plantation, or a process-integrated on-site dryer. Figure 9 illustrates the three scenarios considered in this work:

- Scenario 1: transport of wet biomass + drying by integrated indirect steam-tube dryer that is either
    a. heated by steam extracted from the IP/LP crossover pipe or
    b. heated by steam extracted from the IP/LP crossover pipe and the LP turbine
- Scenario 2: transport of dry biomass + drying by stand-alone direct rotary dryer that is either
    a. heated by burning wet wood chips or
    b. heated by burning oil
- Scenario 3: transport of wet biomass + drying by integrated direct rotary dryer

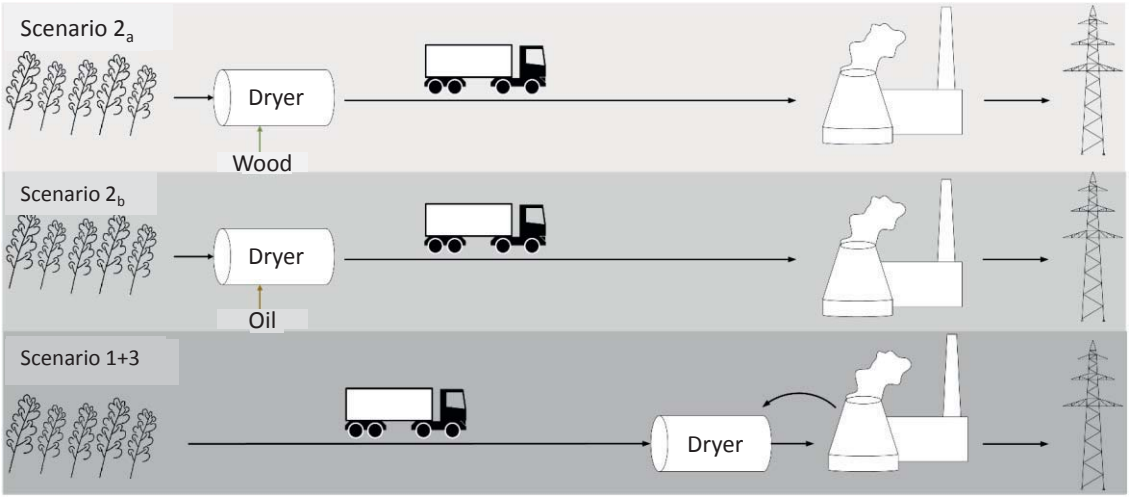

Figure 9: Scenarios of stand-alone drying and integrated on-site drying

As the indirect steam-tube dryer requires steam as a heating medium, it is considered unsuitable for a stand-alone scenario.

The drying processes will be modelled and analysed in detail in the following sections, and technical feasibility and impairments to the power generation process

Dieses Werk ist copyrightgeschützt und darf in keiner Form vervielfältigt werden noch an Dritte weitergegeben werden.
Es gilt nur für den persönlichen Gebrauch.

will be taken into account. In the end, the most favourable drying scenario, regarding CO_2 emissions, will be determined by comparing the total resulting CO_2 emissions from transport, drying and power generation. Additionally, the scenario in which the energy input is most efficiently transformed into electrical power is determined. In a final conclusion, the possibilities of technical realisation are estimated and added to the evaluation of drying scenarios.

4.1 Definition of energy utilisation efficiency

To compare the integrated and decentralised drying scenarios on an equal basis, the additional effort for drying in the decentralised scenarios needs to be taken into account. Therefore, a new overall energy utilisation efficiency has to be defined to compare all scenarios, as the gross and net efficiency, which are used to rate the power generation process, are not sufficient to evaluate a complete biomass co-firing scenario, which includes a pre-treatment process like drying.

The following figures schematically show the energies needed for power generation and biomass drying, as well as the auxiliary power demand and resulting electrical power output. The energy balance to calculate the overall energy utilisation efficiency (see Eq. 4.3) of all scenarios must include all required energy inputs and the resulting energy output.

In Figure 10, all essential energies considered in Scenario 1_a are shown. The fuel heat input by biomass $\dot{Q}_{\mathrm{bm,PG}}$, which is required for power generation, enters the energy balance and is dried prior to co-firing. As the following equations show for 10 % CFR, the fuel energy of the wet biomass $\dot{Q}_{\mathrm{bm,PG}}^{50\%\mathrm{H_2O}}$ is equivalent to the fuel energy of the dried biomass $\dot{Q}_{\mathrm{bm,PG}}^{10\%\mathrm{H2O}}$:

$$\dot{Q}_{\mathrm{bm,PG,10\%CFR}}^{50\%\mathrm{H_2O}} = \dot{m}_{\mathrm{bm,PG,10\%CFR}}^{50\%\mathrm{H_2O}} \cdot LHV_{\mathrm{bm}}^{50\%\mathrm{H_2O}} = 22.187\ \frac{kg}{s} \cdot 8.60\ \frac{MJ}{kg} = 190.8\ MW_{\mathrm{th}}, \tag{4.1}$$

$$\dot{Q}_{\mathrm{bm,PG,10\%CFR}}^{10\%\mathrm{H_2O}} = \dot{m}_{\mathrm{bm,PG,10\%CFR}}^{10\%\mathrm{H_2O}} \cdot LHV_{\mathrm{bm}}^{10\%\mathrm{H_2O}} = 12.326\ \frac{kg}{s} \cdot 15.48\ \frac{MJ}{kg} = 190.8\ MW_{\mathrm{th}}. \tag{4.2}$$

This assumption requires that the temperature of the biomass mass flow is the same when entering the drying process and when entering the power generation process. No thermal decomposition of the dried biomass must occur. The process model

Dieses Werk ist copyrightgeschützt und darf in keiner Form vervielfältigt werden noch an Dritte weitergegeben werden.
Es gilt nur für den persönlichen Gebrauch.

development and simulation analyses are carried out in a way which ensures these assumptions are met in all cases.

The numbers for the biomass mass flow for power generation with a fuel moisture content of 50 % H_2O $\dot{m}_{\mathrm{bm,PG,10\%CFR}}^{50\%H_2O}$ and for the biomass mass flow for power generation with a fuel moisture content of 10 % H_2O $\dot{m}_{\mathrm{bm,PG,10\%CFR}}^{10\%H_2O}$ are results of simulations, which are described in more detail in Chapter 7. The lower heating values of the wood chips for either 10 % fuel moisture content ($LHV_{\mathrm{bm}}^{10\%H_2O}$) or 50 % fuel moisture content ($LHV_{\mathrm{bm}}^{50\%H_2O}$) correspond to the results shown in Figure 1.

In addition to the biomass fuel heat input, the coal fuel heat input $\dot{Q}_{\mathrm{C,PG}}$ enters the energy balance. The drying process is heated by steam, extracted from the IP/LP crossover pipe in the power generation process. The occurring condensate is reintegrated in the power generation process. The electrical gross power output is reduced by the auxiliary power demand of the drying process and the auxiliary power demand of the power generation process. Only the net electrical power output $P_{\mathrm{el,PG,net}}$ is considered as energy output, leaving the energy balance limit.

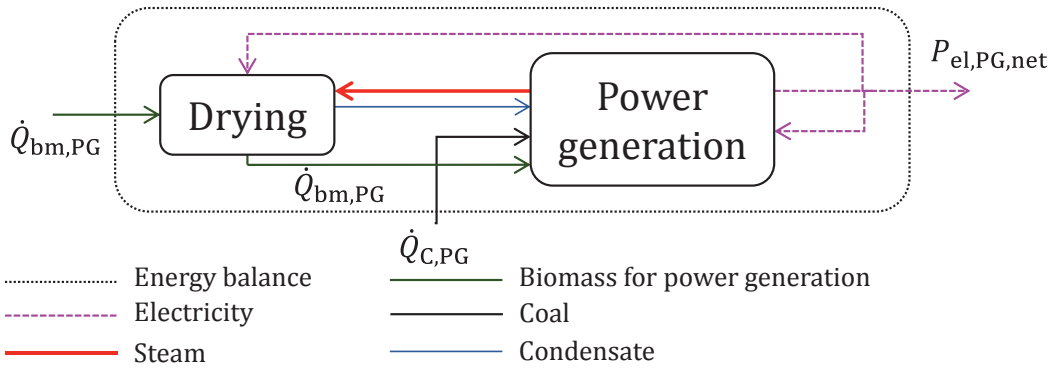

Figure 10: Energy balance for Scenario 1_a

The energies considered in Scenario 1_b are shown schematically in Figure 11. The only difference to Scenario 1_a consists in the multi-stage integration of the drying process. Drying steam is extracted from the IP/LP crossover pipe as well as from the LP turbine. The fuel heat inputs by biomass and coal remain as energy input in this energy balance. The electrical net power output remains as the only energy output in the energy balance.

Dieses Werk ist copyrightgeschützt und darf in keiner Form vervielfältigt werden noch an Dritte weitergegeben werden.
Es gilt nur für den persönlichen Gebrauch.

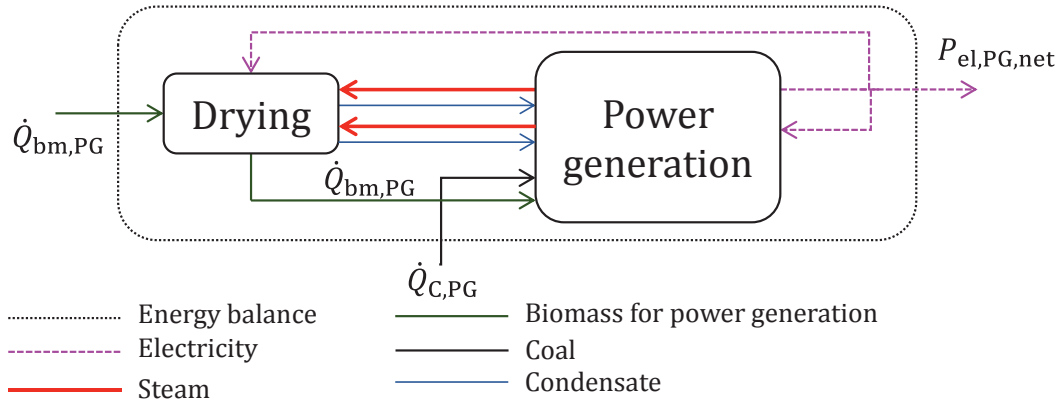

Figure 11: Energy balance for Scenario 1_b

Figure 12 shows all essential energies for biomass co-firing with coal in Scenario 2_a. As opposed to Scenario 1, the drying process is not coupled to the power generation process. A biomass fuel energy for drying $\dot{Q}_D$ is therefore required to heat the drying process in a way that ensures the desired fuel moisture content in the dried biomass is achieved and all thermal losses in the drying process are covered. This biomass fuel heat input for drying needs to be considered as input energy in the energy balance together with the fuel heat inputs by biomass and coal for power generation. Additionally, the electrical demand of the dryer $P_{el,D}$ enters the energy balance as energy input. The electrical net power generation remains as the only output energy in the energy balance for this scenario.

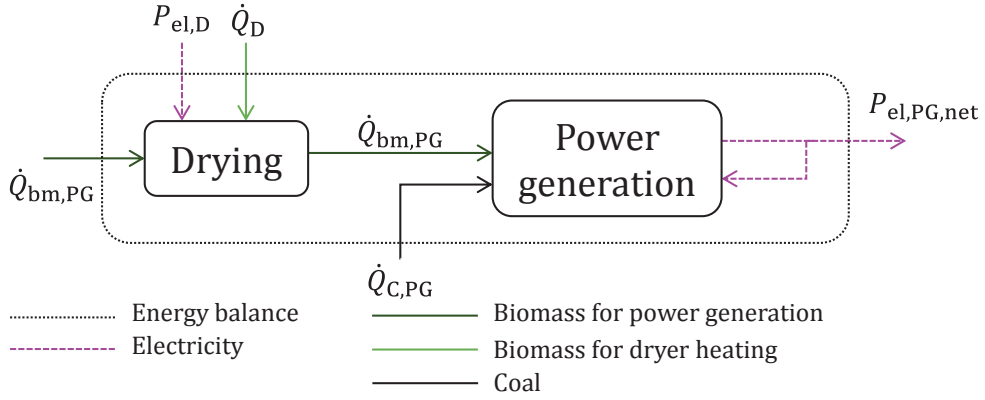

Figure 12: Energy balance for Scenario 2_a

Figure 13 shows the energies considered for Scenario 2_b. As Scenario 2_b differs from Scenario 2_a only in the energy input for drying heat supply, all other energies considered in the energy balance remain as in Scenario 2_a. Here the fuel energy required to heat the drying process is provided by oil instead of biomass.

Dieses Werk ist copyrightgeschützt und darf in keiner Form vervielfältigt werden noch an Dritte weitergegeben werden.
Es gilt nur für den persönlichen Gebrauch.

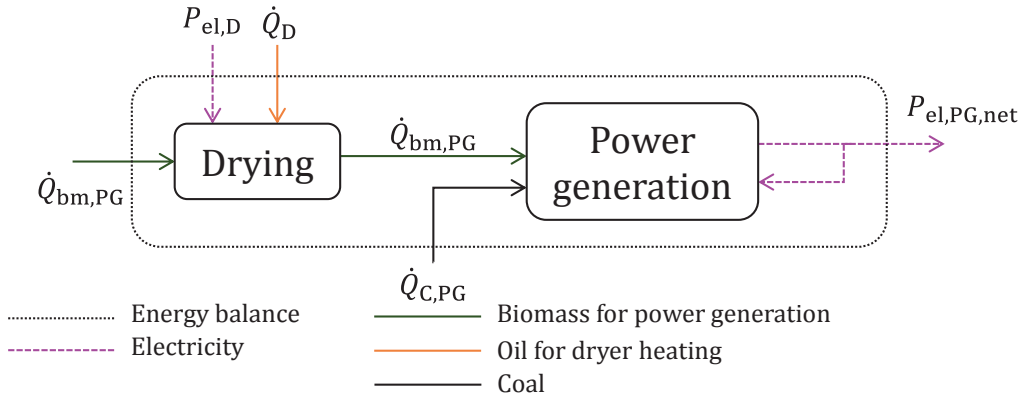

Figure 13: Energy balance for Scenario 2b

In Scenario 3 the drying process is again integrated into the power generation process. Figure 14 shows the energy balance, which is used to define the overall energy utilisation efficiency of the overall process and all essential energies. As in Scenario 1, the two fuel energy inputs by biomass and coal are considered as energy input in the energy balance and the net electrical power generation is considered as energy output. To provide the required drying heat, flue gas is extracted for the power generation process and re-integrated after usage.

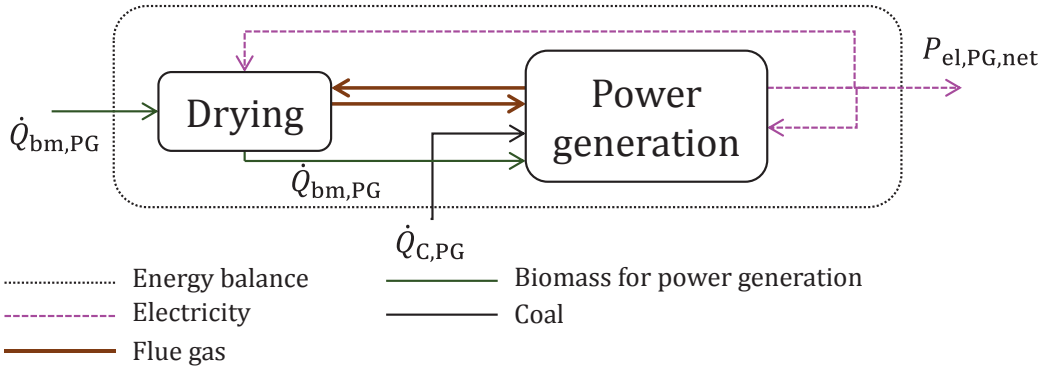

Figure 14: Energy balance for Scenario 3

An approach that allows the comparison of the integrated and decentralised drying scenarios on an equal basis, like described above, needs to consider the additional effort for drying of the decentralised scenarios. The overall energy utilisation efficiency ζ is therefore defined in Eq. 4.3 as the ratio between electrical power output and total thermal heat input:

$$\zeta = \frac{P_{el,PG,net} - P_{el,D}}{\dot{Q}_{C,PG} + \dot{Q}_{bm,PG} + \dot{Q}_D}. \quad (4.3)$$

Dieses Werk ist copyrightgeschützt und darf in keiner Form vervielfältigt werden noch an Dritte weitergegeben werden.
Es gilt nur für den persönlichen Gebrauch.

Here, the dryer's electricity consumption $P_{\mathrm{el,D}}$ is subtracted from the power generation process's net electrical power output $P_{\mathrm{el,PG,net}}$ to determine the resulting power output from the overall process. The required heat input is the sum of the fuel heat input by coal for power generation $\dot{Q}_{\mathrm{C,PG}}$, fuel heat input by biomass for power generation $\dot{Q}_{\mathrm{bm,PG}}$ and fuel heat input by oil or biomass for drying in a direct rotary dryer $\dot{Q}_{\mathrm{D}}$. The sum of $\dot{Q}_{\mathrm{C,PG}}$ and $\dot{Q}_{\mathrm{bm,PG}}$ remains constant. However, their ratio changes according to the co-firing rate.

The results of the scenario analyses in the following sections will be used to calculate the according ζ for each scenario.

Dieses Werk ist copyrightgeschützt und darf in keiner Form vervielfältigt werden noch an Dritte weitergegeben werden.
Es gilt nur für den persönlichen Gebrauch.

5 MODEL DEVELOPMENT

The software used for modelling in this work is EBSILON®*Professional,* which is widely used for simulating thermodynamic cycle processes [61] and allows system analyses for stationary processes. All the common components of a power plant system are available in the modelling software, and further components can be created by the user. During the model development process several components, such as mills and dryers, were programmed. These custom-made components allow the simulation of processes that have not as yet been analysed.

A model of the overall power generation process of a large-scale pulverised coal power plant was developed, as well as a detailed boiler model for the same power plant. Both of the previously selected dryers were modelled and, in a second stage, integrated into the power generation process. The direct rotary dryer is additionally modelled as a stand-alone variant. A detailed dryer design is neither possible nor aspired to with the developed models.

5.1 Steam power plant for biomass co-firing

The power plant model used for the direct and indirect co-firing analyses is based on an existing large-scale pulverized coal-fired power plant. To analyse the effects of biomass co-firing, a boiler model is first developed, and its results are then integrated into the power plant's overall process model in a second stage. The information necessary for modelling was provided by a utility. The coal-only case was specifically validated with regard to steam temperatures, steam pressures, net power output and net efficiency.

5.1.1 Power plant overall process modelling

The existing large-scale pulverized coal-fired power plant operates at full load with live steam conditions of 530 °C and 210 bar, and reheat steam conditions of 525 °C and 39 bar. The resulting gross power output is 827 $MW_{el,}$ with a gross efficiency of 42.92 % and a net efficiency of 39.60 %, related to LHV. The water-steam cycle and also the air and flue gas side were modelled and form the baseline for all analyses concerning the partial substitution of fossil fuel with renewable biomass [49], [62]. Figure 15 shows a simplified flowsheet of the modelled hard coal-fired steam power plant, which already includes a biomass mill. Key parameters of the process at full-load operation without co-firing of biomass (coal-only) are listed in Table 5.

Dieses Werk ist copyrightgeschützt und darf in keiner Form vervielfältigt werden noch an Dritte weitergegeben werden.
Es gilt nur für den persönlichen Gebrauch.

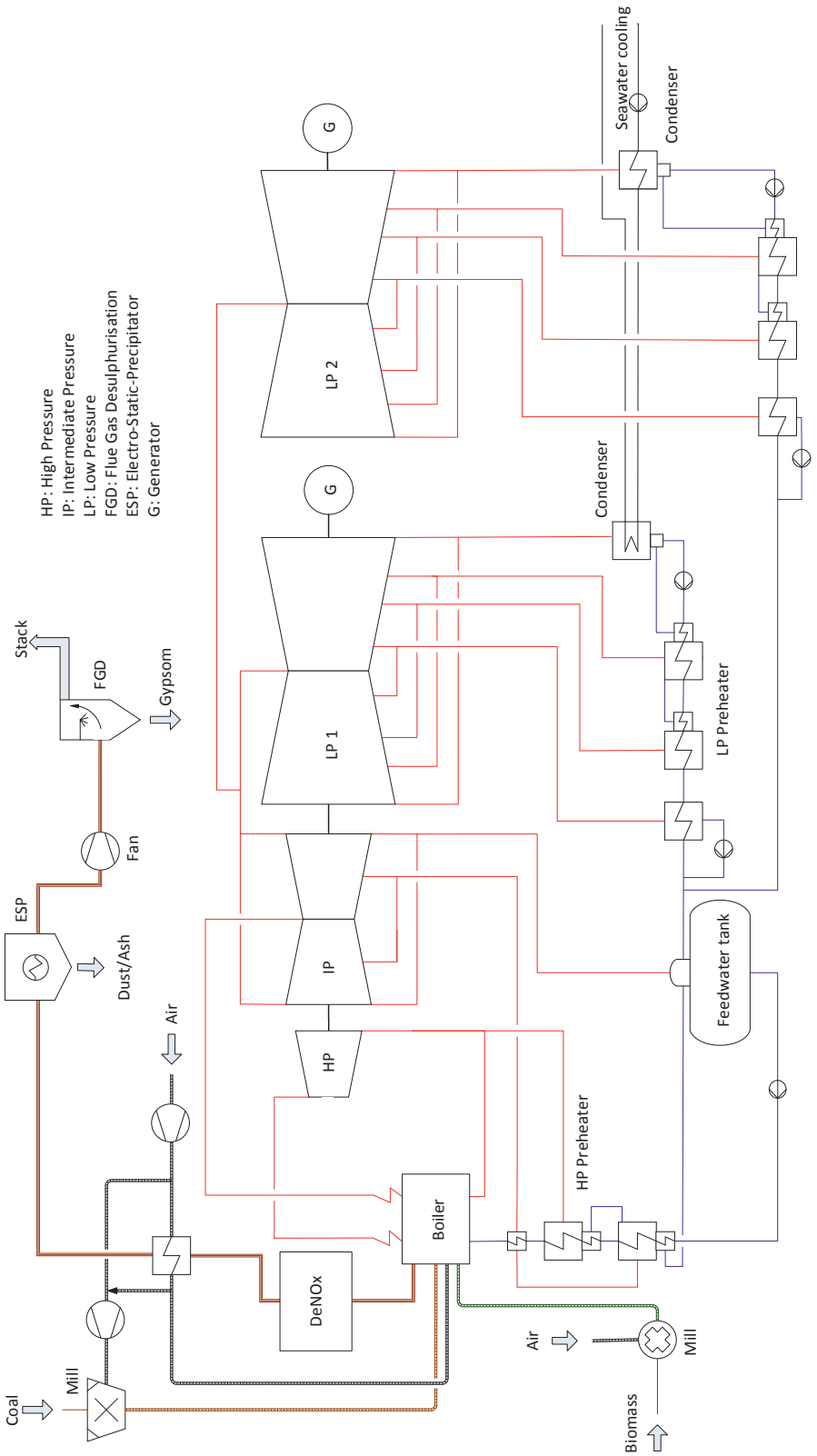

Figure 15: Simplified flowsheet of the modelled steam power plant

Dieses Werk ist copyrightgeschützt und darf in keiner Form vervielfältigt werden noch an Dritte weitergegeben werden.
Es gilt nur für den persönlichen Gebrauch.

Table 5: Key parameters of the power plant process (coal-only at full load)

Fuel heat input	1908 MW_{th}
Net power output	763 MW_{el}
Gross power output	827 MW_{el}
Net efficiency	39.60 %
Gross efficiency	42.92 %
Live steam mass flow	642 kg/s
Live steam pressure	210 bar
Live steam temperature	530 °C
Reheat steam pressure	39 bar
Reheat steam temperature	525 °C
Boiler feedwater temperature	245 °C
Condenser pressure LP1	0.087 bar
Condenser pressure LP2	0.060 bar
IP/LP crossover pressure	5.4 bar
Feedwater tank pressure	5.2 bar
Cooling water temperature LP1	21 °C
Cooling water temperature LP2	17 °C
Flue gas temperature downstream of the ECO	365 °C
Flue gas temperature downstream of the air preheater	149 °C
LHV coal (10.7 wt.-% H_2O)	25.9 MJ/kg
LHV biomass (10 wt.-% H_2O)	15.5 MJ/kg

One uncommon characteristic of this power plant is the second low-pressure turbine (LP2 in Figure 15), which was added several years after the power plant was first commissioned and therefore supplies a second generator. A second condenser and a low-pressure feedwater preheating section were also added. Low-pressure

Dieses Werk ist copyrightgeschützt und darf in keiner Form vervielfältigt werden noch an Dritte weitergegeben werden.
Es gilt nur für den persönlichen Gebrauch.

feedwater preheating is carried out in three stages, with steam extracted from the associated low-pressure turbine. High-pressure feedwater is also preheated in three stages, and is supplied by high-pressure and intermediate-pressure steam.

To reduce emissions, a selective catalytic reduction (SCR) $DeNO_x$ unit, an electrostatic precipitator (ESP) and a flue gas desulphurisation (FGD) unit are installed. To benefit from the flue gases' high temperature, the combustion air streams through the air preheater, which is located upstream of the ESP. A partial mass flow of preheated air is used to fluidise the mills and thus transports the pulverised fuels to the boiler.

Hard coal is pulverised in a vertical spindle mill. To reduce the particle size of the co-fired wood chips, a hammer mill is used. Details of the hammer mill model can be found in [63]. The following equation Eq. 5.1 for the required grinding energy E_{1-2} was developed by TEMMERMAN [64]:

$$E_{1-2} = MH\left(\frac{1}{z_2} - \frac{1}{z_1}\right) \text{ in Wh/kg.} \tag{5.1}$$

Here, the factor M is characteristic for the ground material, H is the moisture content in mass per cent, and z_2 and z_1 are the particle sizes of feed (1) and product (2) in millimetres (also see [63]). Experimental experience showed that grinding wood as fine as pulverised coal is unnecessary. Therefore, 1 mm is chosen as the product particle size. As no experimental analyses were carried out by TEMMERMAN for poplar wood chips, the resulting factor $M = 9.65$ for pine wood chips will be used for calculations in this work. According to KALTSCHMITT [2], poplar and pine are both softwoods and should therefore show similar grinding characteristics.

The lower heating value (LHV) of the hard coal usually fired in the modelled power plant is 25.9 MJ/kg. The biomass fuel considered for most co-firing analyses in this work is poplar wood chips, which have a lower heating value of 15.5 MJ/kg at a moisture content of 10 %.

Even though part-load considerations will not be part of this paper, calculations of some components cannot be carried out in nominal capacity mode. As the fuel heat input will remain constant at 1908 MW_{th}, various parameter changes will occur due to changed fuel characteristics when co-firing biomass with coal. A part-load calculation mode is therefore chosen for all components of the baseline process, whereas new components, which are added for co-firing or fuel pre-treatment, are set to calculate in nominal capacity mode during simulations.

Dieses Werk ist copyrightgeschützt und darf in keiner Form vervielfältigt werden noch an Dritte weitergegeben werden.
Es gilt nur für den persönlichen Gebrauch.

5.1.2 Boiler modelling

The boiler in this power plant is a once-through steam generator with a boiler efficiency of 95 % at full load (coal-only). A separate boiler model containing all heating surfaces was designed, and a simplified flowsheet is shown in Figure 16. Radiation heat transfer in the furnace is modelled in two steps, followed by nine convective heating surfaces for superheating (SH1–SH5B). Steam reheating is realised by three convective heating surfaces (RH1–RH2). The remaining heat in the flue gas mass flow downstream of the reheat surface RH1A is used to warm up the feedwater mass flow in the economizer (ECO).

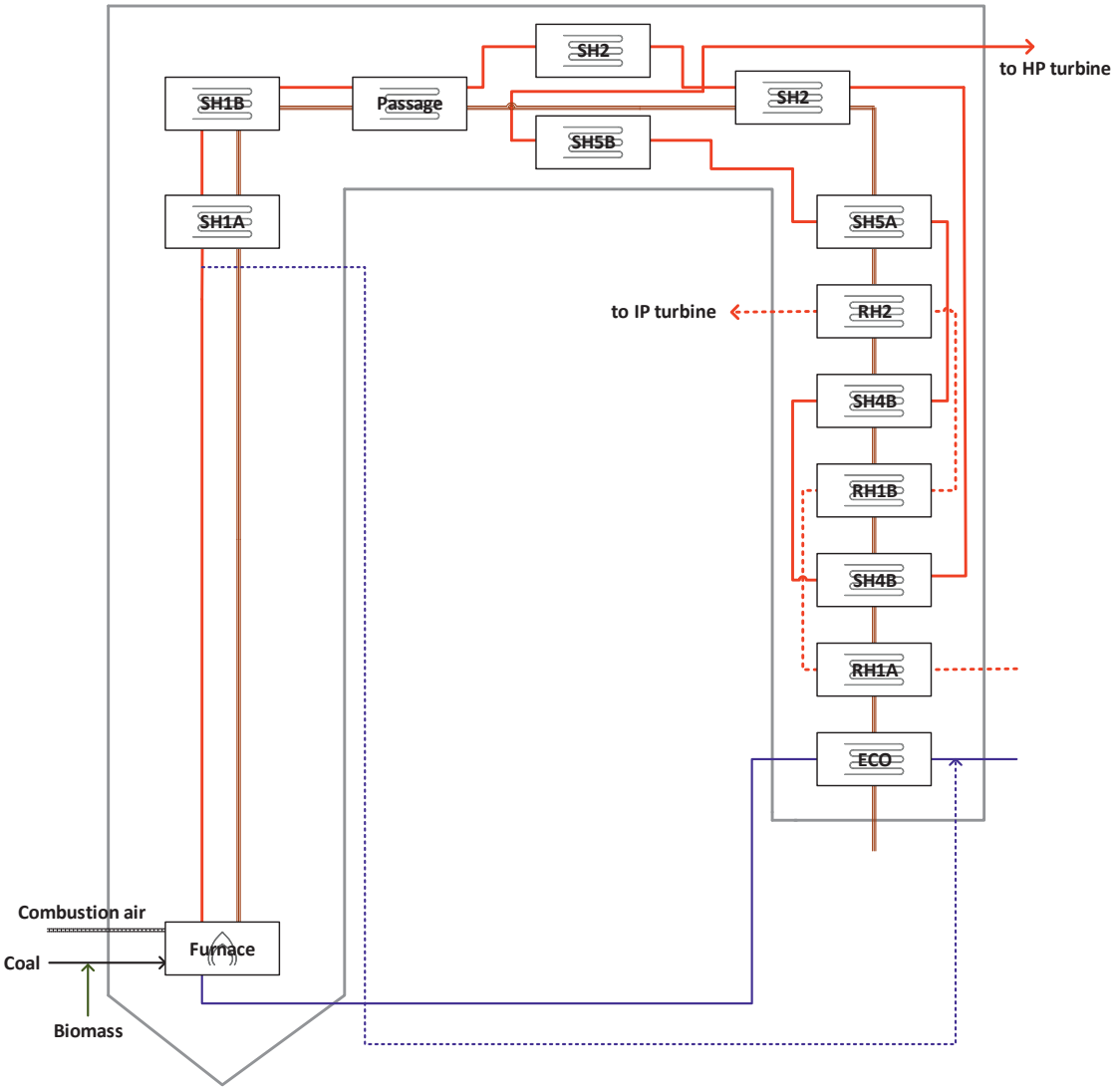

Figure 16: Simplified flowsheet of the boiler model

Dieses Werk ist copyrightgeschützt und darf in keiner Form vervielfältigt werden noch an Dritte weitergegeben werden.
Es gilt nur für den persönlichen Gebrauch.

With the regular coal-only combustion case forming the baseline of simulations, the co-firing rate (CFR) can be varied by substituting the according fuel heat input share with poplar wood. In simulations, the total fuel heat input will remain constant, with the combustion air mass flow being adjusted to the changed minimum air demand, while the amount of excess air also remains constant. Based on practical experience, the flue gas furnace end temperature and the live steam temperature are also assumed to remain constant for all co-firing rates.

The boiler model's simulation results show shifts in the following key process parameters:

- live steam mass flow
- reheat steam temperature
- flue gas temperature downstream of the ECO

After analysing the impacts of biomass co-firing on the boiler, these results are integrated into the power plant's overall process model.

5.2 Indirect steam-tube dryer

As described in Chapter 3.2, an indirect steam-tube dryer requires saturated or slightly superheated steam as a heating medium, which is condensed in tubes transferring the required heat demand to the wood chips. The calculation of the required heat demand and the model layout will be described in the following section.

5.2.1 Dryer modelling

The mass flows in the dryer modelled in this work are shown schematically in Figure 17. After condensing in the heating tubes, the water exits the dryer. Wet biomass enters the dryer on one side and is transported by gravity and rotation, as the dryer is set up to have a small slope. The dry biomass exits the dryer on the opposite side, with an exit temperature of about 70 °C.

To transport the exhaust vapours, air is used. The ventilation air mass flow needs to be sufficient to ensure a relative humidity of less than 100 % in the exit mass flow. The ratio of ventilation air mass flow to raw biomass mass flow is described by the ventilation ratio Φ (kg_{air}/kg_{bm}). As the air mass flow needs to be heated up from an inlet temperature of 15 °C, an optimal air to biomass ratio Φ needs to be found to minimize the required heating demand [49].

Dieses Werk ist copyrightgeschützt und darf in keiner Form vervielfältigt werden noch an Dritte weitergegeben werden.
Es gilt nur für den persönlichen Gebrauch.

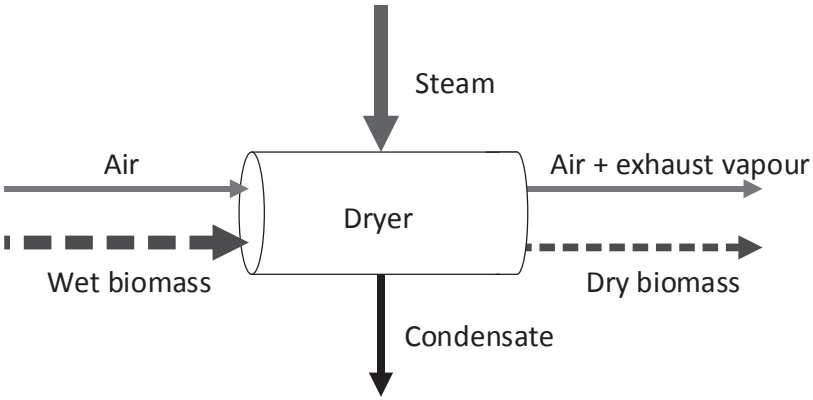

Figure 17: Considered feed and product mass flows of an indirect steam-tube dryer for drying biomass [49]

The required absolute heating duty depends on the feed-biomass mass flow, the raw-biomass moisture content and the desired moisture content of the dried product biomass mass flow. The specific heating duty per kilogram of evaporated water requires the energy for the following actions:

- heating up the feed mass flow including
  - dry matter
  - fuel moisture
- heating up the ventilation air mass flow
- evaporating fuel moisture
- overcoming binding energy

The specific heat of dry wood is calculated according to the empirical equation Eq. 5.2 developed by DUNLAP [65]:

$$c_{\mathrm{w,db}} = 1.114 + 0.00486 \cdot T_{\mathrm{w,m}} \text{ in kJ/kgK.} \quad (5.2)$$

Here, $T_{\mathrm{w,m}}$ is the arithmetic mean value of the solid's temperature when entering the dryer and the solid's temperature when leaving the dryer in °C.

The binding energy specifies the energy necessary for the transportation of moisture to the surface of a wood particle. FORTUIN [66] identified the following empirical equation (Eq. 5.3) as suitable for estimating the binding enthalpy of water in woody biomass:

$$h_{\mathrm{bind}}(u) = 74{,}68 - \frac{4{,}1868 \cdot 22 \cdot \mathrm{u}}{0{,}07 + \mathrm{u}} \text{ in kJ/kg}_{\mathrm{dm.}} \quad (5.3)$$

Dieses Werk ist copyrightgeschützt und darf in keiner Form vervielfältigt werden noch an Dritte weitergegeben werden.
Es gilt nur für den persönlichen Gebrauch.

Here, *u* is the amount of water per dry matter. Special attention needs to be paid to the specific binding enthalpy as it refers to the dry matter. All other specific enthalpies refer to the mass of evaporated water.

Additionally, a thermal loss of 6 % of the total heat demand is assumed, and the dryer's electrical power consumption is set to 115 kW/kg_{H2Oev} for all drying scenarios [67]. The dried poplar wood chips leave the dryer with a temperature of 70 °C while the temperature of ventilation air and exhaust vapour mass flow is typically 15 K higher [67]. All the important modelling parameters are listed in Table 6. The required ventilation ratio was determined by simulations and ensures a sufficient difference from the ventilation air dew point temperature, as condensation of exhaust vapours should be avoided.

Table 6: Modelling parameters for the indirect steam-tube dryer

Ventilation ratio	1.606	
Temperature of solids leaving the dryer	70 °C	[67]
Temperature of gases leaving the dryer	85 °C	[59]
Electrical demand per kilogram evaporated water	115 kW	[67]
Thermal loss relative to total heat demand	6 %	[67]
Ambient air temperature	15 °C	
Temperature difference condensate to dew point	-2 K	
Condensate pressure loss in dryer	100 mbar	
Ventilation air pressure loss	50 mbar	

5.2.2 Integration into the power plant process

The steam required to cover the dryer's heating duty can be provided by the power plant's water-steam cycle. When integrating the drying process into the water-steam cycle, the right position for steam extraction needs to be identified. Two variations will be analysed:

- drying steam extracted from the IP/LP crossover pipe
- drying steam extracted from both IP/LP crossover pipe and LP turbine

All variations are described in the following section.

Dieses Werk ist copyrightgeschützt und darf in keiner Form vervielfältigt werden noch an Dritte weitergegeben werden.
Es gilt nur für den persönlichen Gebrauch.

Drying steam extracted from IP/LP crossover pipe

For an effective drying process, a condensation temperature of around 140 °C is required, which corresponds to a saturated steam pressure of 3.615 bar. The initial IP/LP crossover pressure is 5.4 bar and is thereby suitable for providing the steam for the dryer. The required steam mass flow is extracted from the IP/LP crossover pipe, condensed while drying wood chips and reintegrated into the low-pressure feedwater preheating section. Figure 18 shows a simplified flow chart of the power plant's water-steam cycle, with the integrated biomass dryer described above. The steam pressure losses occurring in the connecting pipe between steam extraction and dryer are 10 %, relative to the initial steam pressure.

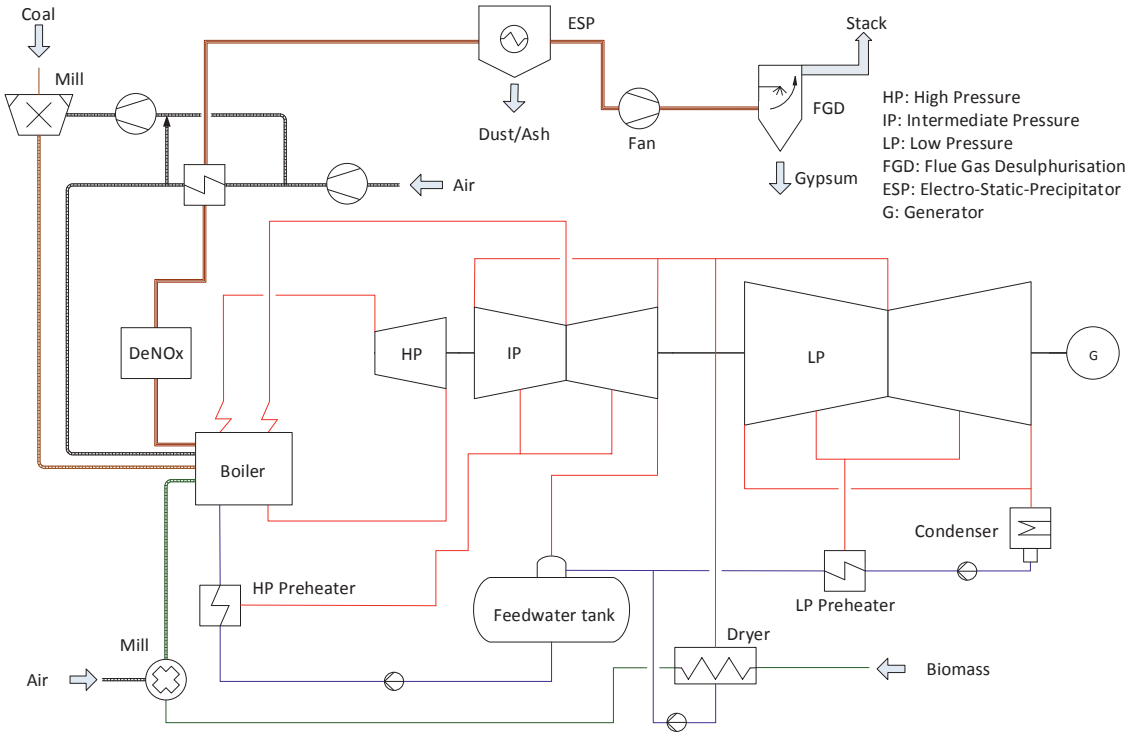

Figure 18: Indirect steam-tube dryer integrated into the power plant process – drying steam is extracted from the IP/LP crossover pipe

The steam temperature after extraction is still above 250 °C. To reduce the steam temperature, dryer condensate is recycled and injected into the superheated steam until a temperature approach of 10 K to saturated steam temperature is reached in front of the dryer.

For optimal efficiency at full-load operation, the condensate downstream of the dryer is returned into the preheating section at the point where the feedwater

Dieses Werk ist copyrightgeschützt und darf in keiner Form vervielfältigt werden noch an Dritte weitergegeben werden.
Es gilt nur für den persönlichen Gebrauch.

temperature is most similar; this is the case directly upstream of the feedwater tank, where the condensate temperature is 120 °C. A pump is used to overcome the pressure difference between drying condensate and low-pressure feedwater.

Drying steam extracted from both IP/LP crossover pipe and LP turbine

In this variation, a combined steam-tube dryer with two heating zones is used. The first dryer half is heated with steam extracted from the LP turbine, and the second is heated with steam extracted from the IP/LP crossover pipe. With this design, the advantage of a shortened retention time can be combined with the usage of lower quality steam. A larger share of the steam mass flow can be used for power generation in the LP turbines and is extracted afterwards for drying at a lower temperature level. Thus, efficiency losses in the power generation process can be reduced. The steam pressure of the LP turbine extraction is initially 2.3 bar, which corresponds to a condensation temperature of 125 °C. According to the reference coal-only process, the initial steam pressure in the IP/LP crossover extraction is 5.4 bar, which corresponds to a condensation temperature of 155 °C.

Figure 19 shows how a steam-tube dryer provided with two qualities of drying steam, as described above, is integrated into the power plant's water-steam cycle. Steam extraction and condensate reintegration for the higher pressure level is realised in the same way as before. The additional condensate, which is on a lower pressure level, is reintegrated at the same location, upstream of the feedwater tank. A pump is used to overcome the occurring pressure differences.

Dieses Werk ist copyrightgeschützt und darf in keiner Form vervielfältigt werden noch an Dritte weitergegeben werden.
Es gilt nur für den persönlichen Gebrauch.

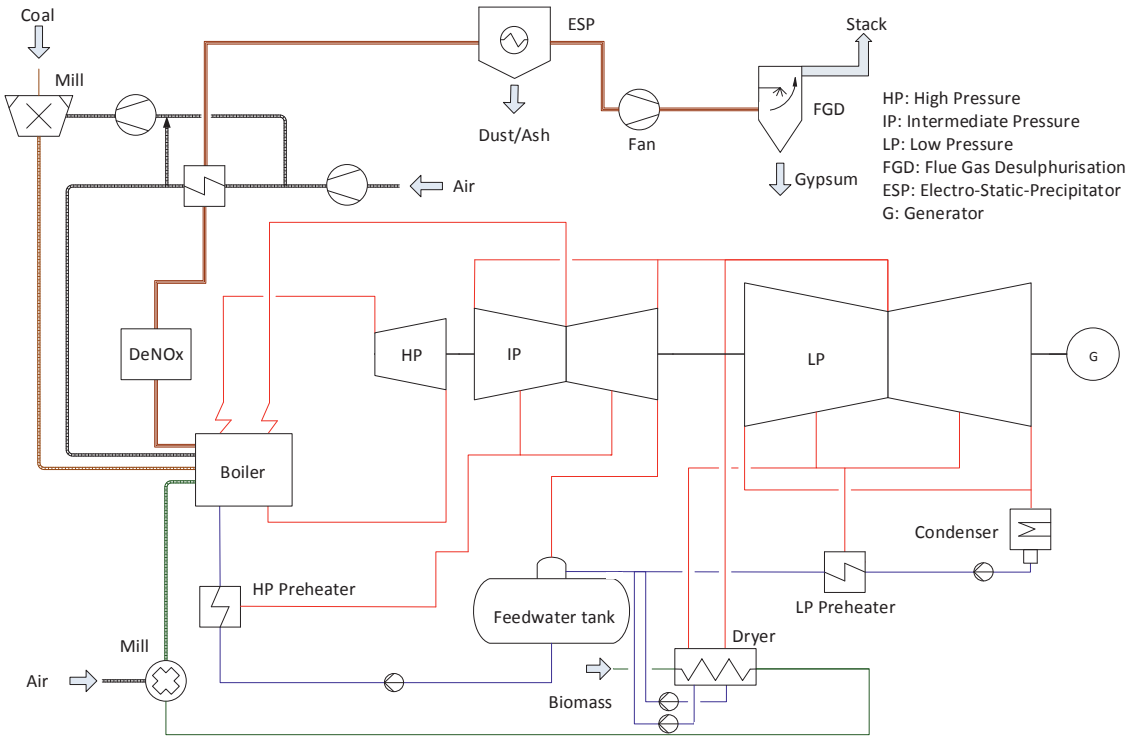

Figure 19: Indirect steam-tube dryer integrated in the power plant process – drying steam is extracted from the IP/LP crossover pipe and the LP turbine

The two integration variations are compared and evaluated in the drying scenario analyses in Chapter 6. In both variations, further process improvement should be possible by ventilation air heat integration.

Ventilation air heat integration

The evaporated moisture mass flow needs to be transported out of the dryer by a ventilation air mass flow. Further heat integration using this humid air mass flow is beneficial, regarding the efficiency of the power plant process. The dryer's ventilation ratio is set in such a way that the temperature difference to the dew point temperature is 15 K. Due to the high relative humidity in the air mass flow, a heat potential exists not only in sensible heat, which is determined by the air temperature, but also in latent heat, which can be used by condensing the exhaust vapours.

Firstly, the maximal theoretical potential of heat integration for low-pressure feedwater preheating by ventilation air heat integration is determined. To maximise the effect of heat integration, the air heat exchangers (AHE1+AHE2) are located upstream of the low-pressure feedwater preheater with the greatest heating steam

Dieses Werk ist copyrightgeschützt und darf in keiner Form vervielfältigt werden noch an Dritte weitergegeben werden.
Es gilt nur für den persönlichen Gebrauch.

demand. Placing the air heat exchangers right downstream of the condensers would cause a partial evaporation of condensate in the first supercooler located downstream of the according low pressure preheater (LPPH2.1 or LPPH1.1). Therefore, the air heat exchangers AHE1 and AHE2 have to be placed downstream of the low pressure preheaters LPPH1.1 and LPPH 2.1, respectively. As the low pressure feedwater temperature is increased by only 2 K by either LPPH1.1 or LPPH2.1, the resulting loss in heat integration potential is small. Figure 20 shows how AHE1 and AHE2 are integrated into the low-pressure preheating sections.

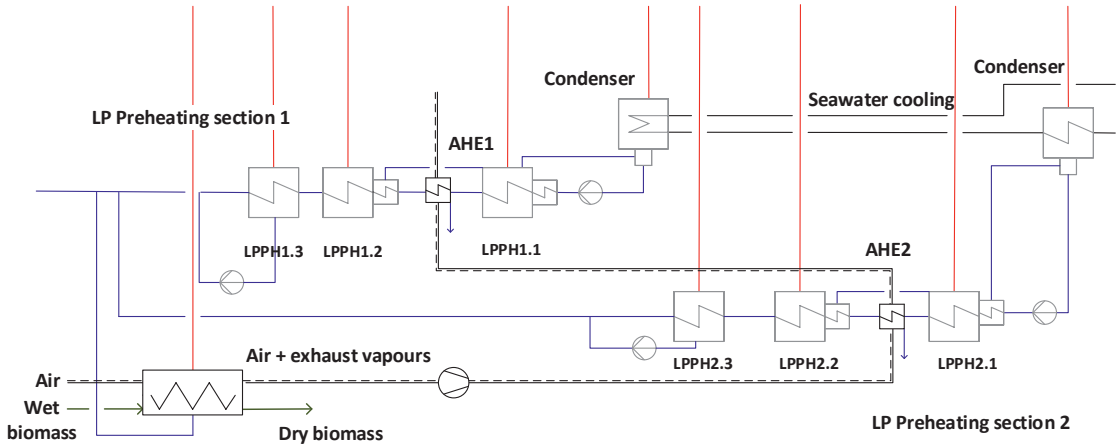

Figure 20: Heat integration of ventilation air and exhaust vapours – theoretical evaluation of potential for low-pressure feedwater preheating

All the components added for heat integration are set to operate in nominal capacity mode. Disregarding aspects of technical realisation, the air heat exchangers are set to calculate an ideal heat transfer in order to identify the maximal theoretical potential of low-pressure feedwater preheating. The air heat exchangers therefore determine the heat transfer according to a method which calculates the resulting air and low-pressure feedwater temperatures based on a given heat transfer efficiency of 100 %, while respecting a given minimum terminal temperature difference of 5 K. The heat integration regarding the share of heat transfer in AHE1 and AHE2 will be optimised by simulation during the drying scenario analyses.

The ventilation air heat integration is considered in more technical detail in two variations:

- Variation A – low-pressure feedwater preheating with an additional heat transfer cycle
- Variation B – ventilation air preheating

Dieses Werk ist copyrightgeschützt und darf in keiner Form vervielfältigt werden noch an Dritte weitergegeben werden.
Es gilt nur für den persönlichen Gebrauch.

A direct air-to-low-pressure feedwater heat transfer, as described above, would face many difficulties in technical realisation. For a start, the low-pressure feedwater heaters are located directly under the low-pressure steam turbine, which leaves little room for channels carrying high volume air flows. Also, the air heat exchangers would have to be designed for latent heat exchange, which would require plastic components due to the formation of condensate. As the ventilation air is likely to carry small wood particles out of the dryer, it is also recommendable to place a small ESP or bag filter unit downstream of the dryer. Otherwise, any condensate occurring will also contain particles and will therefore be more difficult to handle in any disposal processes.

Figure 21 shows the process flowsheet for Variation A, which includes examples of resulting temperatures. In Chapter 7.1.2 these will be analysed in more detail. An additional heat transfer cycle is modelled for low-pressure feedwater preheating. An air-to-water heat exchanger is placed in the ventilation air mass flow. A terminal temperature difference of 25 K is assumed to model the heat transfer between ventilation air and water. For the heat transfer in the low-pressure feedwater preheater (LPFWPH), a terminal temperature difference of 5 K is assumed.

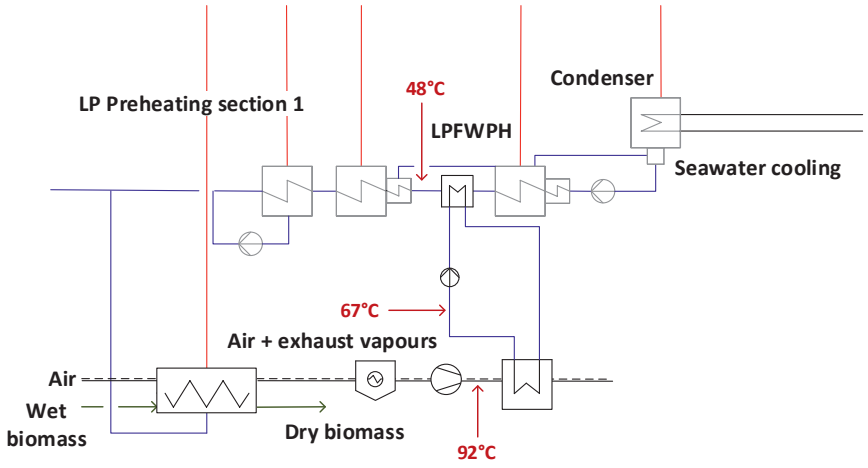

Figure 21: Heat integration of ventilation air and exhaust vapours – Variation A

Another option, which might require less constructional effort, is considered in Variation B. Figure 22 shows the relevant process flowsheet. Again, examples of the resulting temperatures, which will be regarded in detail in Chapter 7.1.2, are shown as well. The ventilation air enters the process with an ambient air temperature of 15 °C. Heating up the ventilation air is part of the total heat demand for drying. This can be reduced by installing a ventilation air preheater (VAPH).

Dieses Werk ist copyrightgeschützt und darf in keiner Form vervielfältigt werden noch an Dritte weitergegeben werden.
Es gilt nur für den persönlichen Gebrauch.

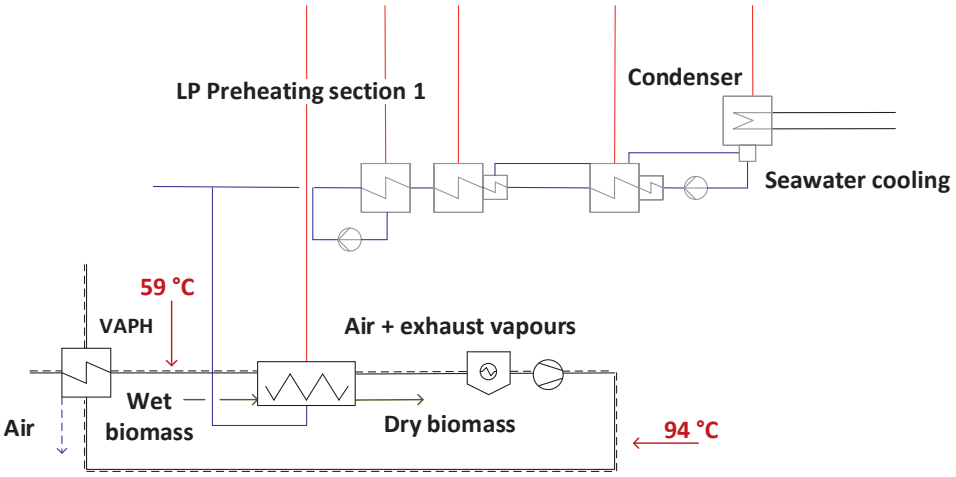

Figure 22: Heat integration of ventilation air and exhaust vapours – Variation B

To reduce the share of fine particles in the ventilation air mass flow, a small ESP unit is recommendable, as in Variation A. Depending on the ventilation air dew point temperature and the terminal temperature difference, the exhaust vapours will condense in the ventilation air preheater. This is the desired reaction, as most of the ventilation air's heat potential is present as latent heat potential. The terminal temperature difference in the VAPH is assumed to be 35 K.

Both ventilation air integration variations and their resulting effects on the power generation process will be analysed in Chapter 7.1.

5.3 Direct rotary dryer

A direct rotary dryer uses flue gas as a drying medium. Unlike the indirect steam-tube dryer, this allows a comparatively easy realisation of a stand-alone dryer alternatively to an integrated drying process. Both variations of direct rotary drying are modelled and compared below in different drying scenarios.

5.3.1 Dryer modelling

The feed and product mass flows considered in the dryer model are shown in Figure 23. Flue gas enters the dryer and the energy necessary for drying is transferred to the particles by convective heat transfer; evaporated water increases the water vapour partial pressure in the drying gas.

Dieses Werk ist copyrightgeschützt und darf in keiner Form vervielfältigt werden noch an Dritte weitergegeben werden.
Es gilt nur für den persönlichen Gebrauch.

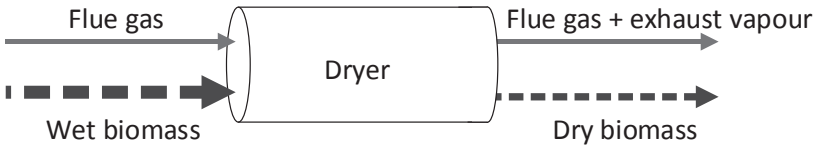

Figure 23: Feed and product mass flows of a direct rotary dryer

Starting with a certain incoming moisture content in the wet biomass, the dryer model calculates the resulting moisture content in the dried biomass, which will depend on the heat input from the drying gas [62]. The energy balance includes all the aspects necessary to determine the required drying heat demand:

- warming up of the dry biomass
- warming up of all water contained in the biomass
- energy necessary for overcoming binding energy
- evaporation and overheating of evaporated water
- direct heat losses of the dryer

Heat capacity of dry biomass and binding energy are calculated according to Eq. 5.2 and Eq. 5.3, in the same way as in the indirect steam-tube dryer model.

Some of the largest direct rotary dryers that are industrially available have an operation range that meets the requirements of a biomass mass flow corresponding to 10 % CFR, with an inlet moisture content of 50 % and a product moisture content of 10 % [68]. Therefore, a dryer model was developed which was designed to process a fixed biomass mass flow of 11 kg_{dm}/s. Depending on the detailed dryer design and the reachable volumetric heat transfer coefficient, the dimensions of such a dryer would be 6.5–7 m in diameter and 25–30 m in length [68]. When considering higher co-firing rates, the number of dryers should be multiplied accordingly.

Heat losses depend on the dryer surface area and temperature, as well as the mean temperature inside the dryer and the surrounding temperature. They are determined to be 788.65 W/m^2, according to KONIDIS [59]. The electrical demand for turning the dryer is 450 kW [68]. The drying gases' pressure loss while passing through the dryer shell is estimated to be 30 mbar [59]. The volumetric heat transfer coefficient is assumed to be 275 W/m^3 [68], [59].

Dieses Werk ist copyrightgeschützt und darf in keiner Form vervielfältigt werden noch an Dritte weitergegeben werden.
Es gilt nur für den persönlichen Gebrauch.

5.3.2 Stand-alone dryer

In the stand-alone variation, the drying gas necessary to heat the direct rotary dryer is flue gas from a combustion chamber. Usually, the fuel combustion serves solely to cover the dryer's heat duty, and no further heat utilising units are on-site. Figure 24 shows the process flowsheet of the modelled dryer [62]. Here, wet biomass is used as fuel in a stoker-fired furnace, but other fuels can also be used for heat generation (see Chapter 7).

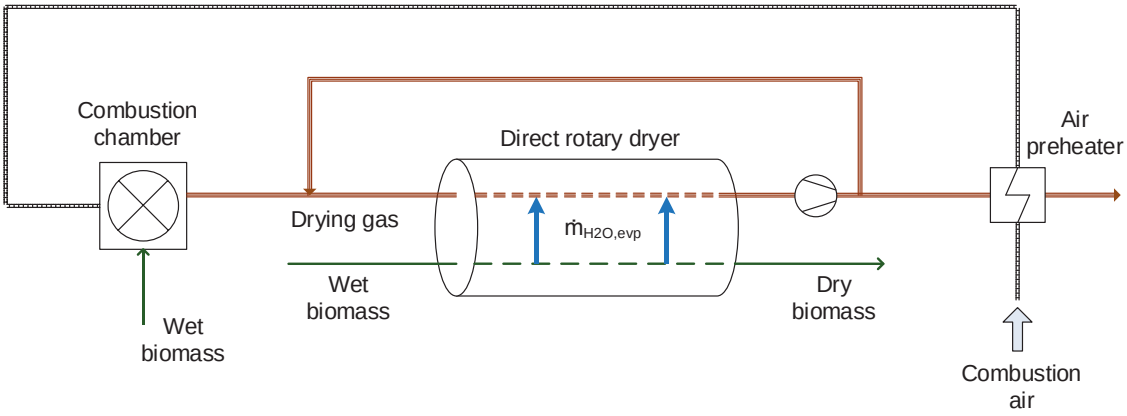

Figure 24: Process flow sheet of the stand-alone direct rotary dryer

Upstream of the combustion chamber, the combustion air is preheated using energy still contained in the dryer's exhaust gases. This increases the efficiency of the overall drying process by reducing the fuel demand. The influence of the air preheater's terminal temperature difference on the total heat demand of the process is evaluated in Chapter 7. The resulting flue gases have to be cooled down to the desired temperature at the entrance of the dryer by being mixed with the partially recycled mass flow of the dryer's exhaust gases. To keep the risk of wood particle ignition at a minimum and limit undesired torrefaction reactions, the maximum drying gas temperature at the dryer inlet is limited. Also, the oxygen content in the drying gas must not exceed 10 % [55].

The drying gas mass flow and the wet biomass mass flow enter the dryer, and the desired amount of fuel moisture evaporates. The cooled-down drying gas and the dried biomass leave the dryer. Fans are required to overcome pressure losses in the dryer and the cyclones, which are necessary for reducing particle emissions. Table 7 contains further parameters and boundary conditions used for modelling the stand-alone direct rotary dryer. During the drying process, the wood chips are heated up to 80 °C [68]. A higher particle temperature should be avoided, not only

Dieses Werk ist copyrightgeschützt und darf in keiner Form vervielfältigt werden noch an Dritte weitergegeben werden.
Es gilt nur für den persönlichen Gebrauch.

for safety reasons but also to avoid volatile organic compound (VOC) emissions caused by degradation of the biomass due to high temperatures.

Table 7: Modelling parameters and boundary conditions of a stand-alone direct rotary dryer

Excess air ratio in combustion chamber	2.0	[4]
Ambient air temperature	15 °C	
Electrical demand for dryer turning	450 kW	[68]
Pressure loss in dryer	30 mbar	[59]
Pressure loss in cyclones	20 mbar	[69]
Minimum exhaust gas temperature downstream of the dryer	105 °C	[68]
Temperature of dried biomass	80 °C	[68]
Terminal temperature difference in air preheater	35 K	

The resulting biomass moisture content is determined depending on the incoming drying gas heat flow and the set drying gas exhaust temperature. The result for the required heat input is thereby not only dependent on the drying gas temperature and mass flow but also on the drying gas composition and resulting heat capacity [62]. The dryer's heat demand also depends on the exhaust gas temperature, which should be chosen with consideration of the fact that condensation of evaporated moisture on biomass particles or other surfaces in the dryer must be avoided [68].

5.3.3 Integration of a direct rotary dryer into the power plant

The direct rotary dryer can also be heated with flue gas from the power plant process. To do this, flue gas has to be first extracted from the flue gas track and reintegrated after passing through the dryer. The dryer model itself remains unchanged and is integrated into the power plant process. As can be seen in [62], the dryer inlet temperature should be as high as possible to enable efficient drying. The highest available flue gas temperature is found downstream of the SCR. A partial flue gas mass flow is extracted here, flows through the dryer and is reintegrated upstream of the electrostatic precipitator (ESP). By doing this, fine particle emissions can be minimised as the dryer's exhaust gas is led through the power plant's flue gas cleaning track. Figure 25 illustrates the schematic integration of a

Dieses Werk ist copyrightgeschützt und darf in keiner Form vervielfältigt werden noch an Dritte weitergegeben werden.
Es gilt nur für den persönlichen Gebrauch.

rotating drum dryer into a steam power plant's flue gas side. Impairments are expected, as the flue gas extracted for drying cannot serve for air preheating anymore. To balance declining performance in the air preheater, operation of the steam air heater will be necessary to ensure the required minimum medium temperature in the air preheater. A fan is necessary to overcome the pressure loss in the dryer and to balance the pressure difference between the dryer exhaust gas and the flue gas upstream of the ESP.

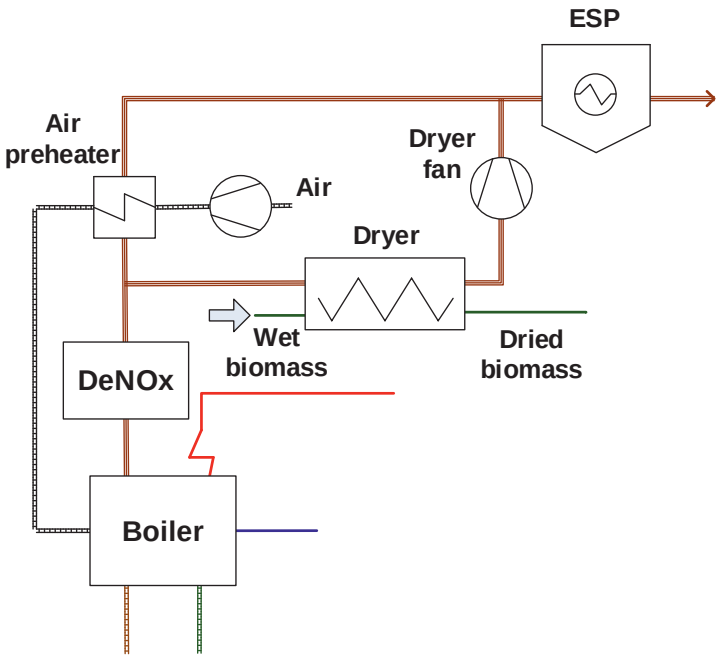

Figure 25: Process flow sheet of the integrated direct rotary dryer

The dried biomass mass flow corresponds to the co-firing rate. As in the stand-alone model, the wood chips are dried to 10 % moisture and leave the dryer with a temperature of 80 °C. The drying gas temperature at dryer inlet is 360 °C; the required flue gas mass flow depends on the co-firing rate. The dryer's exhaust gas temperature is not fixed and variations will be part of the analyses in Chapter 7.

Dieses Werk ist copyrightgeschützt und darf in keiner Form vervielfältigt werden noch an Dritte weitergegeben werden.
Es gilt nur für den persönlichen Gebrauch.

6 EFFECTS OF BIOMASS CO-FIRING ON THE POWER GENERATION PROCESS

The effects of substituting a certain share of fuel heat input by biomass in a usually coal-fired steam power plant will be analysed in the following sections. Firstly, a close look will be taken at the boiler and the development of its output parameters. These are then integrated into the overall process model to gain more general insight on the effects of biomass co-firing on the power generation process.

Unless otherwise stated, only direct co-firing of poplar wood chips with a moisture content of 10 % will be considered in this chapter.

6.1 Effects on the boiler

According to SAMI [10], co-firing approximately 10–15 % wood with coal results in a decrease in boiler efficiency of less than 1.5 % relative to coal-only operation. This suggests that only small effects on the boiler should be expected due to co-firing. To confirm this, simulation results from the boiler model described in Chapter 5.1.2 were analysed. The co-firing rate (CFR) is raised in steps from 0 % to 50 %, based on fuel heat input.

Due to its composition, wood differs from coal in its combustion characteristics. As Table 2 shows, wood generally has a lower carbon content and a significantly higher oxygen content than coal. Figure 26 shows the changes that occur in adiabatic flame temperature and flue gas mass flow for co-firing rates up to 50 %. The decline in adiabatic flame temperature is a result of the decreasing mean calorific value of the incoming fuel mass flow with increasing CFR. The adiabatic flame temperature is 2053 °C for coal-only combustion, and would be 1938 °C if only wood chips with a moisture content of 10 % were used as fuel. Another consequence of the altered fuel composition is a change in minimum air demand per kilogram of fuel. In the coal-only case, 9.57 kg_{air}/kg_{fuel} are required as the minimum air demand. Due to poplar wood chips' high oxygen content and thus resulting low carbon and hydrogen content, this demand is reduced to 6.64 kg_{air}/kg_{fuel} for 50 % CFR. However, due to the significantly lower LHV of poplar wood chips, the resulting increase in total fuel mass flow outbalances the decline in combustion air demand. So, following the mass balance, the flue gas mass flow grows with increasing CFR. As the flue gas temperature declines and the flue gas mass flow increases with biomass co-firing,

Dieses Werk ist copyrightgeschützt und darf in keiner Form vervielfältigt werden noch an Dritte weitergegeben werden.
Es gilt nur für den persönlichen Gebrauch.

the heat transfer in the boiler is affected accordingly. The resulting changes in heat flows in all boiler heating surfaces are shown in Figure 27.

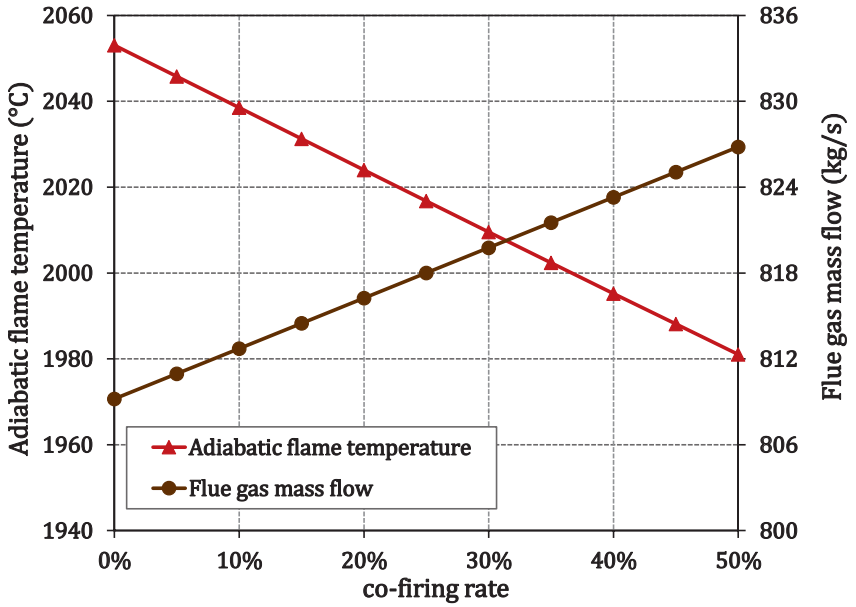

Figure 26: Changes in adiabatic flame temperature and flue gas mass flow when co-firing poplar wood chips (10 % H_2O) with hard coal, in relation to the co-firing rate

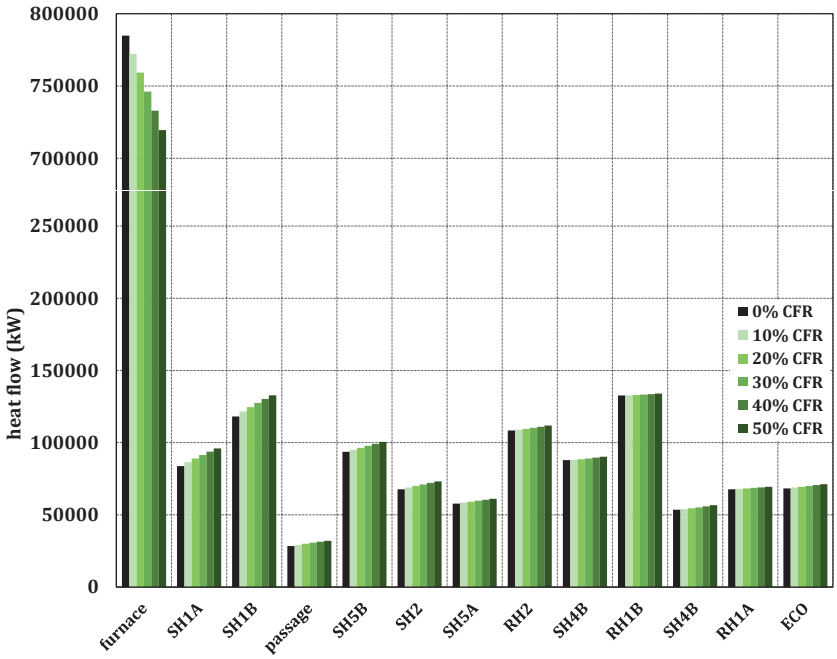

Figure 27: Heat flow changes in all boiler heating surfaces when co-firing poplar wood chips with 10 % fuel moisture content, in relation to the co-firing rate

Dieses Werk ist copyrightgeschützt und darf in keiner Form vervielfältigt werden noch an Dritte weitergegeben werden.
Es gilt nur für den persönlichen Gebrauch.

The reduced flue gas temperature causes a decline in radiation heat transfer in the furnace, where the largest amount of heat is transferred from the flue gas to the water-steam side of the power generation process. On the other hand, the increased flue gas mass flow improves heat transfer in the convective heating surfaces. This effect is clearest for the superheaters 1A and 1B (see Figure 27) and loses intensity for heating surfaces located further downstream.

Nevertheless, the decline in radiation heat transfer which occurs with increasing CFR cannot be outbalanced by an improved convective heat transfer. To maintain a constant live steam temperature, the live steam mass flow has to be adjusted and slowly declines with higher CFR (see Figure 29). The resulting steam heat output for live steam and reheat steam is shown in Figure 28, together with the resulting live steam heat output for co-firing poplar wood chips with a moisture content of 20 %.

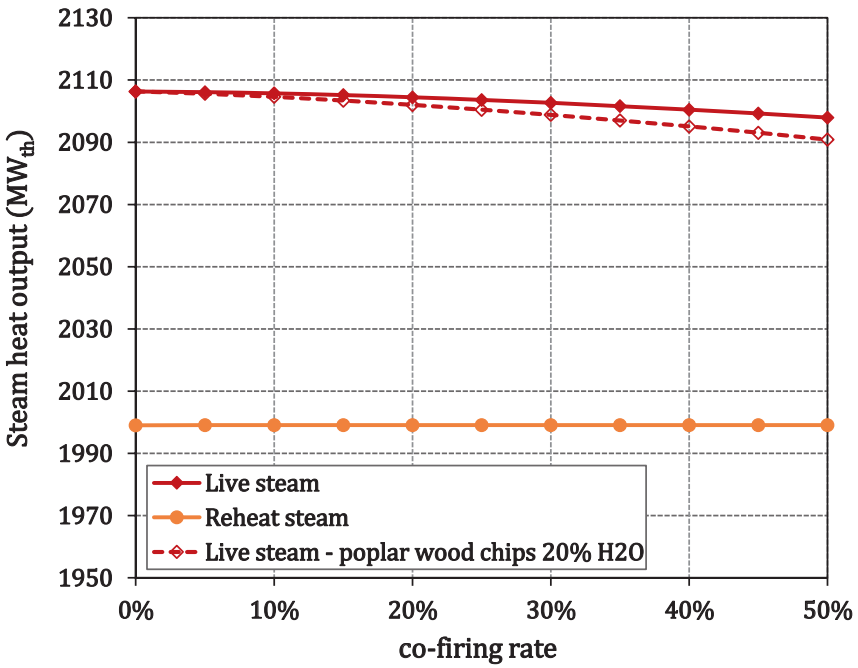

Figure 28: Changes in live and reheat steam heat output in relation to the co-firing rate

While the live steam heat output slightly declines, the reheat steam output remains constant. As only convective heat transfer is applied for reheat steam production, it remains largely uninfluenced by the reduced radiation heat transfer and increases only slightly (see Figure 29). However, the temperature is kept at coal-only level by spray water injection. The reheat steam mass flow also remains at coal-only level. It can also be seen that co-firing fuels with a higher moisture content of 20 % further reduces the achievable live steam heat output. The effects of co-firing wood chips

Dieses Werk ist copyrightgeschützt und darf in keiner Form vervielfältigt werden noch an Dritte weitergegeben werden.
Es gilt nur für den persönlichen Gebrauch.

with a higher moisture content are considered in more detail later on in this chapter and in Chapter 6.2.

Figure 29, furthermore, shows the relative changes of the following boiler parameters: flue gas temperature downstream of the ECO, live steam temperature and live steam mass flow. As the flue gas temperature downstream of the combustion chamber remains constant for all co-firing rates, the decline in flue gas temperature downstream of the ECO might indicate less flue gas losses and a higher heat transfer yield in the convective heating surfaces. This is indeed the case, as the increasing flue gas mass flow leads to higher flow velocities and thus enables a better heat transfer on the flue gas side of the convective heating surfaces. Additionally, the specific heat capacity of the flue gas changes when co-firing biomass, due to the increasing moisture content. This further enhances the resulting slight decrement in flue gas temperature.

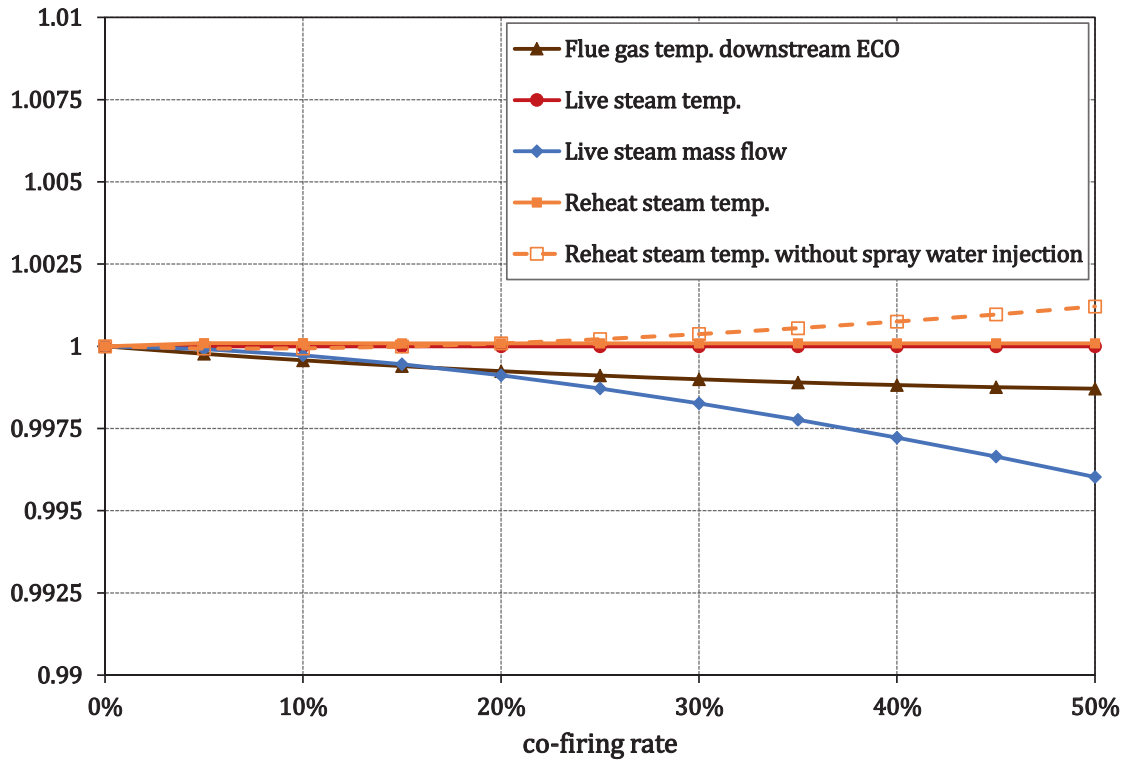

Figure 29: Relative changes of boiler parameters for co-firing wood chips with a moisture content of 10 %, in relation to the co-firing rate

Figure 29 also shows the previously mentioned development of the reheat steam temperature. Without spray water injection, the slightly reinforced convective heat transfer causes a minimum increase of the reheat steam temperature. However, in

Dieses Werk ist copyrightgeschützt und darf in keiner Form vervielfältigt werden noch an Dritte weitergegeben werden.
Es gilt nur für den persönlichen Gebrauch.

total, it can be concluded that, due to biomass co-firing, all relevant boiler process parameters change by approximately less than 1 % relative to their initial value for coal-only. Practically this means that in reality there will be almost no influence on any important process parameters and the resulting boiler performance.

The changes in heat transfer can also affect the boiler efficiency, which is defined in Eq. 6.1:

$$\eta_{\mathrm{b}} = \frac{\dot{Q}_{\mathrm{ls}} - \dot{Q}_{\mathrm{fw}} + \dot{Q}_{\mathrm{hrh}} - \dot{Q}_{\mathrm{crh}}}{\dot{Q}_{\mathrm{f}}} \tag{6.1}$$

with the live steam heat flow $\dot{Q}_{\mathrm{ls}}$, feedwater heat flow $\dot{Q}_{\mathrm{fw}}$, hot reheat steam flow $\dot{Q}_{\mathrm{hrh}}$ and cold reheat steam flow $\dot{Q}_{\mathrm{crh}}$. The boiler efficiency is 95.03 % for coal-only. It declines to 94.9 % for 50 % CFR. This corresponds to a relative change of 0.14 % and is thus in the range mentioned by SAMI [10]. Again, it can be underlined, that co-firing biomass with a very low moisture content shows no considerable effects on the boiler.

When co-firing poplar wood chips with a fuel moisture content of 20 %, the previously described effects – of a declining adiabatic flame temperature and an increasing flue gas mass flow – intensify. The resulting heat flow changes in the boiler heating surfaces can be seen in Figure 30.

Dieses Werk ist copyrightgeschützt und darf in keiner Form vervielfältigt werden noch an Dritte weitergegeben werden.
Es gilt nur für den persönlichen Gebrauch.

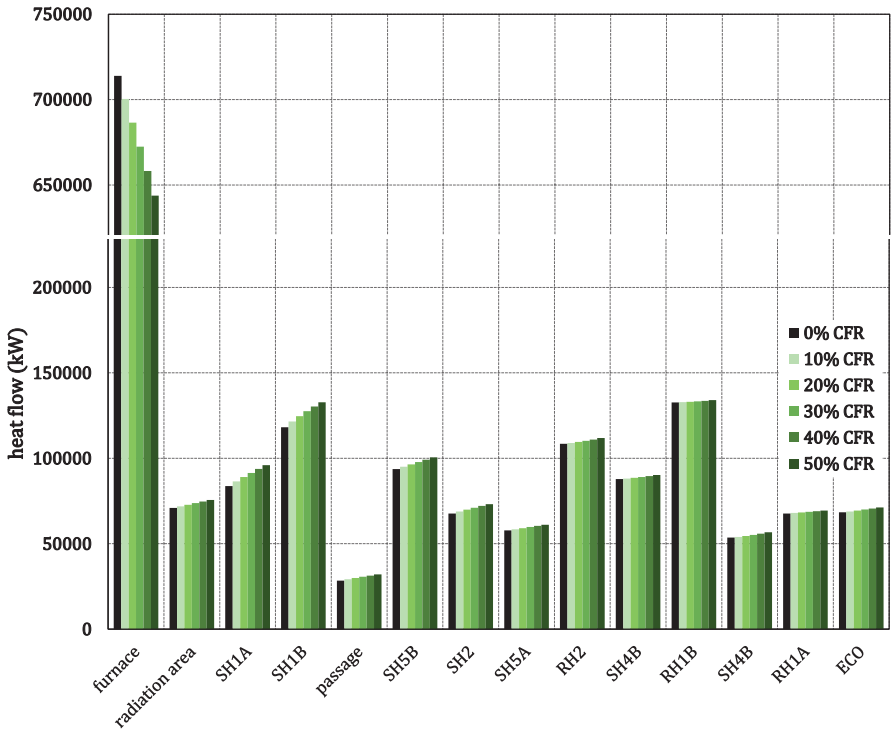

Figure 30: Heat flow changes in all boiler heating surfaces when co-firing poplar wood chips with 20 % fuel moisture content, in relation to the co-firing rate

Due to an even more strongly declining adiabatic flame temperature, less heat can be transferred by radiation compared to co-firing wood chips with a lower moisture content. When comparing with the results shown in Figure 27, it is clear that less heat can be transferred in the furnace when co-firing poplar wood chips with a fuel moisture content of 20 %.

As a result, the live steam heat output declines more strongly than for co-firing poplar wood chips with a moisture content of 10 % (see Figure 28). The resulting relative changes of boiler parameters are also slightly more intense than those shown in Figure 29. The boiler efficiency declines to 94.8 % for a co-firing rate of 50 %. Co-firing wood with a low moisture content is therefore not essential to maintain high boiler efficiency. How the overall process is affected by co-firing wood with 10 % or 20 % moisture content is considered in the following chapter.

Dieses Werk ist copyrightgeschützt und darf in keiner Form vervielfältigt werden noch an Dritte weitergegeben werden.
Es gilt nur für den persönlichen Gebrauch.

6.2 Effects on the overall process

To further analyse the effects of biomass co-firing in coal-fired steam power plants, the results for relative changes of live steam mass flow and flue gas temperature downstream of the ECO were implemented into the power plant overall process model that is described in Chapter 5.1.1. Figure 31 shows the most important results.

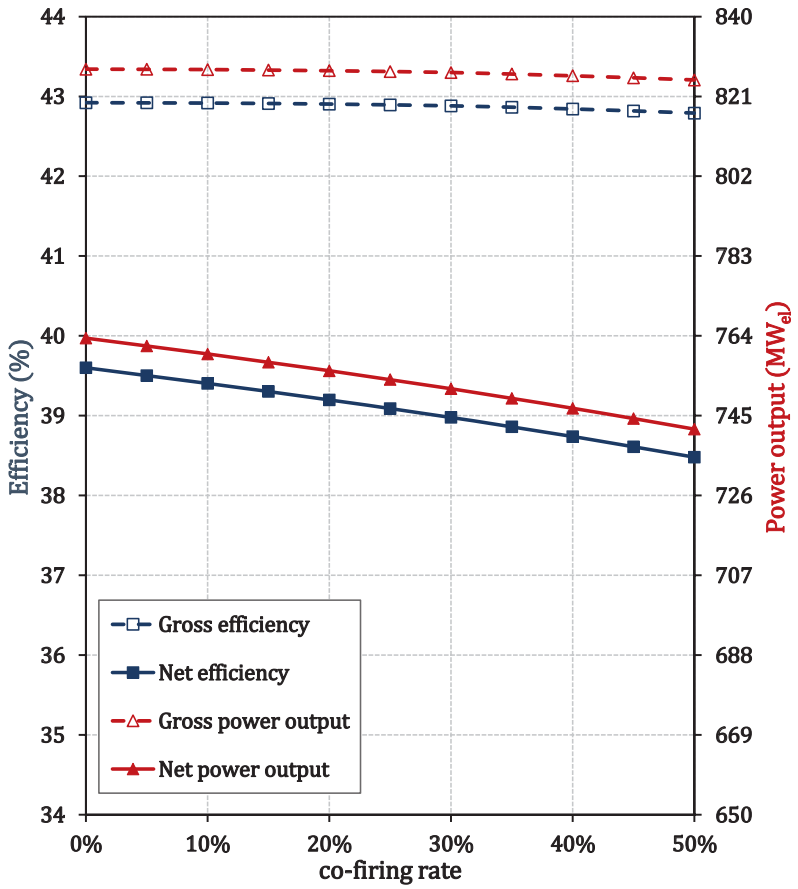

Figure 31: Net and gross efficiency and power output for direct co-firing of wood chips with moisture content of 10 % in relation to the co-firing rate

Here, results for the key process parameters (net and gross efficiency, as well as net and gross electrical power output) for co-firing poplar wood chips with a moisture content of 10 % up to a co-firing rate of 50 % are shown. The slightly declining development of gross efficiency and power output is proportional to the live steam power output's development, which was presented in Figure 28.

Dieses Werk ist copyrightgeschützt und darf in keiner Form vervielfältigt werden noch an Dritte weitergegeben werden.
Es gilt nur für den persönlichen Gebrauch.

The development of net efficiency and net power output declines remarkably. As the only reason for this is significantly growing auxiliary power demand, the electrical power demand of the main consumers feedwater pump, flue gas fan, air fan, coal mill and biomass mill, are shown in Figure 32.

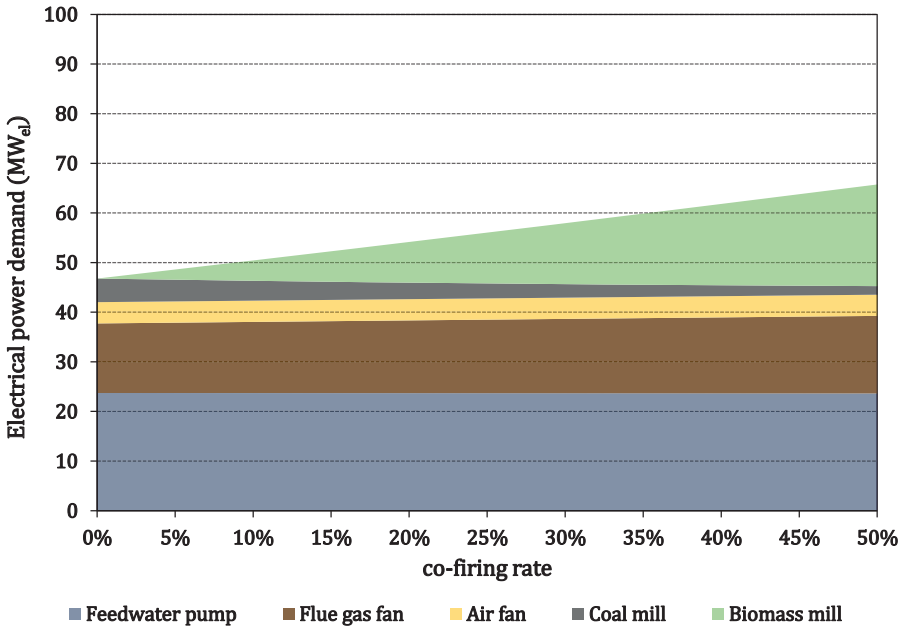

Figure 32: Distribution of main shares in auxiliary power demand for direct co-firing of wood chips in relation to the co-firing rate

The feedwater pump's auxiliary power demand remains constant, at almost 24 MW, for all direct co-firing variations and has the highest share in total auxiliary power demand when only coal is fired. Also largely unaffected by biomass co-firing are the auxiliary power demands of the flue gas and air fans. They add up to 18.3 MW for 0 % CFR and increase up to 19.9 MW for 50 % CFR. As expected, the auxiliary power demand of the coal mill declines with increasing CFR. The biomass mill's auxiliary power demand increases significantly as CFR increases and thereby causes the remarkable drop in net efficiency and net power output. For 50 % biomass co-firing, the auxiliary power demand increases by more than 30 % compared to coal-only usage.

The boiler analyses in Chapter 6.1 showed only very moderate shifts in combustion air demand, as well as in flue gas mass flow and temperature. Nonetheless, the resulting effects on air preheating will now be analysed further. Figure 33 shows the flue gas temperatures downstream of the air preheater and downstream of the economiser (according to Figure 29), the air temperature upstream of the boiler, as

Dieses Werk ist copyrightgeschützt und darf in keiner Form vervielfältigt werden noch an Dritte weitergegeben werden.
Es gilt nur für den persönlichen Gebrauch.

well as the flue gas and air mass flows through the air preheater, for a CFR of up to 50 %. The air temperature upstream of the air preheater is not shown but remains constant at 39 °C.

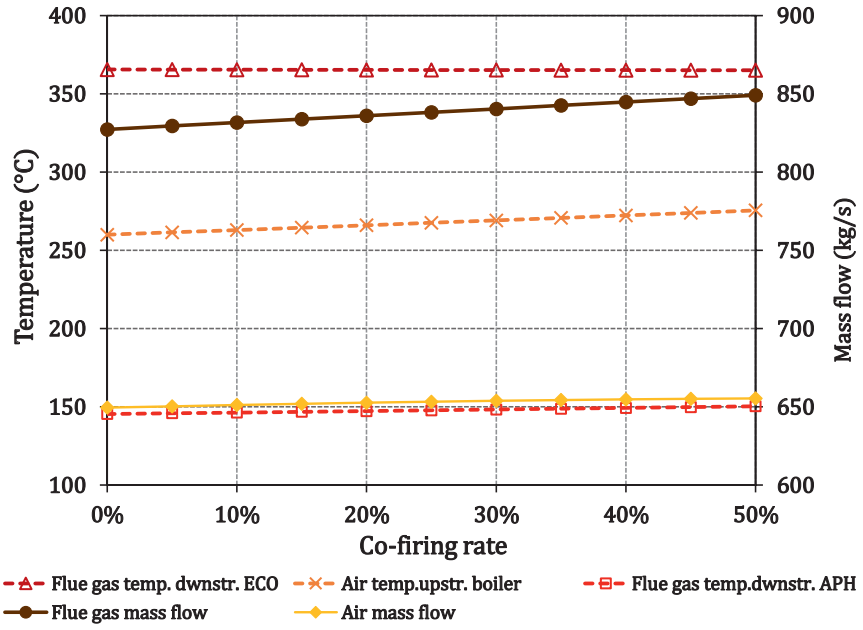

Figure 33: Air and flue gas temperatures and mass flows in the air preheater for direct co-firing of wood chips in relation to the co-firing rate

As the combustion air demand declines with rising CFR, an increase of air mass flow through the air preheater seems surprising at first sight. However, as less air is required to fluidise the coal mills, less cold air, which bypasses the air preheater, is required to regulate the mill outlet temperature. As the mill air demand of the biomass hammer mill is typically smaller than the mill air demand of the coal mill, a higher share of the air mass flow can flow through the air preheater.

The slight decline in flue gas temperature is balanced out by the rising flue gas mass flow so that, in total, a higher flue gas heat flow is available for air preheating when co-firing biomass with coal. Even though the air mass flow slightly increases, the air temperature upstream of the boiler can also be increased. The increasing flow velocities cause an improved heat transfer and therefore reduce the terminal temperature difference in the air preheater for high CFR.

Even though the power plant process is slightly affected by the changed thermodynamics of biomass co-firing, it can be concluded that, for direct co-firing of poplar wood chips, the main influence on the power generation process is the very high auxiliary power demand of the biomass hammer mill.

Dieses Werk ist copyrightgeschützt und darf in keiner Form vervielfältigt werden noch an Dritte weitergegeben werden.
Es gilt nur für den persönlichen Gebrauch.

To underline the significance of moisture content in the biomass fuel, the results of direct co-firing of poplar wood chips with a moisture content of 20 % are shown in Figure 34 and Figure 35.

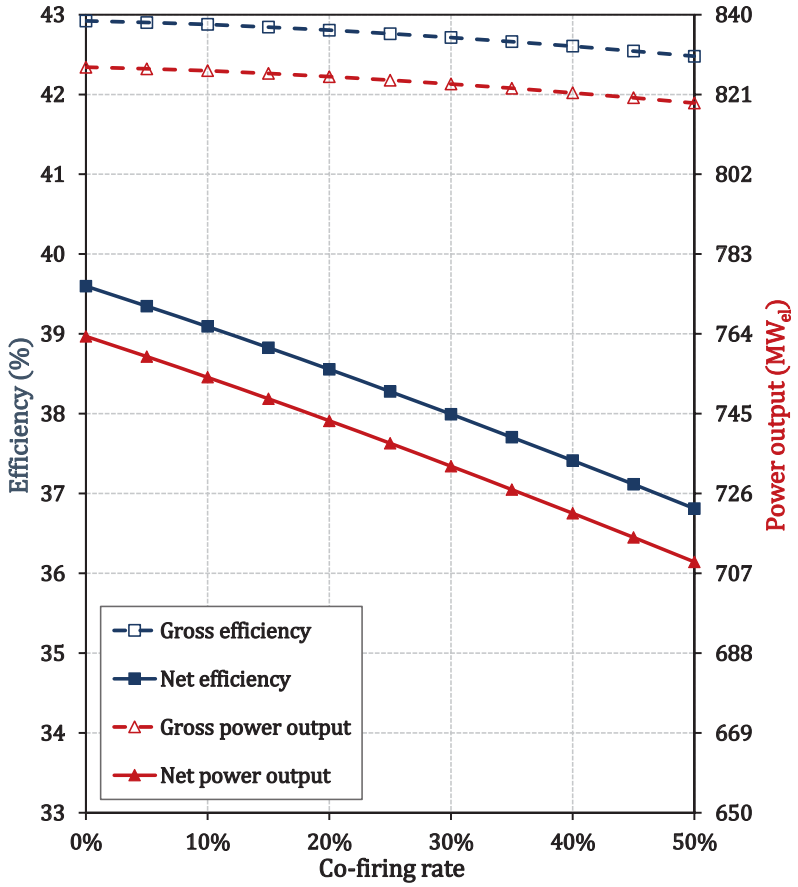

Figure 34: Net and gross efficiency and power output for direct co-firing of poplar wood chips with a moisture content of 20 % in relation to the co-firing rate

As the live steam heat output declines more strongly for a fuel with a higher moisture content (see Figure 28), the decline in gross efficiency and power output is stronger compared to co-firing poplar wood chips with a moisture content of 10 % (see Figure 31). Even more severe is the decline in net efficiency and power output. Again, this decline is primarily caused by the biomass hammer mill's auxiliary power demand.

The shares in auxiliary power demand for direct co-firing of poplar wood chips with a moisture content of 20 % are shown in Figure 35.

Dieses Werk ist copyrightgeschützt und darf in keiner Form vervielfältigt werden noch an Dritte weitergegeben werden.
Es gilt nur für den persönlichen Gebrauch.

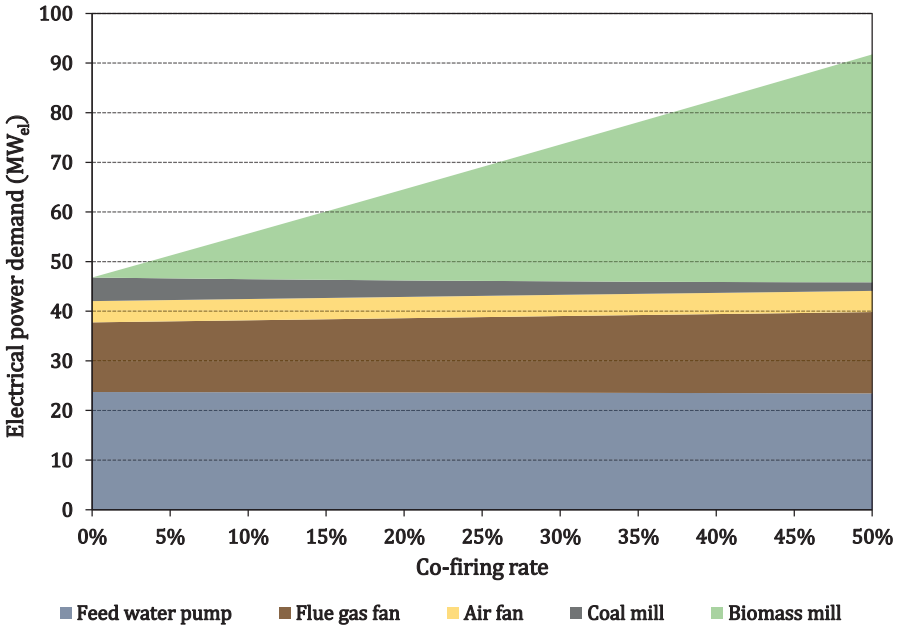

Figure 35: Distribution of main shares in auxiliary power demand for direct co-firing of poplar wood chips with a moisture content of 20 % in relation to the co-firing rate

The auxiliary power demand of the biomass hammer mill reaches 46 MW_{el} at 50 % CFR, which is roughly double the energy demand of grinding poplar wood chips with a moisture content of 10 %. The energy demand for grinding the wood chips is linearly dependent on the fuel moisture content (see Eq. 5.1). To avoid this extreme increase in auxiliary power demand, and also to limit the decrease in steam generation, drying the biomass fuel to a moisture content of 10 % is mandatory when co-firing biomass with coal.

Dieses Werk ist copyrightgeschützt und darf in keiner Form vervielfältigt werden noch an Dritte weitergegeben werden.
Es gilt nur für den persönlichen Gebrauch.

Dieses Werk ist copyrightgeschützt und darf in keiner Form vervielfältigt werden noch an Dritte weitergegeben werden.
Es gilt nur für den persönlichen Gebrauch.

7 ANALYSIS OF DRYING SCENARIOS

The analyses of direct co-firing in Chapter 6 showed that little impairment is caused by using woody fuel with a moisture content of 10 %. As freshly harvested wood chips have a moisture content of around 50 %, drying is therefore essential. The drying scenarios described in Chapter 4 are analysed in this chapter regarding their impacts on the power generation process and possible technical limitations. A comparison of the total resulting CO_2 emissions and energy utilisation efficiency (see Chapter 4) of each scenario aims to identify the most favourable scenario for co-firing wood chips with coal in a large-scale steam power plant.

7.1 Scenario 1 – integrated on-site drying by an indirect steam-tube dryer

The models described in Chapter 5.2 are used to analyse the effects of indirect co-firing of poplar wood chips for co-firing rates of up to 50 %. Wet wood chips with a moisture content of 50 % need to be dried to a moisture content of 10 %, with the wood chips mass flow always corresponding to the co-firing rate.

In Scenario 1_a the dryer's heat demand is covered by steam extracted from the IP/LP crossover pipe. Firstly, in the base case integration, the steam-tube dryer is connected to the power plant's water-steam cycle, but the ventilation air heat integration (see Figure 20) is at first not considered. How the overall process can be improved further by such ventilation air heat integration is analysed in the second stage.

In Scenario 1_b the dryer's heat demand is covered by steam extracted from the IP/LP crossover pipe and steam that is extracted from the LP turbine. The dryer is integrated in the power plant's water-steam cycle and ventilation air heat integration is varied, which is found as most beneficial in Scenario 1_a.

7.1.1 Scenario 1_a – drying steam extracted from IP/LP crossover pipe

Here, the dryer's heat demand is covered completely by steam extracted from the IP/LP crossover pipe and the base case integration of the drying process into the water-steam cycle is analysed. The possibilities of additional ventilation air heat integration are analysed later on.

Dieses Werk ist copyrightgeschützt und darf in keiner Form vervielfältigt werden noch an Dritte weitergegeben werden.
Es gilt nur für den persönlichen Gebrauch.

Base case integration

The initial IP/LP crossover pipe steam pressure of 5.4 bar corresponds to a condensation temperature of 155 °C. However, due to pressure losses, the final drying steam temperature will be slightly lower. Also, efficiency and power generation will be affected by the drying steam extraction.

Figure 36 shows the dependence of net and gross efficiency and net and gross electrical power output on the co-firing rate, for co-firing rates of up to 50 %. Starting from 39.6 % for coal-only firing, the net efficiency drops by 3.6 %-pts to 36 % for 50 % CFR. The electrical net power output is reduced by 9 % to 693 MW_{el}.

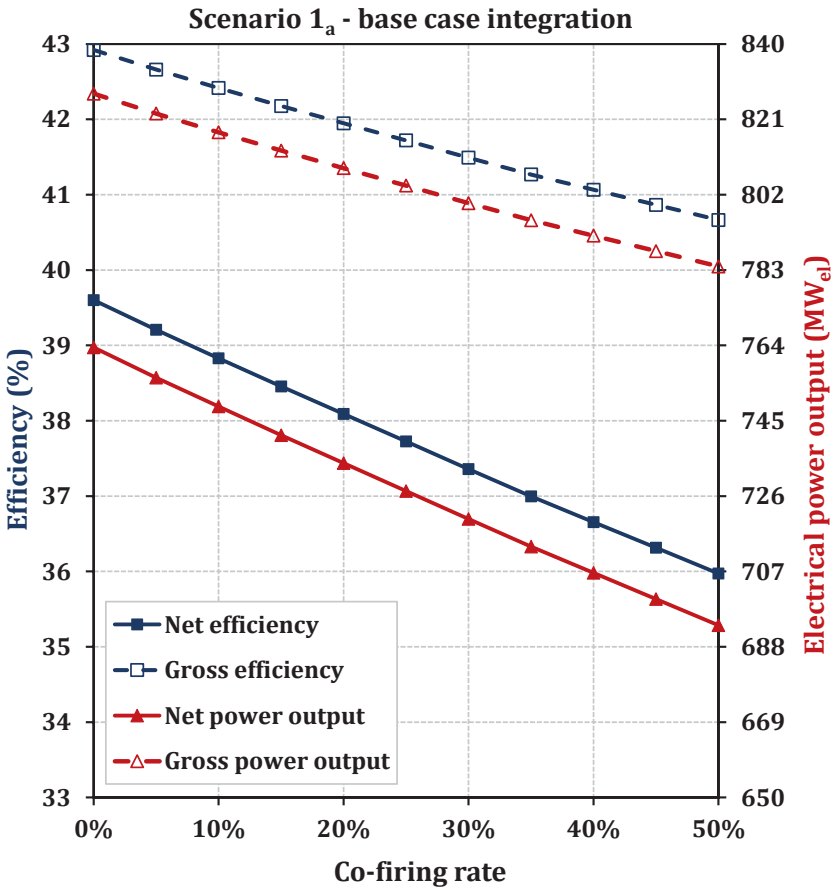

Figure 36: Net and gross efficiency and power output for co-firing of wood chips (10 % H_2O) dried with a steam-tube dryer in relation to the co-firing rate, integrated Scenario 1_a

Due to the steam extraction for drying, less steam is available for power generation in the low-pressure turbines, which causes the decline in gross efficiency and power output. The power generation in the steam turbines is also affected negatively by a

Dieses Werk ist copyrightgeschützt und darf in keiner Form vervielfältigt werden noch an Dritte weitergegeben werden.
Es gilt nur für den persönlichen Gebrauch.

declining steam pressure and temperature. On the other hand, the turbine outlet pressure declines, due to part-load operation of the turbine condenser. This is beneficial for the turbine performance, but cannot sufficiently counteract the negative influences. Net efficiency and power output are additionally affected by the growing on-site power demand due to the biomass hammer mills (see Figure 32).

Figure 37 shows the declines of steam pressure and mass flow upstream of the LP turbine, which result from the drying stream extraction from the IP/LP crossover pipe. For a co-firing rate of 50 %, the steam mass flow upstream of the LP turbines is reduced by almost 13 %. The steam pressure drops by around 14 % compared to coal-only usage.

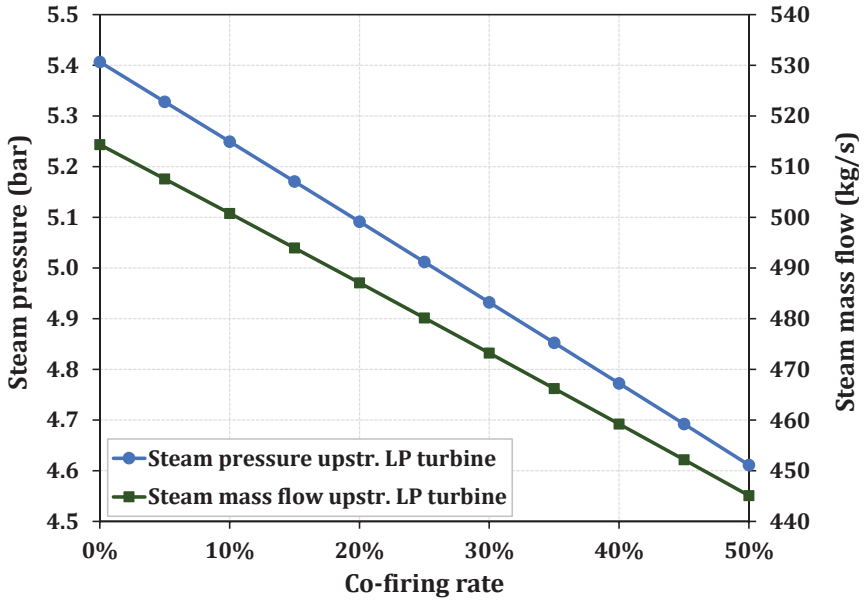

Figure 37: Steam pressure and mass flow decline upstream of the LP turbine due to drying steam extraction from IP/LP crossover pipe in relation to the co-firing rate

Consequently, power generation in the LP turbines is greatly affected by the dryer's integration into the water-steam cycle. Both the quantity and quality of the steam reaching the LP turbines are reduced, represented by a declining steam pressure. These effects are direct results of the extraction of steam for drying and thus reduce the possible power output.

Furthermore, the decline in steam pressure affects the drying process itself. Figure 38 shows the development of drying steam pressure and the resulting drying steam condensation temperature for increasing co-firing rates. Due to pressure losses in

Dieses Werk ist copyrightgeschützt und darf in keiner Form vervielfältigt werden noch an Dritte weitergegeben werden.
Es gilt nur für den persönlichen Gebrauch.

the drying steam pipe (see Chapter 5.2.2), the drying steam pressure is lower than the steam pressure in the IP/LP crossover pipe.

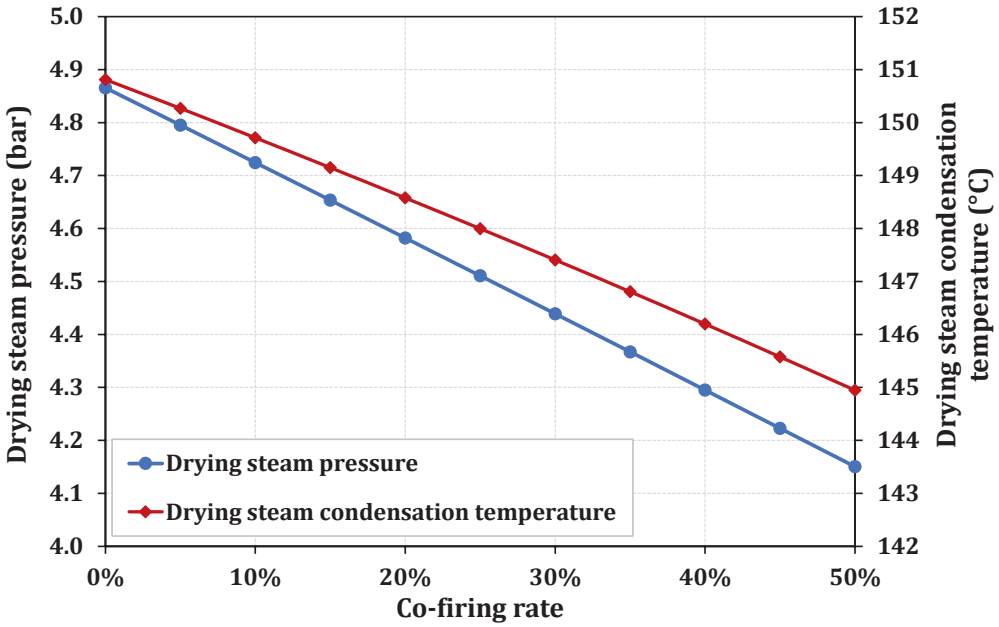

Figure 38: Development of drying steam pressure and resulting drying steam condensation temperature in Scenario 1_a in relation to the co-firing rate

The drying steam condensation temperature drops from 150 °C (for 5 % CFR) to 145 °C (for 50 % CFR). As most of the required drying heat is transferred by condensation, this temperature largely defines the drying process. A drop in the drying steam condensation temperature results in a comparatively longer necessary residence time of the drying product in the dryer, and probably requires adjustments in the rotation speed of the dryer. However, the resulting moderate decline in drying temperature is not a critical issue for the drying process, and so additional pressure-maintaining measurements upstream of the LP turbines are not required.

To consider the heat demand for drying wood chips in more detail, the total heat demand without heat losses $\dot{Q}_{\mathrm{dry,tot}}$ for drying a wood chips mass flow corresponding to 10 % CFR, is listed in Table 8.

Dieses Werk ist copyrightgeschützt und darf in keiner Form vervielfältigt werden noch an Dritte weitergegeben werden.
Es gilt nur für den persönlichen Gebrauch.

Table 8: Energy demand of a steam-tube dryer for 10 % CFR

$\dot{Q}_{\mathrm{dry,air}}$ ($\mathrm{MW_{th}}$)	$\dot{Q}_{\mathrm{dry,bm}}$ ($\mathrm{MW_{th}}$)	$\dot{Q}_{\mathrm{dry,ww}}$ ($\mathrm{MW_{th}}$)	$\dot{Q}_{\mathrm{dry,evp}}$ ($\mathrm{MW_{th}}$)	$\dot{Q}_{\mathrm{dry,bind}}$ ($\mathrm{MW_{th}}$)	$\dot{Q}_{\mathrm{dry,tot}}$ ($\mathrm{MW_{th}}$)
1.837	0.805	2.551	23.520	0.201	28.910

The total heat demand is the sum of heat demand for ventilation air heating $\dot{Q}_{\mathrm{dry,bm}}$, heat demand for heating of the dry biomass mass flow $\dot{Q}_{\mathrm{dry,air}}$, heat demand for warming up all water contained in the wood chips $\dot{Q}_{\mathrm{dry,ww}}$, heat demand for evaporating the desired amount of water $\dot{Q}_{\mathrm{dry,evp}}$ and heat demand required to overcome binding enthalpy $\dot{Q}_{\mathrm{dry,bind}}$. As expected, the heat demand for evaporation dominates the total drying heat demand. However, the energy required for warming up the ventilation air and the wet wood chips accounts for 18 % of the total drying heat demand.

Ventilation air heat integration – theoretical potential

The water evaporated through the drying process is removed from the dryer by a ventilation air mass flow. Downstream of the dryer fan, the ventilation air has a moisture content of 21.7 % and a temperature of 92 °C. It reaches a mass flow of 227 kg/s at a co-firing rate of 50 %, with a dew point temperature of around 70 °C. How the losses in efficiency and power generation caused by the drying steam extraction can be reduced by integrating this heat flow into the power generation process will be considered in the following section.

The maximum potential of low pressure feedwater (LPFW) preheating by ventilation air is analysed as a first step. There are three possibilities for ventilation air heat integration for LPFW preheating (see Figure 20):

- heat exchanger AHE1 in main turbine (MT) low-pressure preheating section
- heat exchanger AHE2 in second turbine (ST) low-pressure preheating section
- heat exchangers in both preheating sections

The model described in Chapter 5.2.2 is used for the following simulation analyses. To estimate the theoretical heat integration potential, the heat flow generated by condensing all moisture contained in the ventilation air flow is determined and

Dieses Werk ist copyrightgeschützt und darf in keiner Form vervielfältigt werden noch an Dritte weitergegeben werden.
Es gilt nur für den persönlichen Gebrauch.

shown in Figure 39, together with the maximum heat flow in AHE1 and AHE2. The maximum heat flows are determined by assuming an ideal heat transfer to the according relevant LPFW mass flow. In the coal-only case, the LPFW temperature upstream of AHE1 is 44.7 °C and the LPFW temperature upstream of AHE2 is 58.4 °C. This results in a lower maximum heat flow in AHE2.

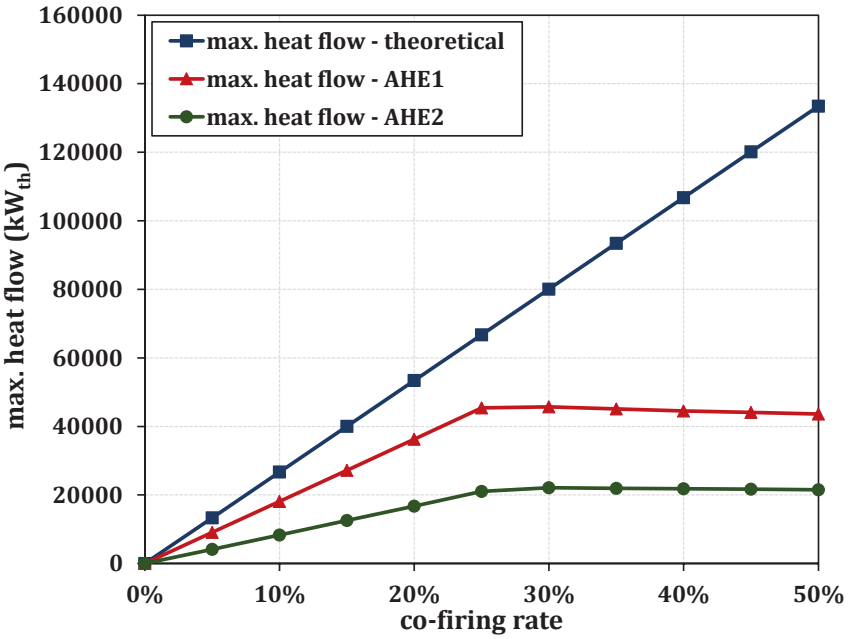

Figure 39: Ventilation air heat integration potential in relation to the co-firing rate

In general, the heat available for integration rises continuously with rising co-firing rates as the ventilation air mass flow, which carries the vapours, increases. Whereas temperature and water vapour partial pressure remain constant, as these depend on the dryer's feed and product moisture content and the ventilation ratio (see Chapter 5.2).

Even so, the amount of heat that can be integrated into the preheating section is limited due to LPFW temperature, pressure and mass flow. Evaporation of the LPFW in the preheating section must be avoided, and a minimum temperature difference of 6 K to the pinch point needs to be maintained. The comparatively lower feedwater temperature in the main turbine's preheating section allows a higher heat flow and therefore a higher heat integration potential for AHE1. Heat integration of up to 40 MW_{th} can be expected when using AHE1 and up to 20 MW_{th} when using AHE2. Even more successful heat integration might be possible by using both AHE1 and AHE2 heat exchangers. However, the resulting benefits for the overall process not

Dieses Werk ist copyrightgeschützt und darf in keiner Form vervielfältigt werden noch an Dritte weitergegeben werden.
Es gilt nur für den persönlichen Gebrauch.

only depend on the amount of heat transferred but also on the temperature level of the heat source.

Furthermore, the potential for heat integration is limited by the LPFW mass flow. As more steam needs to be extracted for drying, the LPFW mass flow declines with rising co-firing rates, and less heat can be integrated. This results in a maximum for the integrable heat.

The development of heat transfer in air heat exchanger 1 (AHE1) is shown in Figure 40, the heat transfer in air heat exchanger 2 (AHE2) is shown in Figure 41. Water vapour is condensed and extracted in both heat exchangers. This enables very effective heat transfer with high heat transfer coefficients and thus small heat exchanger surfaces.

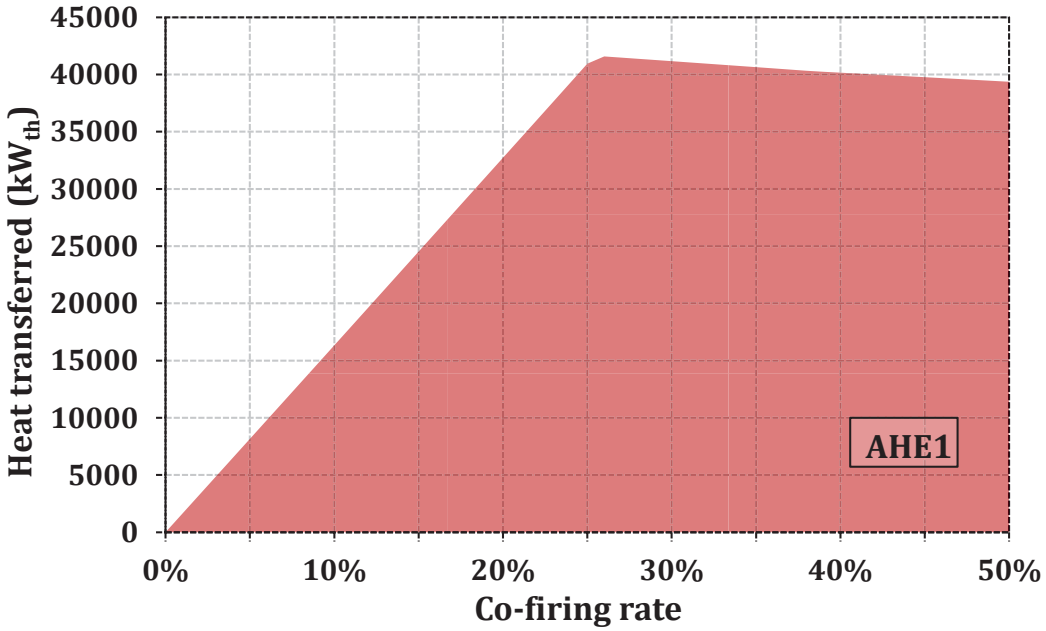

Figure 40: Heat transfer for heat integration – air heat exchanger 1

As had been expected, both variations show a maximum level of heat integration at 26 % CFR. For higher co-firing rates, the heat transfer slightly declines. As more steam is extracted for drying with higher CFR, less steam is condensed in the condenser downstream of the LP turbines. Due to the declining condensate mass flow, less heat can be integrated into a turbine's preheating section. In a comparison, using AHE 1 seems more favourable than using AHE 2, as around twice as much heat can be gained for low-pressure feedwater preheating.

Dieses Werk ist copyrightgeschützt und darf in keiner Form vervielfältigt werden noch an Dritte weitergegeben werden.
Es gilt nur für den persönlichen Gebrauch.

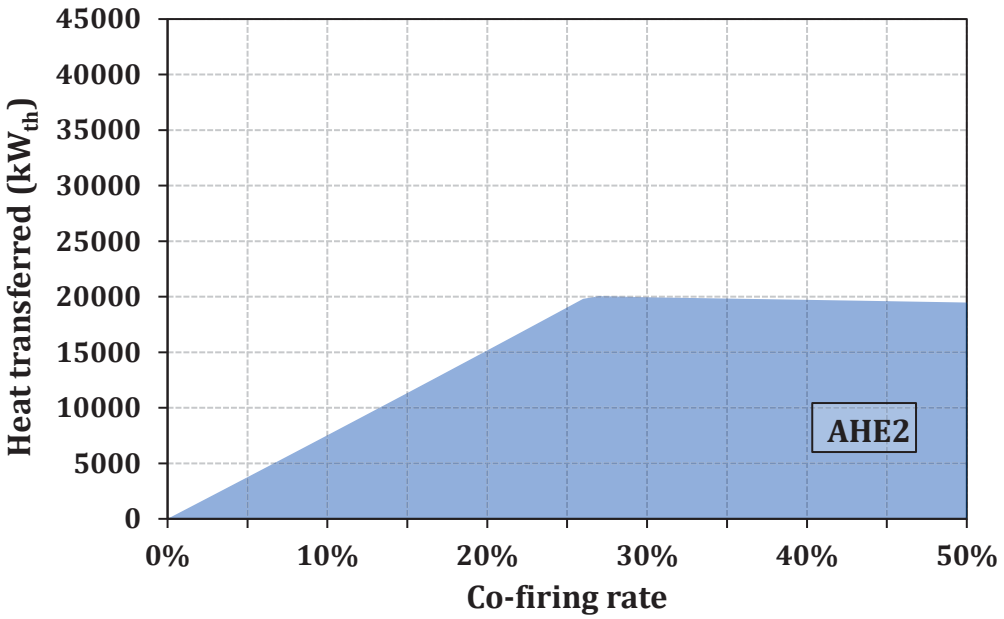

Figure 41: Heat transfer for heat integration – air heat exchanger 2

The resulting heat transfer from using both preheaters in a row is shown in Figure 42Figure 42.

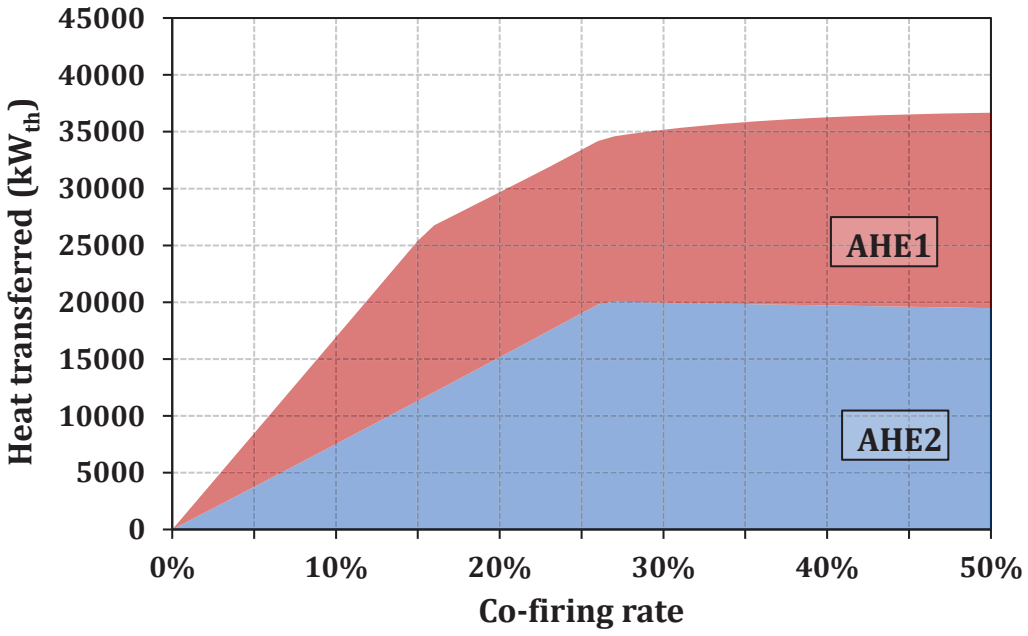

Figure 42: Heat transfer for heat integration – air heat exchangers 1 and 2

If both air preheaters are used, AHE2 is located upstream of AHE1. This means that the heat transfer in AHE2 remains unchanged. The additional heat transfer in AHE1

Dieses Werk ist copyrightgeschützt und darf in keiner Form vervielfältigt werden noch an Dritte weitergegeben werden.
Es gilt nur für den persönlichen Gebrauch.

allows further heat integration due to the comparatively lower LPFW temperature in AHE1. Nevertheless, the heat transferred to the preheating sections in this variation is lower than the level of heat integration by using only AHE1. The ventilation air's moisture content is reduced by condensation in AHE2 before reaching AHE1, so the resulting heat transfer in AHE1 becomes comparatively less efficient. Initially the heat transferred in AHE1 increases with the CFR, as more heat is available in the ventilation air mass flow than can be used by AHE2. At about 15 % CFR the heat transfer in AHE1 cannot be increased anymore. The heat transfer in AHE2 is so efficient, and reduces the moisture content in the ventilation air in such a way, that less heat is available for integration in AHE1. However, when the maximum of heat integration in AHE2 is reached at 25 % CFR, but the ventilation air heat flow still increases, more heat is again available for integration in AHE1. The total heat transfer is, of course, improved compared to using only AHE2 but still remains under the level of heat transfer possible by using only AHE1.

Figure 43 shows the temperatures resulting from ventilation air heat integration. When AHE2 is used, the ventilation air can be cooled down to 68 °C. When only AHE1 is used, the ventilation air temperature falls to 65 °C, which is 5 K underneath the dew point temperature. Due to the comparatively lower LPFW temperature, more latent heat transfer is possible in AHE1 than in AHE2, where only a temperature difference to the dew point temperature of 2 K can be reached, and thus less latent heat transfer is possible.

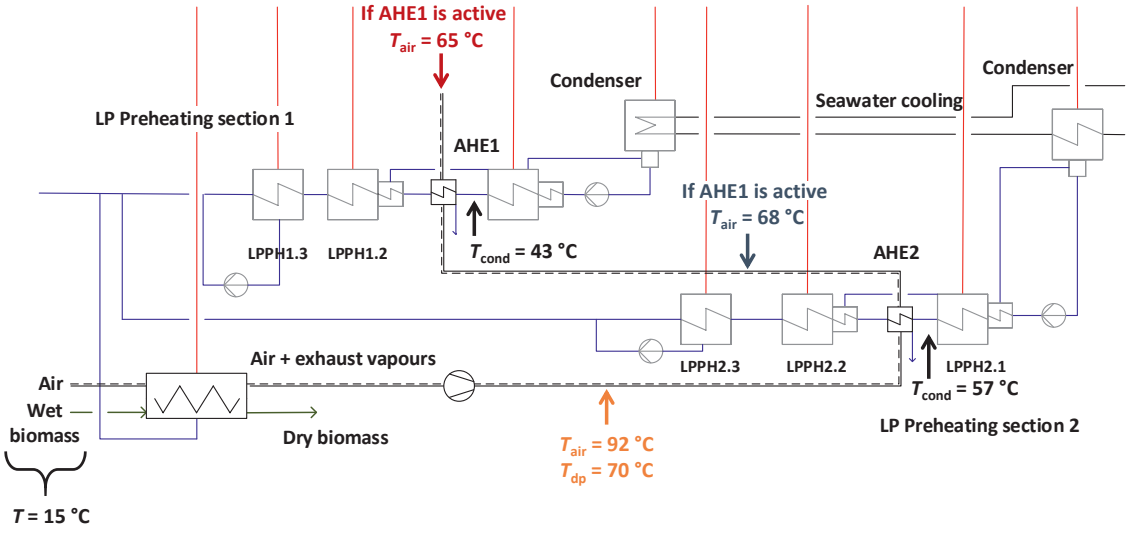

Figure 43: Ventilation air heat integration - resulting ventilation air and dew point temperatures

Dieses Werk ist copyrightgeschützt und darf in keiner Form vervielfältigt werden noch an Dritte weitergegeben werden.
Es gilt nur für den persönlichen Gebrauch.

The resulting theoretical improvements in net efficiency through integrating ventilation air are summarised in Figure 44. The improvement first grows with the co-firing rate and reaches a maximum of 0.3 %-pts. for 25 % CFR when using only AHE1. The potential efficiency improvement then declines as less heat can be integrated for LPFW preheating (see Figure 40).

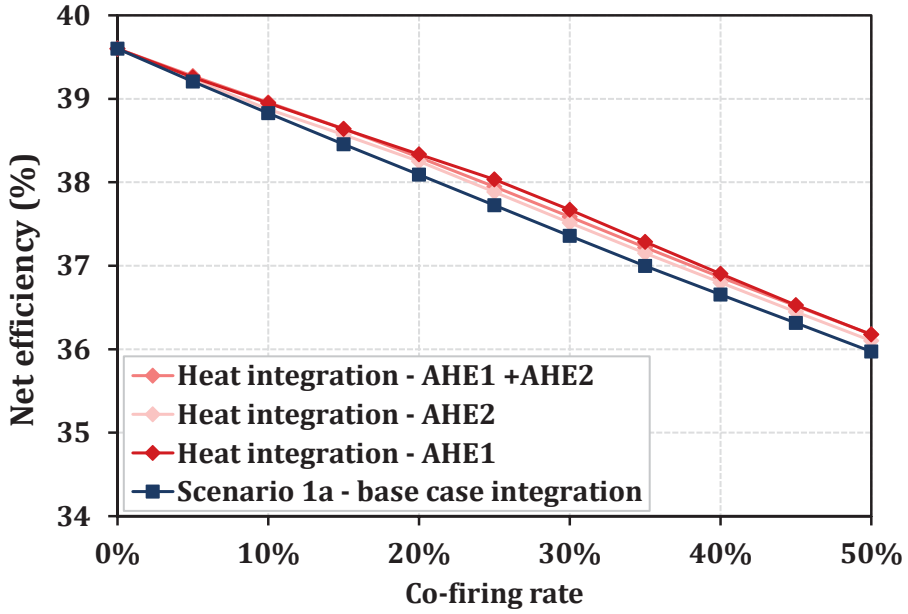

Figure 44: Net efficiency improvement due to heat integration in relation to the co-firing rate

In the scenario of integrated on-site drying with a steam-tube dryer, the highest theoretical potential for ventilation air heat integration exists through the use of one heat exchanger in the main turbine's LPFW preheating section. As the quality and quantity of ventilation air remain unchanged, this conclusion is relevant for both Scenario 1_a and Scenario 1_b.

How this theoretical potential for net efficiency improvement can be realised is now evaluated in two variations. In Variation A, the possibilities of low-pressure feedwater preheating are analysed in more detail. In Variation B, options for improving the drying energy demand are considered.

Ventilation air heat integration – Variation A

As described in Chapter 5.2.2, an additional heat transfer cycle is used for LPFW preheating (also see Figure 21). The additional LPFW preheater is installed in the main turbine's LPFW preheating section as this was identified previously as the most beneficial location.

Dieses Werk ist copyrightgeschützt und darf in keiner Form vervielfältigt werden noch an Dritte weitergegeben werden.
Es gilt nur für den persönlichen Gebrauch.

Figure 45 shows the heat transfer in the additional LPFW preheater. The resulting heat flow stays significantly below the theoretical potential determined in the previous section. Only around 5 MW_{th} can be gained for LPFW preheating at 50 % CFR.

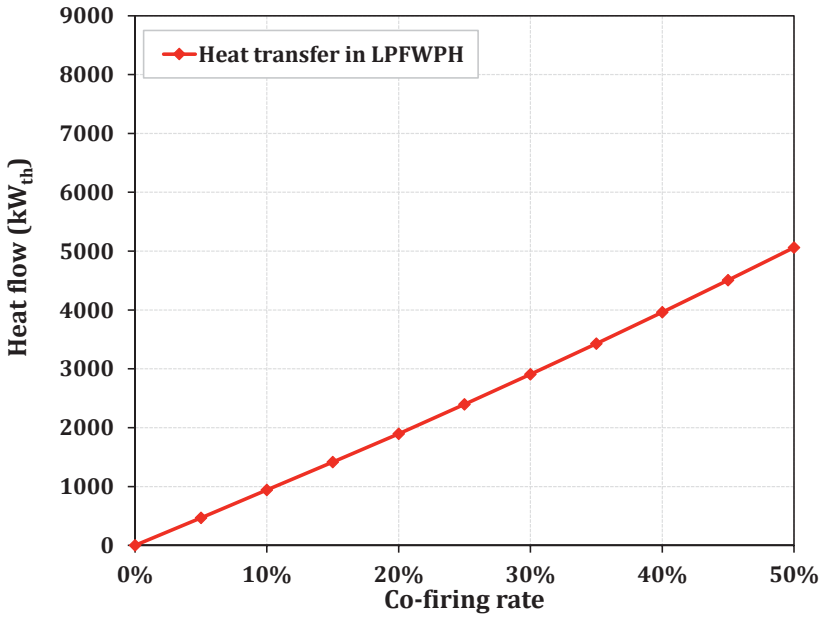

Figure 45: Ventilation air heat integration – Variation A: heat flow in additional LPFW preheater

Due to the terminal temperature differences in the additional low-pressure feedwater preheater (LPFWPH), as well as in the heat exchanger, which transfers heat from the ventilation air mass flow to the additional heating cycle, the final ventilation air temperature is 73 °C. This is still above its dew point temperature (70 °C). The heat potential of a latent heat exchange therefore cannot be used.

Ventilation air heat integration – Variation B

In Variation B, the potential of reducing drying energy demand by using waste heat of the ventilation air mass flow is analysed. A flowsheet of the process is shown in Figure 22. The biomass and the fresh ventilation air enter the drying process with an ambient temperature of 15 °C. Both mass flows are warmed up in the beginning of the drying process by using steam extracted from the power plant's water-steam cycle. As Table 8 shows, around 1.8 MW_{th} are required for ventilation air preheating and around 3.3 MW_{th} are required for wet biomass preheating per 10 % CFR. The resulting drying steam demand could be reduced if air or biomass preheating could be realised by ventilation air integration.

Dieses Werk ist copyrightgeschützt und darf in keiner Form vervielfältigt werden noch an Dritte weitergegeben werden.
Es gilt nur für den persönlichen Gebrauch.

The model described in Chapter 5.2.2 is used to analyse possible benefits of ventilation air preheating. The resulting heat transfer in the additional ventilation air preheater (VAPH) is shown in Figure 46. Both the potential and the demand for ventilation air preheating increase with higher co-firing rates. Up to 8 MW_{th} can be gained for ventilation air preheating at 50 % CFR.

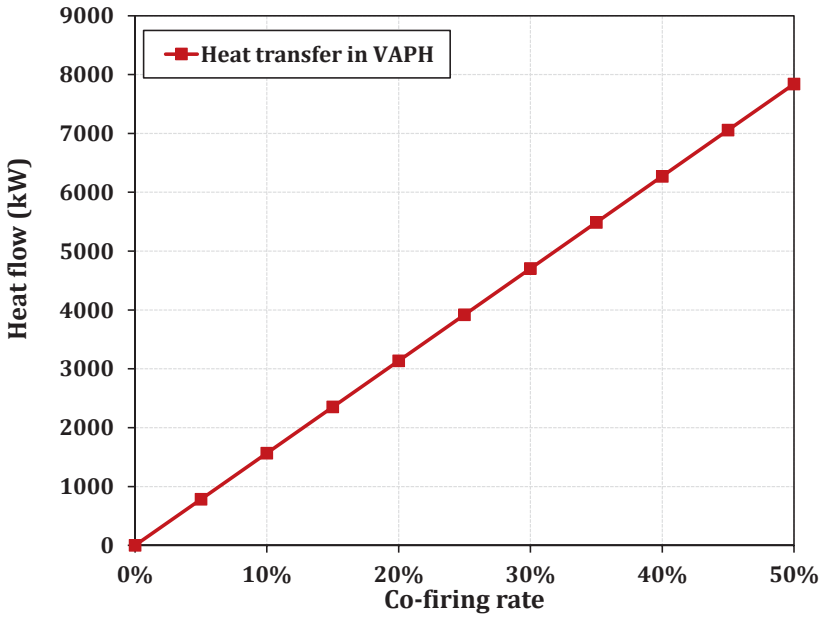

Figure 46: Ventilation air heat integration – Variation B: heat flow in ventilation air preheater

With the chosen terminal temperature difference in the ventilation air preheater, the hot ventilation air is cooled down to 69.9 °C, which is just below the dew point temperature (70 °C). Only a small share of the potential latent heat is used in this variation.

To avoid heat losses, the wet wood chips mass flow could only be preheated immediately upstream of the drying reactor. Also, the retention time for biomass preheating should be short. Otherwise the warm and humid wood will start to decompose. Possible options to achieve this could be heated conveyors that transport the wood chips from a storage space to the dryer or other similar forms of indirect heating. Direct heat transfer should be avoided because the exhaust vapours contained in the ventilation air would condense on the cold wood chips due to the low dew point temperature. Another option to optimise the overall process's heat demand could be to use the heat flow of the dried wood chips, which leave the dryer with a particle temperature of 80 °C.

Dieses Werk ist copyrightgeschützt und darf in keiner Form vervielfältigt werden noch an Dritte weitergegeben werden.
Es gilt nur für den persönlichen Gebrauch.

The resulting net efficiencies for all the considered options for ventilation air heat integration are compared to the resulting net efficiency for base case integration in Table 9. Only the results for 50 % CFR are compared.

Table 9: Net efficiency improvement by ventilation air heat integration in Scenario 1_a

		Ventilation air heat integration		
	Base case	**Max. potential**	**Var A**	**Var B**
η_{net} **(50 % CFR)**	35.97 %	36.17 %	35.99 %	36.03 %

The maximum potential for net efficiency improvement by ventilation air heat integration is 0.20 %-pts. when an ideal heat transfer to the main turbine's low-pressure preheating section is assumed. If this heat transfer is realised with an additional heat transfer cycle, only 0.02 %-pts. net efficiency improvement remains. If the ventilation air heat flow is used to optimise the dryer's heat demand by preheating the incoming ventilation air, a net efficiency improvement of 0.06 %-pts. can be reached.

Variation B is therefore preferable to Variation A and might also involve less investment costs in realisation. The Variation B results are thus used for all further analyses.

7.1.2 Scenario 1_b – drying steam extracted from IP/LP crossover pipe and LP turbine

In Scenario 1_b, the steam-tube dryer operates with two temperature zones. The model described in Chapter 5.2.2 (for flowsheet, see Figure 19) is used for the following analyses. The total drying heat demand is equally distributed to both dryer halves. The first half is heated by drying steam with a condensing temperature of around 125 °C extracted from the LP turbine. The second half is heated by drying steam with a condensing temperature of around 145 °C, extracted from the IP/LP crossover pipe. As ventilation air preheating had previously proven to be the most beneficial option for ventilation air heat integration, it is also carried out in Scenario 1_b. The assumption that it will also be the most beneficial option in this scenario is reasonable, as temperature, moisture content and mass flow of the ventilation air will remain uninfluenced by the mode of drying steam supply. All

Dieses Werk ist copyrightgeschützt und darf in keiner Form vervielfältigt werden noch an Dritte weitergegeben werden.
Es gilt nur für den persönlichen Gebrauch.

results shown therefore already include the benefits gained from this additional heat integration.

The resulting net and gross efficiency and net and gross electrical power output for co-firing up to 50 % dried poplar wood chips are shown in Figure 47. Starting from 39.6 % for coal-only, the net efficiency drops by 3.39 %-pts. to 36.21 % for 50 % CFR. The electrical net power output is reduced by 8.5 % to 698 MW_{el}. As expected, the declines in efficiency and power output are not as strong as in Scenario 1_a.

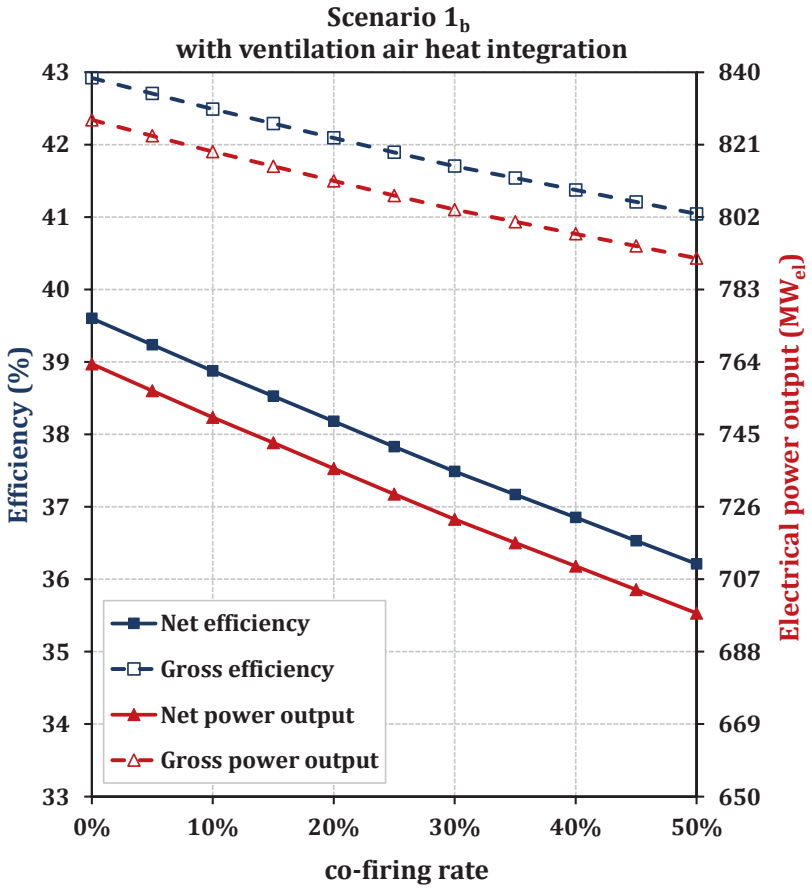

Figure 47: Net and gross efficiency and power output for co-firing of wood chips dried with a steam tube dryer in relation to the co-firing rate, integrated Scenario 1_b

Steam pressure and drying temperature in both dryer halves decline with rising co-firing rates due to mass flow increase in LP turbine extraction and in the IP/LP crossover pipe extraction. Figure 48 shows the development of drying steam pressure and drying steam condensation temperature in the first dryer half, which is heated by steam extracted from the LP turbine. The drying steam condensation temperature declines by around 6 K with an increasing CFR. This decline is

Dieses Werk ist copyrightgeschützt und darf in keiner Form vervielfältigt werden noch an Dritte weitergegeben werden.
Es gilt nur für den persönlichen Gebrauch.

comparatively stronger than the decline in drying steam temperature in Scenario 1_a. However, the quality of the drying steam extracted from the LP turbine is not only reduced by the extraction at this location: as drying stream is already extracted upstream of the LP turbine, the steam quality and quantity are already reduced before reaching the LP turbine inlet.

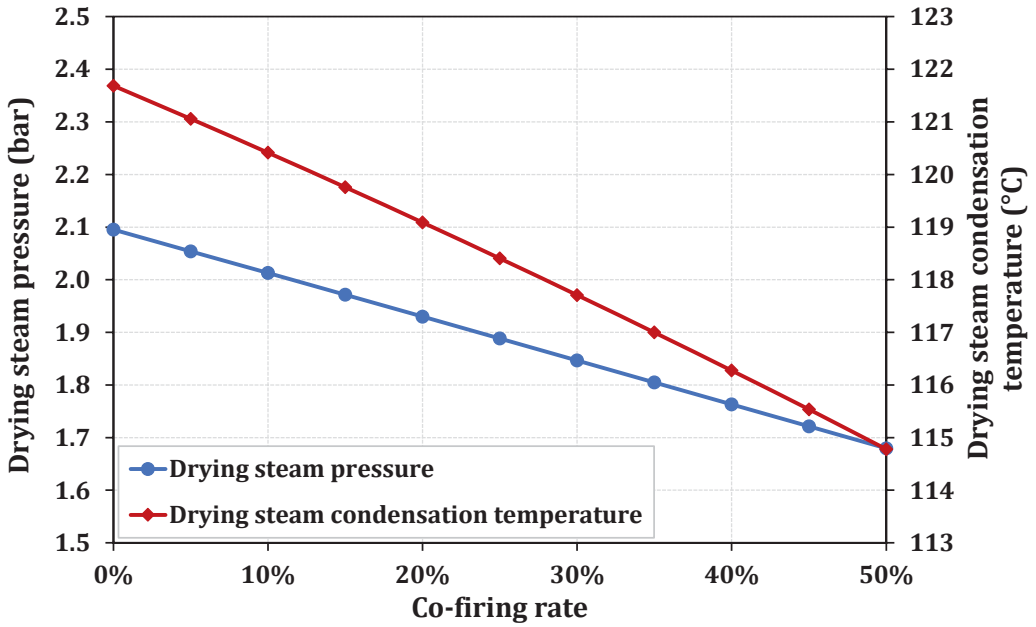

Figure 48: Development of drying steam pressure and drying steam condensation temperature in the first dryer half in relation to the co-firing rate, heated by steam extracted from the LP turbine

The second dryer half is heated with steam extracted from the IP/LP crossover pipe. Figure 49 compares the respective development of drying steam pressure and the drying steam condensation temperature resulting in Scenario 1_a to the drying steam pressure and drying steam condensation temperature development resulting in Scenario 1_b. As opposed to Scenario 1_a, only a part of the dryer's total heat demand is covered by steam extracted from the IP/LP crossover pipe. As expected, the resulting decline in steam pressure and drying steam condensation temperature is less severe and thereby less limiting for power generation in the following LP turbines.

Dieses Werk ist copyrightgeschützt und darf in keiner Form vervielfältigt werden noch an Dritte weitergegeben werden.
Es gilt nur für den persönlichen Gebrauch.

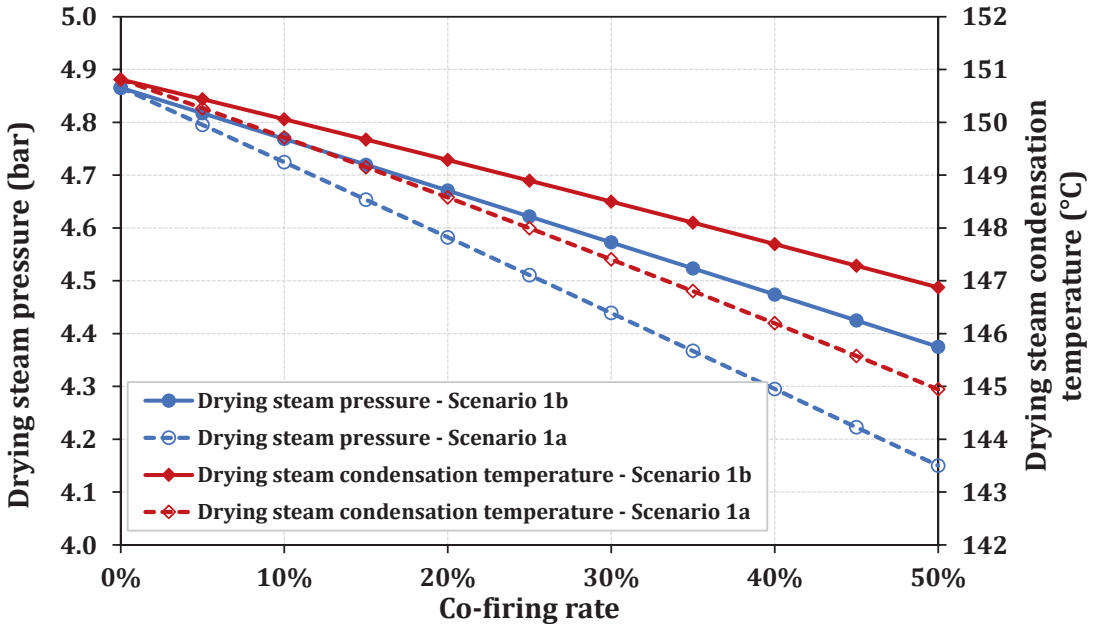

Figure 49: Development of drying steam pressure and drying steam condensation temperature in the second dryer half in relation to the co-firing rate, heated by steam extracted from the IP/LP crossover pipe, compared to the results of Scenario 1_a

As in Scenario 1_a, the required heat demand for drying wood chips will now be regarded in more detail. The first dryer half, which is heated with steam at a pressure level of 2.0 to 1.7 bar depending on the co-firing rate, is named Stage 1. The second dryer half, which is heated with steam at a pressure level of 4.8 to 4.4 bar depending on the co-firing rate, is named Stage 2. Figure 50 illustrates the development of the drying temperature over the drying heat flow for Scenario 1_a and 1_b. The extracted drying steam is still slightly overheated at dryer entry, but the temperature reduction until saturated steam level is reached makes up a near negligible share of the total required drying heat demand, as does the slight condensate supercooling near the dryer exit. The heat transfer in the indirect steam-tube dryer is determined by the condensation temperature of the drying steam. As Figure 50 shows, complete drying heat transfer is achieved at a temperature level of 145 °C (for 50 % CFR) in Scenario 1_a. Whereas, in Scenario 1_b, only half of the total drying heat demand is transferred at an equally high temperature level of 147 °C (for 50 % CFR). As the steam-tube dryer in Scenario 1_b is divided into two heating zones, the first half of the total drying heat demand can be provided at a significantly lower temperature level of 115 °C (for 50 % CFR). Thus, it is not necessary to use steam of a higher temperature level for the complete drying process.

Dieses Werk ist copyrightgeschützt und darf in keiner Form vervielfältigt werden noch an Dritte weitergegeben werden.
Es gilt nur für den persönlichen Gebrauch.

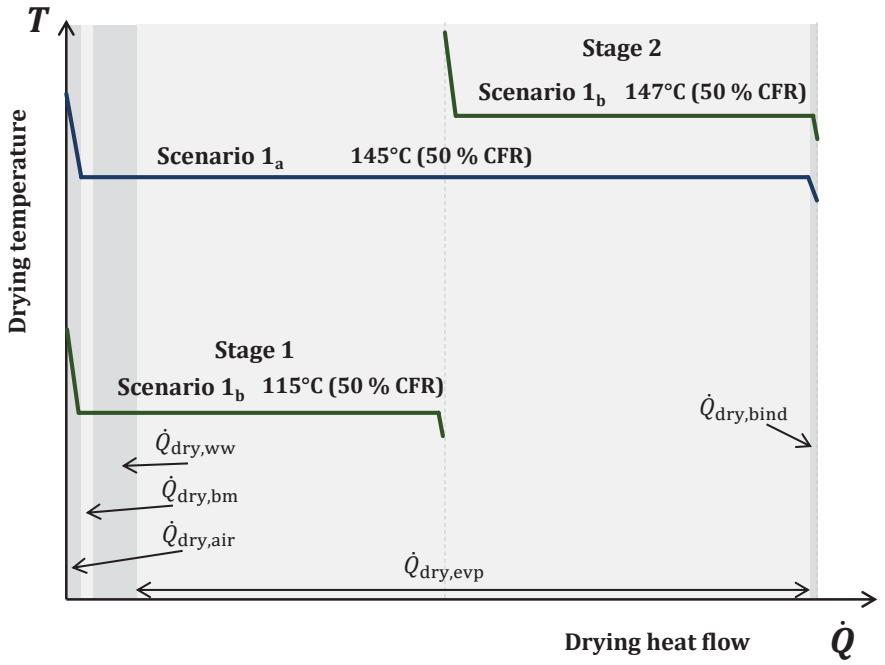

Figure 50: Drying temperature over transferred drying heat flow for Scenario 1_a and the two drying stages of Scenario 1_b

The total heat demand without heat losses $\dot{Q}_{dry,tot}$ for drying a wood chips mass flow corresponding to 10 % CFR in Scenario 1_b, is listed in Table 10. All shares of drying heat demand are listed for both dryer Stage 1 and Stage 2. Their sum is the dryer's complete heat demand for each partial heat demand and the resulting total heat demand $\dot{Q}_{dry,tot}$.

Table 10: Energy demand of a steam-tube dryer for 10 % CFR in Scenario 1_b

	$\dot{Q}_{dry,air}$ (MW_{th})	$\dot{Q}_{dry,bm}$ (MW_{th})	$\dot{Q}_{dry,ww}$ (MW_{th})	$\dot{Q}_{dry,evp}$ (MW_{th})	$\dot{Q}_{dry,bind}$ (MW_{th})	$\dot{Q}_{dry,tot}$ (MW_{th})
Stage 1	0.923	0.805	2.551	9.721	0.000	14.000
Stage 2	0.000	0.000	0.000	13.799	0.201	14.000
Sum	0.923	0.805	2.551	23.520	0.201	28.000

The total drying heat demand is lower than the one listed in Table 8. The reason for this is that the ventilation air preheating is already included here, which can be seen in the reduced heating demand $\dot{Q}_{dry,air}$ and the resulting reduction of the total

Dieses Werk ist copyrightgeschützt und darf in keiner Form vervielfältigt werden noch an Dritte weitergegeben werden.
Es gilt nur für den persönlichen Gebrauch.

heating demand $\dot{Q}_{\mathrm{dry,tot}}$. The share of each heat demand in the total drying heat demand is also visualised in Figure 50. Ventilation air and wet wood chips are heated up in the beginning of the drying process ($\dot{Q}_{\mathrm{dry,air}}$ and $\dot{Q}_{\mathrm{dry,bm}}$). The according heat demand is therefore only required in Stage 1. As $\dot{Q}_{\mathrm{dry,tot}}$ is equally distributed between Stage 1 and Stage 2, a larger share of $\dot{Q}_{\mathrm{dry,evp}}$ is required in the second stage. The binding enthalpy needs to be overcome when drying to a very low end product moisture content. The corresponding heat demand $\dot{Q}_{\mathrm{dry,bind}}$ is thus only required in the end of the drying process and is part of the resulting heat demand of Stage 2.

In Figure 51, the resulting net efficiencies of Scenario 1_a and Scenario 1_b are compared. The results for both scenarios consider the reduced drying heat demand through ventilation air preheating. Even though the thermal energy demand for drying is thus identical for both scenarios, the resulting net efficiencies show a slight difference. The net efficiency reduction is obviously less intense in Scenario 1_b.

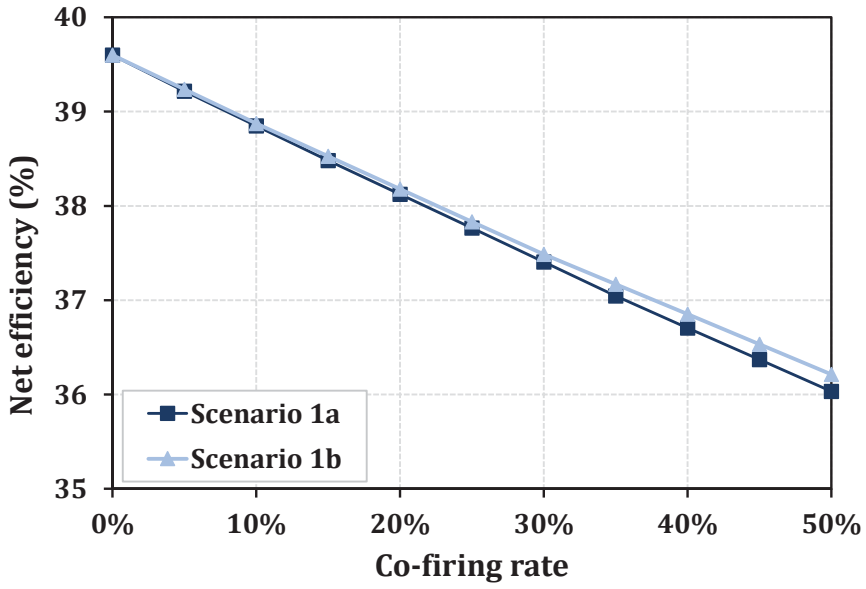

Figure 51: Comparison of net efficiency for Scenario 1_a and Scenario 1_b in relation to the co-firing rate, including ventilation air preheating in both scenarios

It can be concluded that the quality of the steam extracted for drying determines the resulting net efficiency. In Scenario 1_a, only steam extracted from the IP/LP crossover pipe at around 5 bar steam pressure is used for drying. In Scenario 1_b, only half of the drying heat demand is covered by steam extracted from

Dieses Werk ist copyrightgeschützt und darf in keiner Form vervielfältigt werden noch an Dritte weitergegeben werden.
Es gilt nur für den persönlichen Gebrauch.

the IP/LP crossover pipe. The other half is covered by steam extracted from the LP turbine at around 2 bar. The main advantage of partially using drying steam of a lower quality (2 bar) in Scenario 1_b is that a larger amount of the higher quality steam (5 bar) can be used for power generation, before being condensed in the indirect steam-tube dryer. Thus, the net efficiency in Scenario 1_b can be improved by 0.21 %-pts. for a CFR of 50 %, compared to Scenario $1_{a.}$

7.2 Scenario 2 – stand-alone drying by a direct rotary dryer

The direct rotary dryer model described in Chapter 5.3.2 is used for the simulations and analyses for drying Scenario 2. In this subsection, parameter variations will be simulated in order to identify the best-case set of process parameters for comparing the total resulting CO_2 emissions and the overall energy utilisation efficiency later on. The best-case operation point should be the one with the lowest thermal and electrical demands, while still matching technical feasibility and, as a consequence, also having the lowest CO_2 emissions. Furthermore, differences between the two methods of providing the required drying heat (wet wood chips furnace and oil burner) are considered. In Scenario 2_a, wet wood chips are used as fuel to generate the required drying gas; in Scenario 2_b, oil is used as fuel.

In all simulations, poplar wood chips are dried from a moisture content of 50 % to a moisture content of 10 %. In Figure 52, the required fuel heat input for drying wood chip mass flow corresponding to 10 % CFR is shown.

Dieses Werk ist copyrightgeschützt und darf in keiner Form vervielfältigt werden noch an Dritte weitergegeben werden.
Es gilt nur für den persönlichen Gebrauch.

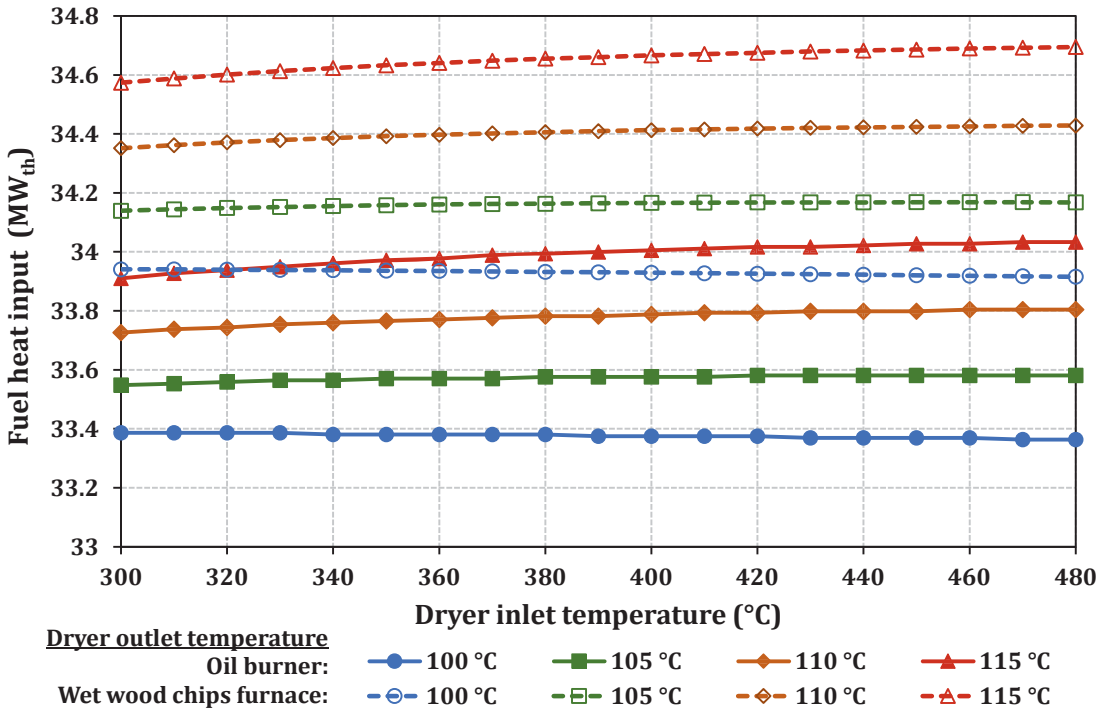

Figure 52: Necessary fuel heat input for a stand-alone direct rotary dryer for drying wood chip mass flow corresponding to 10 % CFR

The dryer inlet temperature is varied from 300 °C to 480 °C, and the dryer outlet temperature is varied from 100 °C to 115 °C, each in steps of 5 K. Due to differing flue gas properties, the required heat input is generally lower if the fuel used for drying gas production is oil, compared to producing drying gas by firing wet wood chips [62]. As oil has a comparatively high hydrogen content, the water vapour content in the resulting drying gas is slightly higher than in the case of the wet wood chips fired furnace. Consequently, different flue gas heat capacities result for the two scenarios. For a constant dryer outlet temperature, the necessary fuel heat input is barely affected by the dryer inlet temperature. In the case of the oil burner, the required heat input from fuel can slightly exceed 34 MW_{th} for an outlet temperature of 115 °C and can be lower than 33.4 MW_{th} for an outlet temperature of 100 °C. If the dryer's heat duty is covered by burning wet wood chips, the required heat input from fuel can reach 34.7 MW_{th} for an outlet temperature of 115 °C and can be as low as 34.9 MW_{th} for an outlet temperature of 100 °C. The chosen dryer outlet temperature should therefore be as low as possible.

The electrical power demand of the stand-alone rotating drum dryer is shown in Figure 53. The dryer inlet temperature is again varied from 300 °C to 480 °C, and the

Dieses Werk ist copyrightgeschützt und darf in keiner Form vervielfältigt werden noch an Dritte weitergegeben werden.
Es gilt nur für den persönlichen Gebrauch.

dryer outlet temperature is varied from 100 °C to 115 °C, each in steps of 5 K.

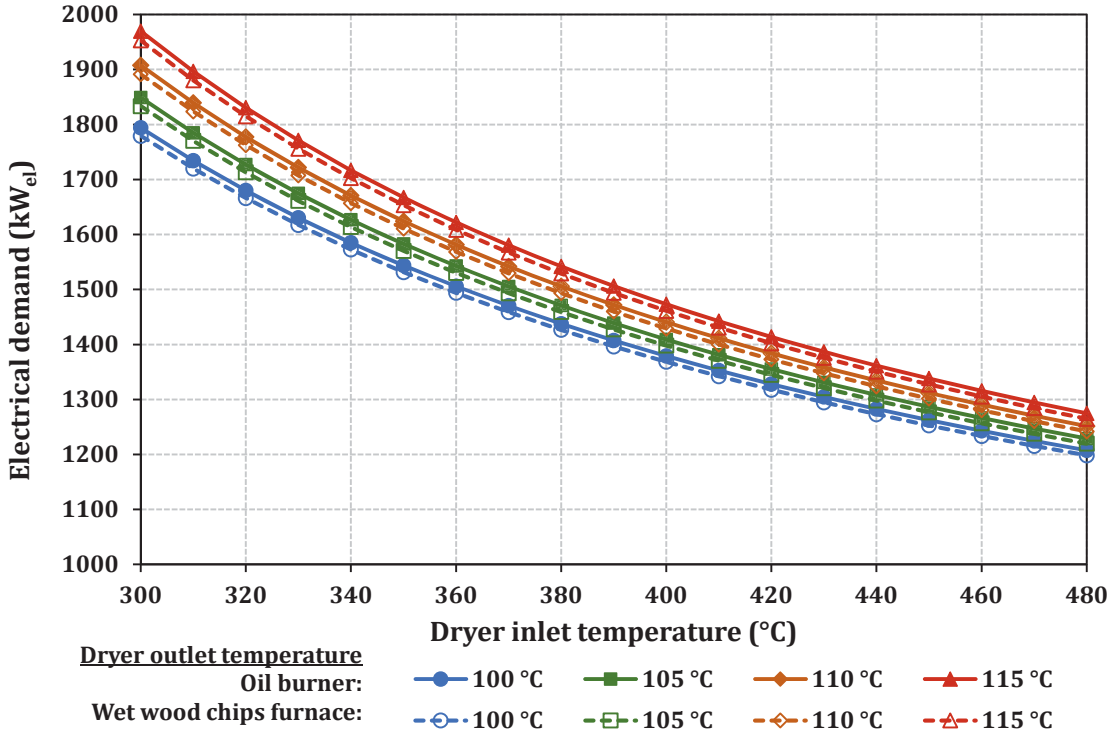

Figure 53: Electrical demand of a standalone direct rotary dryer

The electrical demand of a direct rotary dryer consists of constant demand for turning the dryer and variable demand of the flue gas fan. In contrast to the required heat input, the electrical demand is largely determined by the dryer inlet temperature. With higher dryer inlet temperatures, less drying gas needs to be recycled to cool down the flue gas, and less drying gas mass flow is required [62]. The recycle ratio *R* is defined as the ratio between recycled drying exhaust gas and total exhaust gas. With declining dryer outlet temperatures, less gas needs to be recycled to reach the chosen dryer inlet temperature, and the recycle ratio *R* declines. As a result, electrical demand declines further with declining dryer outlet temperatures [62]. As the wet wood chips furnace produces flue gas of a lower temperature than the oil burner, a lower recycle ratio *R* is necessary. This results in lower electrical demand than for the dryer heated by an oil burner.

To achieve the lowest possible energy demand, the dryer inlet temperature should be as high as possible and the dryer outlet temperature should be as low as possible. The dryer inlet temperature is limited, as self-ignition and any decomposition reactions must be avoided. The dryer outlet temperature is also limited, as

Dieses Werk ist copyrightgeschützt und darf in keiner Form vervielfältigt werden noch an Dritte weitergegeben werden.
Es gilt nur für den persönlichen Gebrauch.

condensation of vapour on particles and operation equipment has to be avoided. For the best-case operation point, the dryer inlet temperature is set to 450 °C and the dryer outlet temperature is set to 105 °C [62], [68].

The terminal temperature difference in the combustion air preheater was 35 K in all previous simulations and analyses. In contrast to most other process parameters, the air preheater's terminal temperature difference is not fixed to a certain value by boundary conditions, but depends on the design of the air preheater. A sensitivity analysis of the terminal temperature difference is carried out to determine this parameter's influence on the drying processes' energy demand. The results for varying the terminal temperature difference in the air preheater from 20 K to 50 K are shown in Figure 54.

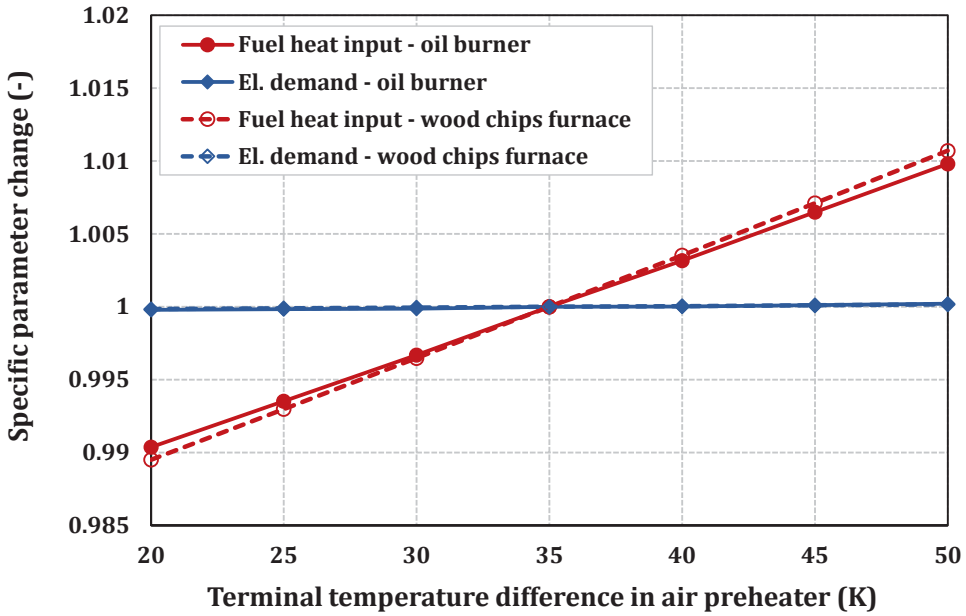

Figure 54: Sensitivity analysis of the air preheater's terminal temperature difference

There is no visible influence on the rotary dryer's electrical demand caused by the air preheater's terminal temperature difference. The required fuel heat input changes by 0.067 % per Kelvin for a varying terminal temperature difference.

Even though setting the terminal temperature difference as low as possible seems desirable to reduce the fuel demand, this is limited by the drying gas dew point temperature. In the case of the wet wood chips fired furnace, condensation of the flue gas mass flow occurs for a terminal temperature difference of 28 K and lower. In the case of the oil burner, condensation will occur with a terminal temperature

Dieses Werk ist copyrightgeschützt und darf in keiner Form vervielfältigt werden noch an Dritte weitergegeben werden.
Es gilt nur für den persönlichen Gebrauch.

difference as low as 33 K, due to the higher initial water vapour content in the flue gas, which is caused by a comparatively high fuel hydrogen content. Therefore, the set terminal temperature difference in the air preheater remains at 35 K. Figure 55 illustrates how the drying gas mass flow can be used to heat up the cold combustion air from 15 °C to 77 °C. The drying gas leaves the dryer with a temperature of 105 °C and reaches a temperature of 112 °C downstream of the drying gas fan. It is cooled down to 80.8 °C in the air preheater.

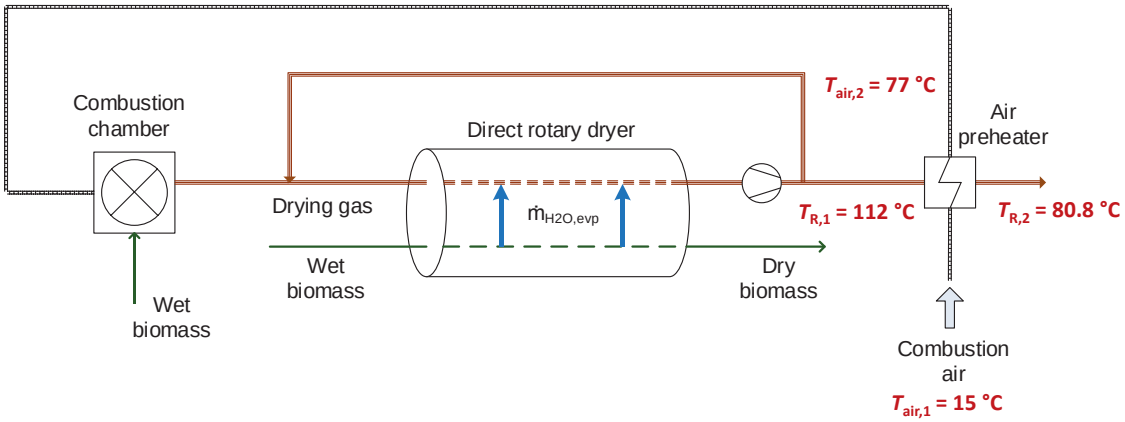

Figure 55: Stand-alone direct rotary dryer - resulting air and flue gas temperatures for combustion air preheating

Table 11 shows the resulting key parameters for the best-case operation point for both variations of heating the direct rotary dryer, the oil burner and the wet wood chips furnace.

Table 11: Drying gas results for a rotary dryer heated by an oil burner or a wet wood chips fired furnace ($T_{dry,in}$ = 450 °C, $T_{dry,out}$ = 105 °C)

	Oil burner	Wet wood chips fired furnace
$x_{H_2O,dg}$ (%)	26.0	25.6
$x_{O_2,dg}$ (%)	8.9	8.3
$\dot{m}_{dg}$ (kg/s)	63.4	63.6
T_{fg} (°C)	1195.3	958.4
R (-)	0.57	0.50
T_R (°C)	112.2	112.1

Dieses Werk ist copyrightgeschützt und darf in keiner Form vervielfältigt werden noch an Dritte weitergegeben werden.
Es gilt nur für den persönlichen Gebrauch.

The water vapour content in the drying gas $x_{H_2O,dg}$ must not be too high as, during the direct contact drying, condensation on cooler particles or equipment surfaces has to be avoided. However, in both cases this risk is sufficiently limited. Due to the fuel composition, the water vapour content in the drying gas is slightly higher when using an oil burner.

The oxygen content in the drying gas $x_{O_2,dg}$ is a critical parameter and for safety reasons must not exceed 10 % [55]. It is slightly higher when the heat demand is covered by the oil burner. Even though both fuels are burnt with the same excess air ratio, the differing fuel composition results in a comparatively higher share of oxygen in the flue gas after combustion when oil is used as fuel.

The differing drying gas composition and thus differing properties, such as heat capacity, lead to small variations in required drying gas mass flow $\dot{m}_{dg}$ and flue gas temperature upstream of the air preheater. This temperature is equivalent to the recycle temperature T_R.

Due to the significantly higher heating value of oil compared to wet wood chips, the adiabatic flame temperature, and thus the flue gas temperature after combustion T_{fg}, is clearly higher in the case of the oil burner. As the flue gas mass flow needs to be cooled down to the same drying gas temperature in both variations, more drying gas needs to be recycled in the case of the oil burner. This is depicted in a higher recycle ratio *R*.

7.3 Scenario 3 – integrated on-site drying by a direct rotary dryer

In Scenario 3, the wet wood chips are transported to the power plant and dried with an integrated direct rotary dryer. The model described in Chapter 5.3.3 is used to analyse how the integrated drying affects the power generation process (see Figure 25).

The results in the previous section clearly showed that the dryer inlet temperature should be as high as possible for an efficient drying process. It is therefore not varied in the simulations and remains at around 360 °C, which is the flue gas temperature upstream of the air preheater. Three dryer outlet temperatures have been chosen to evaluate the effects on the overall power generation process: 140 °C, 150 °C and 160 °C. The dried biomass mass flow always corresponds to the co-firing rate.

Dieses Werk ist copyrightgeschützt und darf in keiner Form vervielfältigt werden noch an Dritte weitergegeben werden.
Es gilt nur für den persönlichen Gebrauch.

As less flue gas will be available in the air preheater, the steam air heater is required to ensure sufficient air preheating. A decline in efficiency is expected as a result of this steam extraction. However, the required air preheating can only be realised up to 30 % CFR, as even with additional air preheating by the steam air heater, the required mean temperature of 90 °C at the cold end of the air preheater could no longer be reached. Co-firing of poplar wood chips that are dried in an integrated rotary dryer is thus limited to a maximum 30 % CFR.

Figure 56 shows the resulting shares of flue gas mass flow available for air preheating and used for drying, in the case of a dryer outlet temperature of 160 °C. To dry the poplar wood chips from a moisture content of 50 % to a moisture content of 10 %, up to 48.5 % (for 30 % CFR) of the total flue gas mass flow is required.

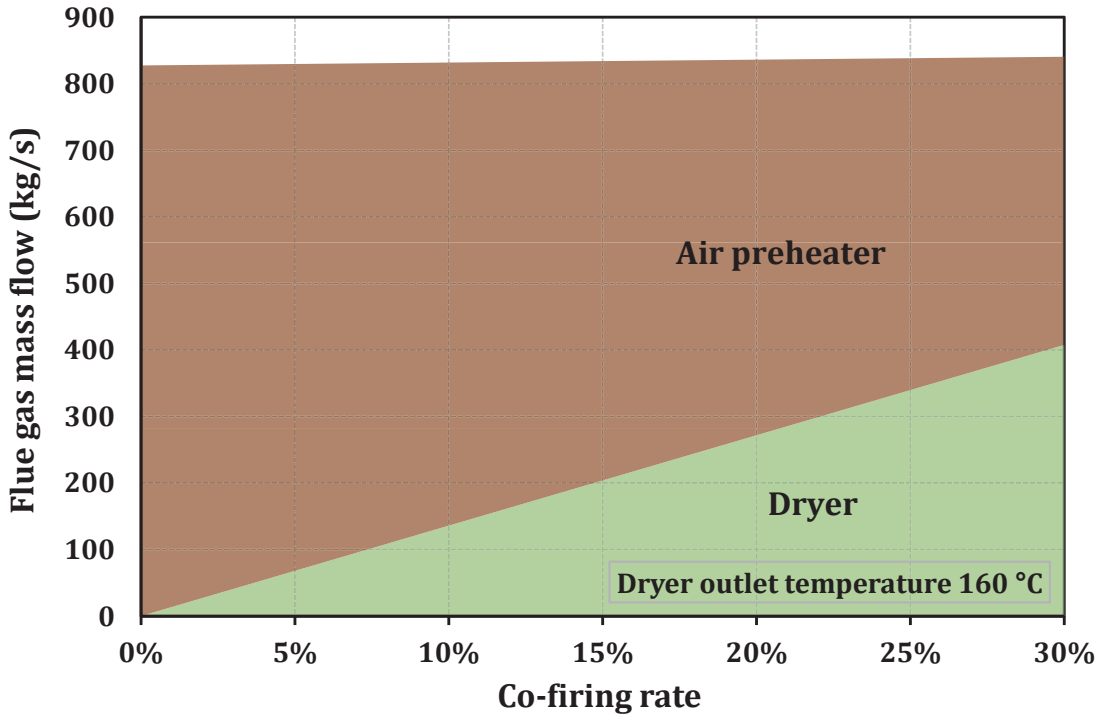

Figure 56: Flue gas mass flow shares for air preheater and dryer for a dryer outlet temperature of 160 °C, in relation to the co-firing rate

As the flue gas temperatures decline in several process steps along the flue gas track due to flue gas extraction for drying, the risks of sulphuric acid corrosion could increase. To determine these risks, the sulphuric acid dew point temperatures are calculated with Eq. 7.1 according to VERHOFF [70]:

Dieses Werk ist copyrightgeschützt und darf in keiner Form vervielfältigt werden noch an Dritte weitergegeben werden.
Es gilt nur für den persönlichen Gebrauch.

$$(1/\vartheta_{DP}) = 0.002276 - 0.00002943 \ln p_{H_2O} - 0.0000858 \ln p_{H_2SO_4} + 0.00000620(\ln p_{H_2SO_4})(\ln p_{H_2O}). \quad (7.1)$$

Here, ϑ_{DP} is the sulphuric acid dew point temperature in K, and p_{H_2O} and $p_{H_2SO_4}$ are the water and sulphuric acid partial pressures in mmHg. The water vapour partial pressure is obtained as a direct simulation result. The sulphuric acid partial pressure is calculated based on the assumption that 2 % of the SO_2 formed during combustion reacts to H_2SO_4 in the furnace and another 0.6 % of SO_2 reacts to H_2SO_4 due to the SCR.

The simulation results for flue gas temperatures downstream of the dryer fan, dryer and air preheater, as well as upstream of the ESP, are presented together with the calculated results for the corresponding sulphuric acid dew point temperatures. The results for a dryer outlet temperature of 140 °C are shown in Figure 57, the results for a dryer outlet temperature of 150 °C are shown in Figure 58 and the results for a dryer outlet temperature of 160 °C are shown in Figure 59.

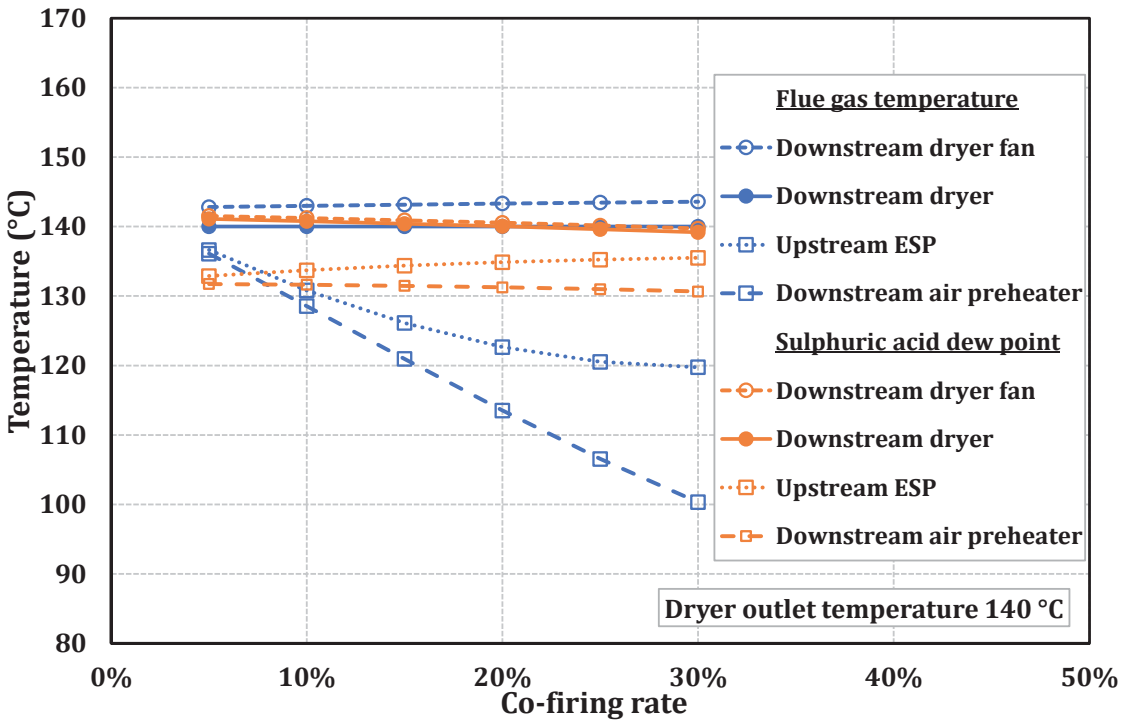

Figure 57: Flue gas and sulphuric acid dew point temperatures of an integrated rotary dryer for a dryer outlet temperature of 140 °C, in relation to the co-firing rate

Dieses Werk ist copyrightgeschützt und darf in keiner Form vervielfältigt werden noch an Dritte weitergegeben werden.
Es gilt nur für den persönlichen Gebrauch.

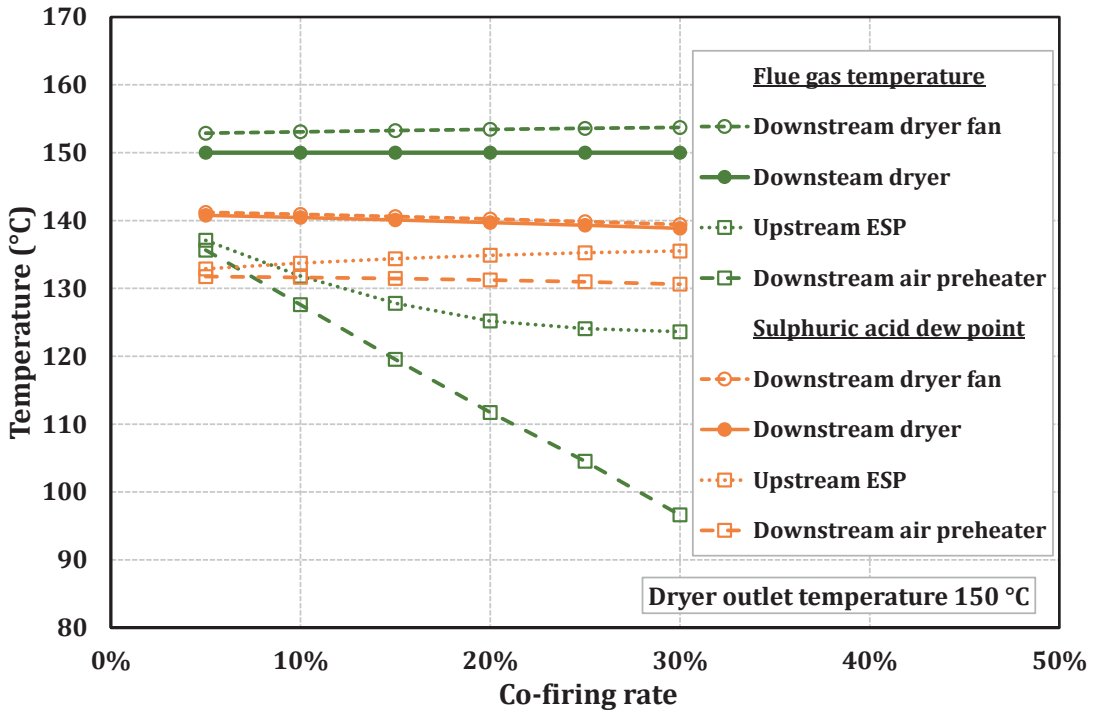

Figure 58: Flue gas and sulphuric acid dew point temperatures of an integrated rotary dryer for a dryer outlet temperature of 150 °C, in relation to the co-firing rate

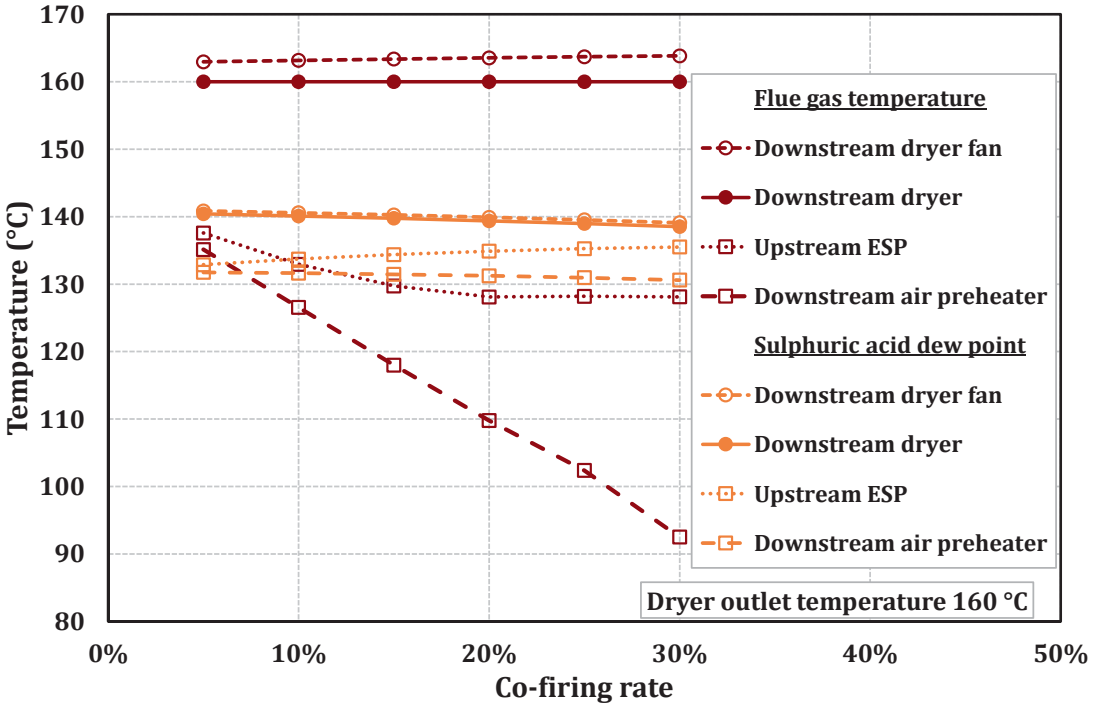

Figure 59: Flue gas and sulphuric acid dew point temperatures of an integrated rotary dryer for a dryer outlet temperature of 160 °C, in relation to the co-firing rate

Dieses Werk ist copyrightgeschützt und darf in keiner Form vervielfältigt werden noch an Dritte weitergegeben werden.
Es gilt nur für den persönlichen Gebrauch.

In all cases, the flue gas temperature downstream of the dryer fan is slightly higher than the flue gas temperature downstream of the dryer. Both temperatures are independent of the co-firing rate and remain constant for each chosen dryer outlet temperature.

As shown in Figure 56, an increasing flue gas mass flow is extracted with rising co-firing rates for drying upstream of the air preheater and reintegrated downstream of it. This results in a significant decline in the flue gas temperature downstream of the air preheater. The higher the dryer outlet temperature, the more flue gas mass flow is required for drying. Therefore, the decline in flue gas temperature downstream of the air preheater is intensified by rising dryer outlet temperatures. The flue gas temperature downstream of the air preheater would be as low as 93 °C for 30 % CFR, in the case of a dryer outlet temperature of 160 °C.

The flue gas temperature upstream of the ESP results from the mixing of the flue gas mass flow that leaves the dryer with the flue gas mass flow that has been cooled down in the air preheater. It declines in all cases, but the decline is always decelerated or almost stopped when the CFR is increased. This is caused by the rising share of flue gas leaving the dryer compared to the amount of flue gas leaving the air preheater. Figure 60 shows the heat flow downstream of the air preheater and downstream of the dryer, for a dryer outlet temperature of 160 °C. The mixed and resulting heat flow upstream of the ESP is also shown in Figure 60. The comparatively warmer drying gas mass flow leads to a weaker decline in flue gas temperature upstream of the ESP. The decline consequently also loses intensity for higher dryer outlet temperatures.

Dieses Werk ist copyrightgeschützt und darf in keiner Form vervielfältigt werden noch an Dritte weitergegeben werden.
Es gilt nur für den persönlichen Gebrauch.

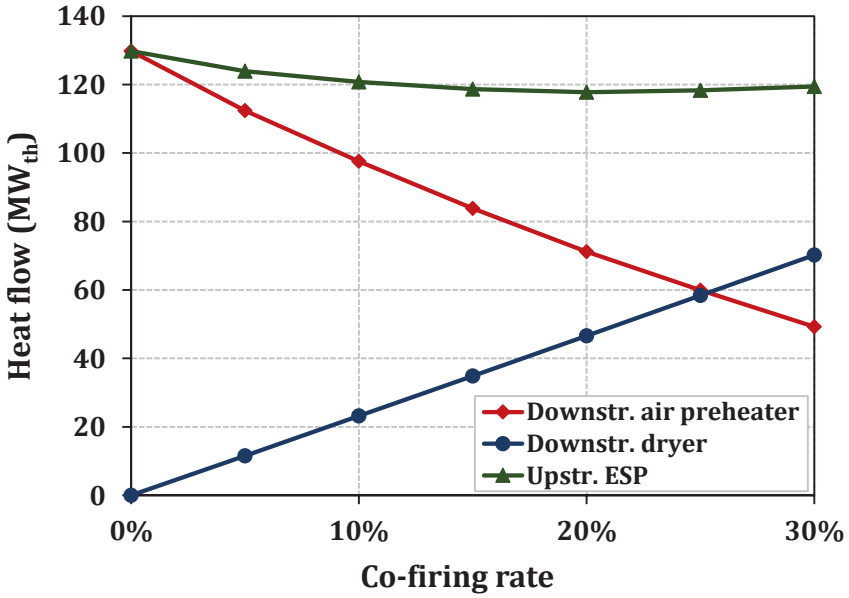

Figure 60: Flue gas heat flow downstream of the air preheater, downstream of the dryer and upstream of the ESP for a dryer outlet temperature of 160 °C, in relation to the co-firing rate

According to Eq. 7.1, the sulphuric acid dew point temperature depends on water vapour partial pressure and sulphuric acid partial pressure. With increasing CFR, the total sulphur content in the fuel declines and, as a direct consequence, the sulphuric acid partial pressure also declines. A slightly decreasing sulphuric acid dew point temperature downstream of the air preheater is the result.

The significant increase in water vapour partial pressure in the dryer causes a noticeably higher sulphuric acid dew point temperature downstream of the dryer and dryer fan compared to downstream of the air preheater. The declining tendency for higher CFR remains.

The flue gas composition, which determines the sulphuric acid dew point temperature upstream of the ESP, is dependent on the share of flue gas mass flow used for drying, which increases with rising CFR. As a result, the water vapour partial pressure and thereby the sulphuric acid dew point temperature upstream of the ESP increase with rising CFR.

To avoid corrosion, the flue gas temperature should always be higher than the sulphuric acid dew point temperature. Figure 57, Figure 58 and Figure 59 show that, for all dryer outlet temperatures, this criterion is only met for 5 % CFR. If the co-firing rate is further increased, the air preheater and also the ESP would be at risk

Dieses Werk ist copyrightgeschützt und darf in keiner Form vervielfältigt werden noch an Dritte weitergegeben werden.
Es gilt nur für den persönlichen Gebrauch.

of severe corrosion. For a dryer outlet temperature of 140 °C, the dryer itself would also be threatened by corrosion, even at 5 % CFR. This leaves only two possible operation points for biomass co-firing with integrated on-site drying using a direct rotary dryer:

- 5 % CFR with a dryer outlet temperature of 150 °C
- 5 % CFR with a dryer outlet temperature of 160 °C

As a low dryer outlet temperature is targeted to realise an energy-efficient drying process, the first operation point is chosen for further analyses and comparisons. Table 12 shows the resulting net efficiency (η_{net}), gross efficiency (η_{gross}), electrical net power output ($P_{\mathrm{el,net}}$) and electrical gross power output ($P_{\mathrm{el,gross}}$).

Table 12: Net and gross efficiency and power output for Scenario 3 (dryer outlet temperature 150 °C)

	η_{net} (%)	η_{gross} (%)	$P_{\mathrm{el,net}}$ ($\mathrm{MW_{el}}$)	$P_{\mathrm{el,gross}}$ ($\mathrm{MW_{el}}$)
0 % CFR	39.60	42.92	763.23	827.41
5 % CFR	39.32	42.26	758.12	826.34

7.4 Comparison of scenarios

This thesis aims to identify the most favourable drying scenario for co-firing poplar wood chips with coal at co-firing rates up to 50 %, based on fuel heat input. The most favourable scenario is determined by technical feasibility, efficient energy utilisation and low total resulting CO_2 emissions. The overall energy utilisation efficiency and the total resulting CO_2 emissions are calculated in the following sections.

The CO_2 emissions caused by power generation are directly reduced by substituting the fossil fuel coal with the renewable fuel wood. As the wood has to be dried, the CO_2 emissions resulting from this process need to be added. For the stand-alone Scenarios 2_a and 2_b, emissions related to drying can be considered separately. For the integrated Scenarios 1_a, 1_b and 3, they are included in the emissions resulting from power generation. In all scenarios, the biomass fuel (either wet or dried) needs to be transported from a short-rotation plantation to the power plant site. To complete the CO_2 balance, the occurring transport-related CO_2 emissions are calculated and added.

Dieses Werk ist copyrightgeschützt und darf in keiner Form vervielfältigt werden noch an Dritte weitergegeben werden.
Es gilt nur für den persönlichen Gebrauch.

In contrast to the gross or net efficiency, which are used to rate the power generation process, the overall energy utilisation efficiency additionally considers the energy spent for the decentralised biomass drying processes. With regard to the decentralised Scenarios 2_a and 2_b this approach is necessary to compare the efficiency of energy utilisation of all scenarios on an equal basis. The resulting net power generation is reduced by the electrical power demand for drying and put into relation with the thermal heat input for power generation and drying.

For a concluding evaluation of the regarded drying processes, the results for total CO_2 emissions and overall energy utilisation efficiency are considered below. Additionally, possibilities and restrictions of technical realisation are discussed for each scenario.

7.4.1 Transport related CO_2 emissions

While power generation and drying have already been analysed in detail in the previous sections, the transportation of the co-fired wood chips is considered separately here. The CO_2 emissions caused by biomass transport mainly depend on the following:

- transportation distance
- means of transport
- bulk density of wood chips

Long transportation distances should be avoided in order to maintain the greenhouse gas-reducing effect of biomass co-firing. The short-rotation plantations are assumed to be 50 km away from the power plant site.

The most common means of transport for wood chips over such a distance is semi-trailer trucks; specialised versions of these trucks that have been designed for the transport of wood chips are available. Their fuel consumption, which determines the resulting CO_2 emissions, depends on the load and thereby on the bulk density of the wood chips. The semi-trailer trucks under consideration can be loaded with a maximum capacity of 24 tonnes. Specific values a_{bm} for CO_2 emissions per tonne and per 100 km are determined using the Eco TransIT World tool [71] and listed in Table 13 together with the resulting specific CO_2 emissions b_{bm} per kilogram of biomass for a transport distance of 50 km.

Dieses Werk ist copyrightgeschützt und darf in keiner Form vervielfältigt werden noch an Dritte weitergegeben werden.
Es gilt nur für den persönlichen Gebrauch.

Table 13: Specific CO_2 emissions for wood chip transport

	Wood chip moisture content	
	10 %	**50 %**
$a_{bm}\left(\frac{kg_{CO_2}}{t_{bm} \cdot 100\ km}\right)$	9.476	7.330
$b_{bm}\left(\frac{g_{CO_2}}{kg_{bm}}\right)$	4.738	3.665

As truck transport is designed for high-density loads, its capacity utilisation is better when transporting wet wood chips with a higher bulk density. This results in specifically higher CO_2 emissions for the transport of dried wood chips with a moisture content of 10 %.

7.4.2 Total resulting CO_2 emissions

The total resulting CO_2 emissions $E_{CO_2,tot}$ for power generation with biomass co-firing, including drying and transport of the biomass fuel, are calculated according to Eq. 7.2. To gain comparable results, the CO_2 mass per electrical power output is specified in g_{CO2} per kWh_{el}:

$$E_{CO_2,tot} = \left(\dot{m}_{CO_2,PG} + \dot{m}_{CO_2,T} + \dot{m}_{CO_2,D}\right) \cdot \frac{3600}{P_{el,PG,net}} \text{ in } \frac{g_{CO_2}}{kWh_{el}}. \quad (7.2)$$

The CO_2 mass flow resulting from power generation $\dot{m}_{CO_2,PG}$, the CO_2 mass flow resulting from transport $\dot{m}_{CO_2,T}$ and the CO_2 mass flow resulting from drying $\dot{m}_{CO_2,D}$ are added together and divided by the net electrical power output $P_{el,PG,net}$. All mass flows need to be in kg/s and the electrical power output in MW_{el}. The calculation method can be applied for all co-firing rates. Here, results are always calculated for full-load operation.

The CO_2 mass flow resulting from power generation is calculated according to Eq. 7.3:

$$\dot{m}_{CO_2,PG} = \dot{m}_{fg,C} \cdot x_{CO_2,fg,C} \text{ in } \frac{kg_{CO_2}}{s}. \quad (7.3)$$

As the combustion of biomass is considered to be carbon neural, the resulting CO_2 emissions are determined by the flue gas mass flow generated by coal

Dieses Werk ist copyrightgeschützt und darf in keiner Form vervielfältigt werden noch an Dritte weitergegeben werden.
Es gilt nur für den persönlichen Gebrauch.

combustion $\dot{m}_{\mathrm{fg,C}}$ and the resulting CO_2 mass share in the according flue gas $x_{\mathrm{CO_2,fg,C}}$, resulting from coal combustion.

The CO_2 mass flow resulting from transporting the required amount of poplar wood chips from a short-rotation plantation to the power plant is calculated with Eq. 7.4:

$$\dot{m}_{\mathrm{CO_2,T}} = b_{\mathrm{bm}} \cdot LHV_{\mathrm{bm}} \cdot \dot{m}_{\mathrm{bm,T}} \text{ in } \frac{\mathrm{kg_{CO_2}}}{\mathrm{s}}. \quad (7.4)$$

The specific emission factor b_{bm} is multiplied by the wood chips' lower heating value $H_{\mathrm{U,bm}}$ and the wood chip mass flow $\dot{m}_{\mathrm{bm,T}}$. The lower heating value depends on the fuel moisture content. The transported fuel mass flow depends on the fuel moisture content as well as on the co-firing rate.

The CO_2 mass flow resulting from drying poplar wood chips in a stand-alone rotary dryer is calculated with Eq. 7.5:

$$\dot{m}_{\mathrm{CO_2,D}} = \dot{m}_{\mathrm{CO_2,D,f}} + \dot{m}_{\mathrm{CO_2,D,el}} \text{ in } \frac{\mathrm{kg_{CO_2}}}{\mathrm{s}}. \quad (7.5)$$

This is the sum of the CO_2 mass flow resulting from fuel combustion $\dot{m}_{\mathrm{CO_2,D,f}}$ and the CO_2 mass flow resulting from electricity consumption $\dot{m}_{\mathrm{CO_2,D,el}}$. The CO_2 emissions due to fuel combustion are calculated with Eq. 7.6:

$$\dot{m}_{\mathrm{CO_2,D,f}} = \dot{m}_{\mathrm{fg,oil}} \cdot x_{\mathrm{CO_2,fg,D}} \text{ in } \frac{\mathrm{kg_{CO_2}}}{\mathrm{s}}. \quad (7.6)$$

Again, the combustion of wet wood chips for drying gas production is considered to be carbon neutral. Therefore, only the flue gas mass flow resulting from oil combustion $\dot{m}_{\mathrm{FG,oil}}$ and the resulting CO_2 mass share in the flue gas $x_{\mathrm{CO_2,fg,D}}$ are considered.

The CO_2 mass flow resulting from the dryer's electricity consumption $P_{\mathrm{el,D}}$ is calculated with Eq. 7.8:

$$\dot{m}_{\mathrm{CO_2,D,el}} = P_{\mathrm{el,D}} \cdot e \cdot \frac{1}{3600} \text{ in } \frac{\mathrm{kg_{CO_2}}}{\mathrm{s}}. \quad (7.8)$$

Here, the factor e is the average value for CO_2 emissions caused by power generation in Germany. For the year 2014, e is 569 g_{CO2}/kWh_{el} [1].

As Scenario 3 (integrated drying with direct rotary dryer) is only possible for 5 % CFR, the total resulting CO_2 emissions are calculated for all three scenarios for

Dieses Werk ist copyrightgeschützt und darf in keiner Form vervielfältigt werden noch an Dritte weitergegeben werden.
Es gilt nur für den persönlichen Gebrauch.

5 % CFR, using the relevant simulation results. The results are compared to the CO_2 emissions resulting from coal-only power generation in Figure 61.

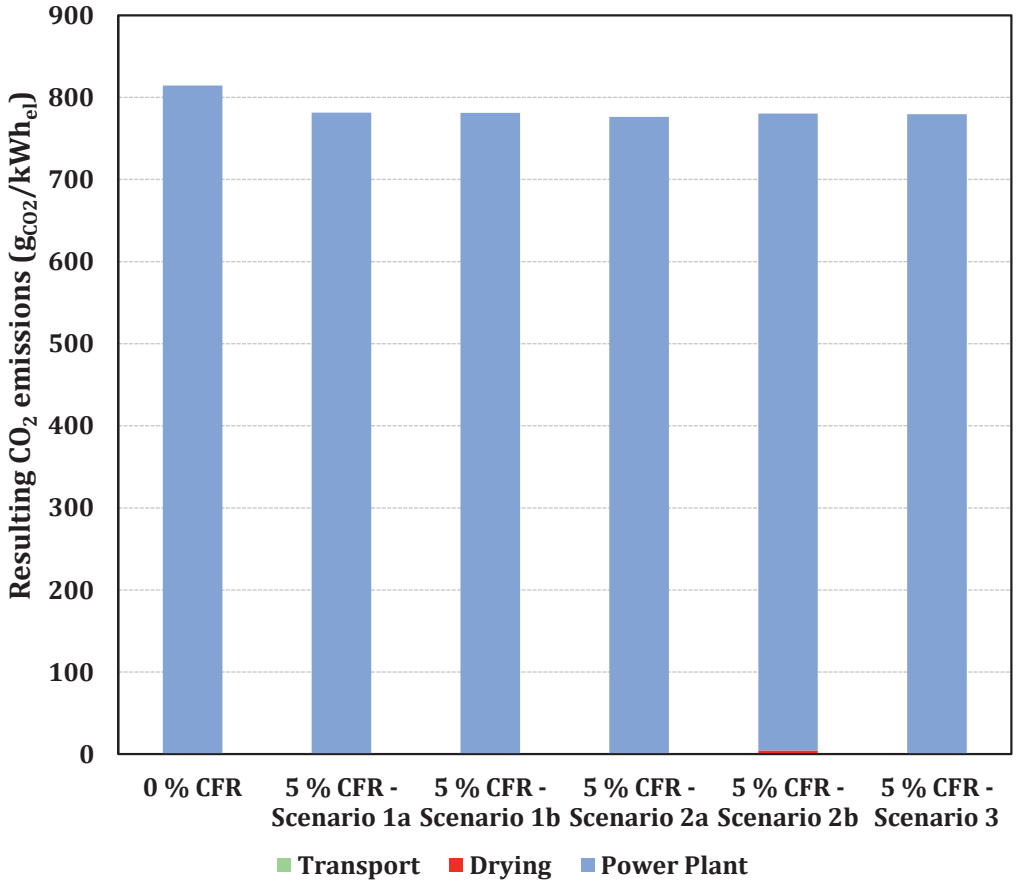

Figure 61: Total resulting CO_2 emissions for all drying scenarios at 5 % CFR compared to coal-only

The CO_2 emissions caused by power generation obviously dominate the total resulting emissions. In all scenarios, the emissions related to biomass transport only make up 0.02 % of the total resulting CO_2 emissions. In Scenario 2_a, almost no CO_2 emissions for drying occur. In Scenario 2_b, around 0.57 % of the total resulting CO_2 emissions are caused by drying. Emissions caused by biomass drying and transport thus barely affect the total resulting CO_2 emissions.

For 5 % CFR, no outstanding differences between the drying scenarios are visible. Nonetheless, Scenario 2_a is most effective in reducing CO_2 emissions by biomass co-firing. Emissions can be reduced by 4.69 %, compared to coal-only. In Scenario 2_b, CO_2 emissions can be reduced by 4.21 %. This difference is due to the CO_2 emissions caused by fossil fuel combustion for drying. Comparing the three integrated

Dieses Werk ist copyrightgeschützt und darf in keiner Form vervielfältigt werden noch an Dritte weitergegeben werden.
Es gilt nur für den persönlichen Gebrauch.

Scenarios 1_a, 1_b and 3 shows that extracting flue gas for drying is slightly more beneficial than extracting steam for an integrated drying process. Scenario 1_b is slightly more effective in reducing emissions than Scenario 1_a, which is due to the higher net efficiency in Scenario 1_b. Emissions can be reduced by 4.05 % in Scenario 1_a, 4.10 % in Scenario 1_b and 4.31 % in Scenario 3. However, due to technical limitations, a higher co-firing rate cannot be realised in Scenario 3. To determine the reachable reduction in CO_2 emissions for high co-firing rates, the total resulting CO_2 emissions for Scenarios 1_a, 1_b, 2_a and 2_b are calculated for 50 % CFR, using the described method and relevant simulation results. The results are again compared to the CO_2 emissions from coal-only power generation and displayed in Figure 62.

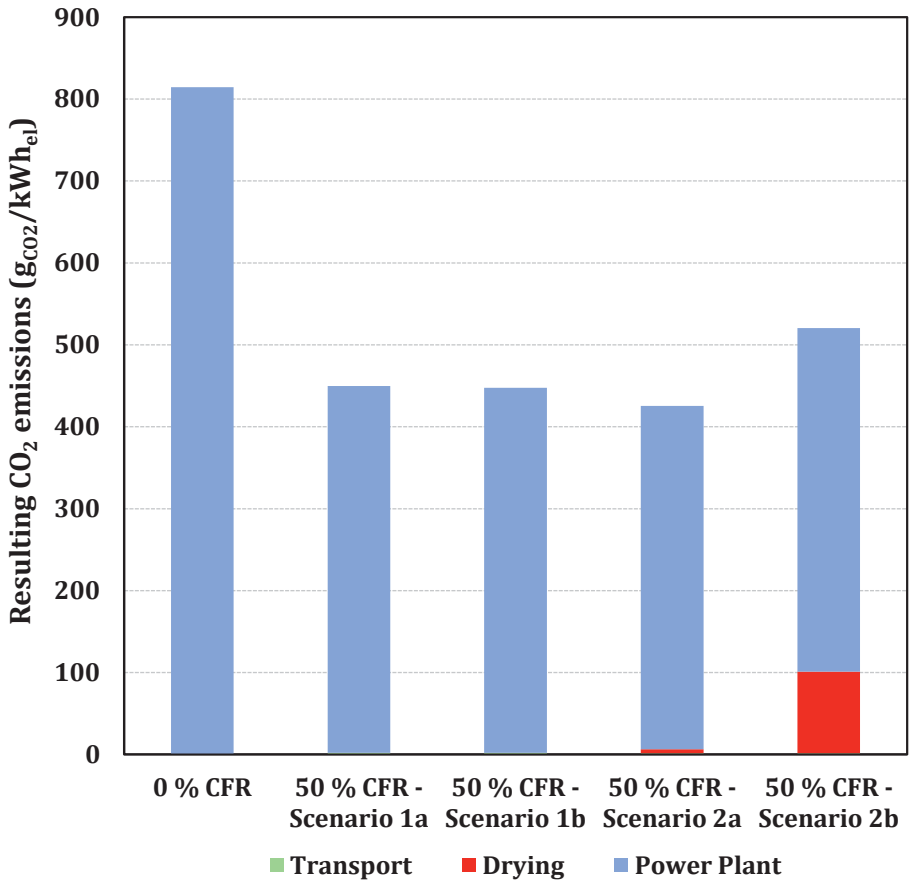

Figure 62: Total resulting CO_2 emissions for Scenarios 1 and 2 at 50 % CFR compared to coal-only power generation

As expected, CO_2 emissions from power generation can be drastically reduced by substituting 50 % of the fuel heat input with a renewable fuel. Again, the

Dieses Werk ist copyrightgeschützt und darf in keiner Form vervielfältigt werden noch an Dritte weitergegeben werden.
Es gilt nur für den persönlichen Gebrauch.

transport-related CO_2 emissions form only a very small part of the total resulting CO_2 emissions. In Scenario 1_a and 1_b, a mass flow of wet poplar wood chips corresponding to half the power plant's fuel heat input needs to be transported. The resulting CO_2 emissions are about 0.5 % of the total emissions in each scenario.

Scenario 2_a, by co-firing dried poplar wood chips cultivated in a nearby short-rotation plantation, is clearly most effective in reducing CO_2 emissions. For 50 % CFR, total CO_2 emissions can be reduced by 47.77%. In Scenario 2_b, as much CO_2 is emitted due to transport and power generation as in Scenario 2_a. In both scenarios, emissions due to power generation are 51.5 % of the CO_2 emissions due to coal-only power generation. Even though 50 % of the fuel heat input is substituted with biomass, the resulting CO_2 emissions cannot be reduced by the same magnitude, since biomass co-firing affects the power generation process and, thus, results in a comparatively lower net electrical power output. The difference in drying-related CO_2 emissions between Scenario 2_a and 2_b is due to fossil fuel utilisation for heat demand covering. In Scenario 2_a, only 1.15 % of the total CO_2 emissions are related to the drying process. In Scenario 2_b, this share is significantly higher and almost 20 % of the total CO_2 emissions are released during the biomass drying process. The total resulting CO_2 emissions can be reduced by 36.04 % for 50 % CFR in Scenario 2_b. The development of the total resulting CO_2 emissions for increasing co-firing rates is shown in Figure 63 for all drying scenarios.

Dieses Werk ist copyrightgeschützt und darf in keiner Form vervielfältigt werden noch an Dritte weitergegeben werden.
Es gilt nur für den persönlichen Gebrauch.

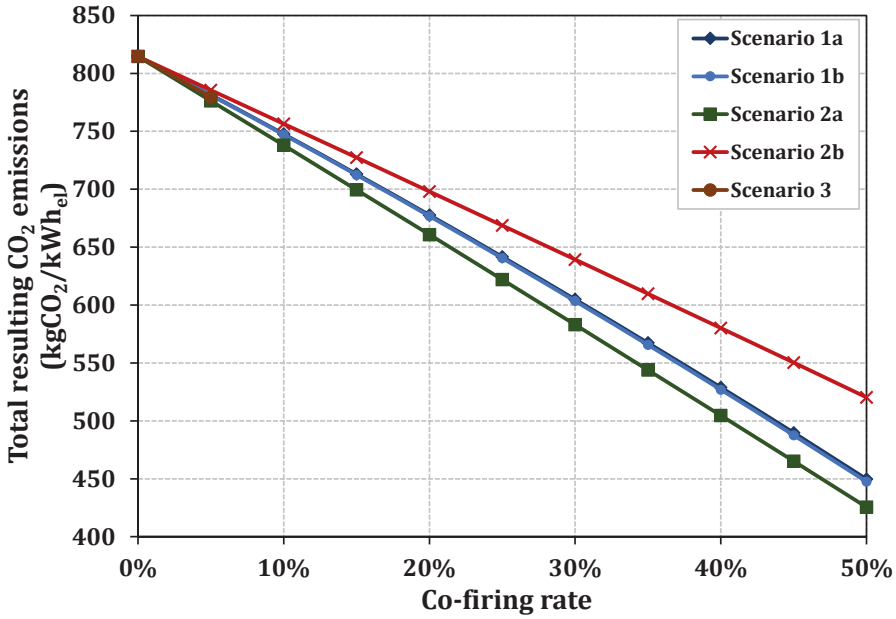

Figure 63: Total resulting CO_2 emissions for co-firing rates up to 50 % for all drying scenarios

The integrated Scenarios 1_a and 1_b show very similar results for CO_2 emission reduction through biomass co-firing, and both are more effective in reducing CO_2 emissions when co-firing biomass with coal than Scenario 2_b. For 50 % CFR, the total resulting CO_2 emissions are reduced by 44.78 % in Scenario 1_a and by 45.06 % in Scenario 1_b. For Scenario 1_a, the emissions resulting solely from power generation are 54.9 % of the emissions caused by coal-only power generation and thereby higher than the CO_2 emissions resulting from power generation in the decentralised scenarios. But the comparatively high CO_2 emissions caused by burning oil to cover the drying heat demand lead to higher total resulting CO_2 emissions in Scenario 2_b compared to Scenario 1_a and 1_b.

Due to steam extraction for drying, the net electrical power output is even further reduced in Scenario 1_a and 1_b than it is in Scenario 2_a and 2_b. The transport-related CO_2 emissions are higher in the integrated scenarios than in the decentralised scenarios. However, the share of transport related CO_2 emissions in the total resulting CO_2 emissions is so small that it could be neglected in further considerations. Of a significantly greater impact are the CO_2 emissions caused by fossil fuel for stand-alone drying in Scenario 2_b. If the same energy demand is covered with a renewable fuel, as in Scenario 2_a, the total resulting CO_2 emissions are lower than for the integrated scenarios. This result is largely determined by

Dieses Werk ist copyrightgeschützt und darf in keiner Form vervielfältigt werden noch an Dritte weitergegeben werden.
Es gilt nur für den persönlichen Gebrauch.

dryers' heat demand, as the electrical demand of all drying processes is only very low and thereby hardly influences the results.

7.4.3 Overall energy utilisation efficiency

Alongside the resulting CO_2 emissions, it is important to consider the degree of energy utilisation when comparing different drying processes and scenarios. So far only the net efficiency has been used to rate the energy utilisation of the power generation process in all scenarios. In this section, the drying scenarios will be compared using the overall energy utilisation efficiency, as defined in Eq. 4.3.

Table 14 shows the simulation and calculation results for $P_{\mathrm{el,PG,net}}$, $P_{\mathrm{el,D}}$, $\dot{Q}_{\mathrm{c,PG}}$, $\dot{Q}_{\mathrm{bm,PG}}$ and $\dot{Q}_{\mathrm{D}}$ for 5 % and 50 % CFR. The energy demand for fuel transport is not included in this analysis. The heat and electricity demand for the decentralised drying processes in Scenario 2_a and 2_b are calculated as linear upscale from the simulation results for 10 % CFR.

Table 14: Electrical net power output, electrical demand for drying and thermal heat input for all drying scenarios for 5 % and 50 % CFR

CFR	Scenario	$P_{\mathrm{el,PG,net}}$ (MW_{el})	$P_{\mathrm{el,D}}$ (MW_{el})	$\dot{Q}_{\mathrm{c,PG}}$ (MW_{th})	$\dot{Q}_{\mathrm{bm,PG}}$ (MW_{th})	$\dot{Q}_{\mathrm{D}}$ (MW_{th})
5 %	$\mathbf{1_a}$	756.06	0.00	1812.89	95.42	0.00
	$\mathbf{1_b}$	756.44	0.00	1812.89	95.42	0.00
	$\mathbf{2_a}$	761.58	0.64	1812.89	95.42	17.02
	$\mathbf{2_b}$	761.58	0.64	1812.89	95.42	16.73
	3	758.12	0.00	1812.89	95.42	0.00
50 %	$\mathbf{1_a}$	694.62	0.00	954.16	954.16	0.00
	$\mathbf{1_b}$	698.08	0.00	954.16	954.16	0.00
	$\mathbf{2_a}$	741.73	6.38	954.16	954.16	170.24
	$\mathbf{2_b}$	741.73	6.43	954.16	954.16	167.35

Even though the total fuel heat input in the power generation process remains constant, the electrical net power output differs, depending on the applied drying process and the co-firing rate. As direct co-firing does not directly affect the power plant's water-steam cycle, the net power output is highest for the decentralised

Dieses Werk ist copyrightgeschützt und darf in keiner Form vervielfältigt werden noch an Dritte weitergegeben werden.
Es gilt nur für den persönlichen Gebrauch.

Scenarios 2_a and 2_b, as expected. The development of the net power output was discussed for all scenarios in more detail in the previous chapters.

The resulting overall energy utilisation efficiency for co-firing rates up to 50 % is shown in Figure 64 for the drying Scenarios 1_a, 1_b, 2_a and 2_b. As biomass drying in an integrated direct rotary dryer is technically limited to very small co-firing rates (Scenario 3), it is only displayed for 5 % CFR.

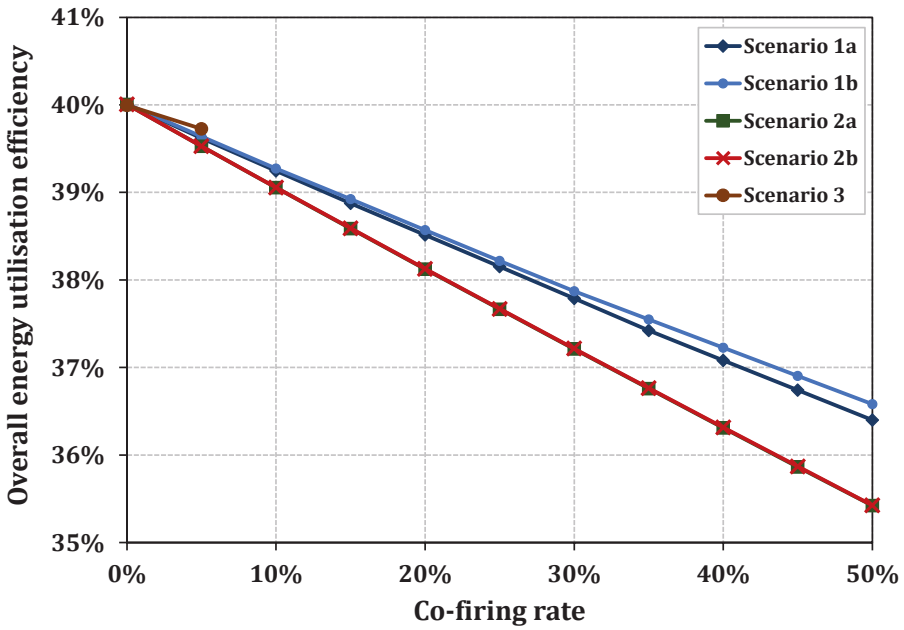

Figure 64: Overall energy utilisation efficiency for co-firing rates up to 50 % for all drying scenarios, in relation to the co-firing rate

However, as Figure 64 clearly shows, Scenario 3 is the most efficient in using the input energy. As in all integrated scenarios, no additional fuel energy is spent on a drying process. Solely the fuel heat input by coal and biomass that match the initial coal fuel heat input in the base case are used for drying and power generation. Nonetheless, the impact on the power generation process is smaller when using flue gas heat for drying than when using steam heat. Flue gas extraction for drying primarily impacts the preheating of combustion air. The resulting drop in combustion air temperature leads to a slight reduction in live steam heat production. However, this reduction has a smaller impact on the resulting net power output than the steam extraction for dryer heating in Scenarios 1_a and 1_b.

As steam of lower quality is partially used for dryer heating in Scenario 1_b, the decline in net power output is slightly less intense than for Scenario 1_a and thus the overall energy utilisation efficiency is slightly higher.

Dieses Werk ist copyrightgeschützt und darf in keiner Form vervielfältigt werden noch an Dritte weitergegeben werden.
Es gilt nur für den persönlichen Gebrauch.

The two decentralised Scenarios 2_a and 2_b show almost no difference in the resulting overall energy utilisation efficiency. The absolute net power output is highest for these scenarios; however, they are nonetheless least efficient in overall energy utilisation. An additional fuel heat input is required, which is used solely for drying, whereas in the integrated scenarios the fuel heat input is converted into steam and used for power generation in a first step, before heat for drying is extracted.

7.4.4 Alternative approach of comparison

So far the co-firing rate (CFR) has been defined as the share of biomass fuel heat input in the boiler. In an alternative approach a new co-firing rate CFR* can be defined as the share of biomass fuel heat input in the total energy balance, as described in Chapter 4. With this new approach, the biomass fuel heat input to heat the direct rotary dryer in Scenario 2_a is added to the biomass fuel heat input for power generation, to calculate the co-firing rate CFR* as in Eq. 7.9:

$$\mathrm{CFR}^* = \frac{\dot{Q}_{\mathrm{bm,D}} + \dot{Q}_{\mathrm{bm,PG}}}{\dot{Q}_{\mathrm{bm,D}} + \dot{Q}_{\mathrm{bm,PG}} + \dot{Q}_{\mathrm{C,PG}}}. \tag{7.9}$$

For a CFR of 50 % in Scenario 2_a 170.25 MW_{th} are needed to heat the direct rotary dryer. With total fuel heat input for power generation of 1908 MW_{th} (see Table 5) and share of biomass fuel heat input in the boiler of 50 %, this corresponds to a CFR* of 54 %. In Table 15 the total resulting CO_2 emissions and energy utilisation efficiency for Scenario 2_a and Scenario 1_b for 54 % CFR* in both scenarios are listed.

Table 15: Total resulting CO_2 emissions and energy utilisation efficiency for Scenario 2_a and Scenario 1_b for 54 % CFR*

	Scenario 2_a	**Scenario 1_b**
Total resulting CO_2 emissions	425.47 g_{CO_2}/kWh_{el}	416.13 g_{CO_2}/kWh_{el}
Energy utilisation efficiency	35.42 %	36.42 %

For 54 % CFR* the required coal mass flow is higher in Scenario 2_a than it is in Scenario 1_b. Thus the total resulting CO_2 emissions are lower in Scenario 1_b, which makes Scenario 1_b the most favourable for co-firing biomass with coal in regard to both energy efficiency and emission reduction, when this approach of comparison is applied. However, in most literature the co-firing rate is defined as biomass share of fuel heat input in the power generation process, without consideration of further fuel heat input for biomass pre-treatment processes.

Dieses Werk ist copyrightgeschützt und darf in keiner Form vervielfältigt werden noch an Dritte weitergegeben werden.
Es gilt nur für den persönlichen Gebrauch.

7.4.5 Concluding evaluation of drying scenarios

In the previous sections, total resulting CO_2 emissions and overall energy utilisation were analysed and compared. For a final concluding evaluation of the drying scenarios, aspects regarding the technical realisation are considered additionally below.

Regarding the total resulting CO_2 emissions, Scenario 2_a, where biomass is dried in a decentralised wet wood chips fired direct rotary dryer, is most beneficial. When regarding the overall energy utilisation, Scenario 1_b, where biomass is dried in an integrated steam-tube dryer supplied with heating steam extracted from the LP turbine and the IP/LP crossover pipe, is most efficient.

A technical advantage of the decentralised drying scenarios is the decoupling of fuel upgrading and power generation. Co-firing operation of the power plant does thereby not depend on the availability of the drying process and vice versa. In this thesis, simulations have only been carried out for full load operation of the power plant. But a hard coal fired steam power plant is estimated to reach only 4000 hours of full load operation per year in Germany. This would of course affect the drying processes in the integrated scenarios.

In part-load operation, the steam pressures in the IP/LP crossover pipe and the LP turbine decrease significantly. As a result, the drying steam quality would be reduced. The extracted steam would condense at a lower temperature than at full load operation. A reduced drying temperature would require a longer retention time of the poplar wood chips in the steam-tube dryer to avoid the product having a higher moisture content than the desired 10 %. To achieve a longer retention time of the wood chips in the dryer, the dryer's rotation speed would have to be reduced. A more favourable possibility for part load operation, in which all dryer operation parameters can remain unaltered, can be achieved in Scenario 1_a, by installing a pressure maintaining valve in the IP/LP crossover pipe downstream of the drying steam extraction. A set steam pressure level for the drying steam can be guaranteed in this way. The resulting additional pressure losses will affect the power generation in the following LP turbines [72] and thus reduce the net efficiency of the power generation process. Nonetheless, using steam extracted from the IP/LP crossover pipe and guaranteeing a certain drying steam pressure level with pressure maintaining value should is the best solution for integrated biomass drying in part-load operation.

Dieses Werk ist copyrightgeschützt und darf in keiner Form vervielfältigt werden noch an Dritte weitergegeben werden.
Es gilt nur für den persönlichen Gebrauch.

An operational advantage of Scenario 2_a and 2_b is the smaller number of trucks necessary for wood chips transportation. This is due to the significantly higher energy density of wood chips, which are dried to a moisture content of 10 %, compared to wet wood chips with a moisture content of 50 %. As was shown in Chapter 6.4.2, the transport related CO_2 emissions are negligible in comparison to those from power generation. However, transporting dried wood chips will require less trucks and thereby cause less stress to the road traffic system between short-rotation plantation and power plant.

It can be concluded that the decentralised Scenarios 2_a and 2_b offer advantages in technical realisation and operation compared to the integrated Scenarios 1_a and 1_b. When wet wood chips are used to cover the drying heat demand, Scenario 2_a is also most effective in reducing CO_2 emissions. Nonetheless, the integrated Scenario 1_b is most efficient in using the overall energy input.

Dieses Werk ist copyrightgeschützt und darf in keiner Form vervielfältigt werden noch an Dritte weitergegeben werden.
Es gilt nur für den persönlichen Gebrauch.

8 SUMMARY AND CONCLUSIONS

Substituting a fossil fuel in a power plant with a renewable fuel is a comparatively easy way to reduce CO_2 emissions. Many European power plants have already been co-firing biomass with coal using a wide range of biomass fuels, with the most important being imported white wood pellets. To avoid the environmental impacts of long transport distances and an energy-intense pre-processing of the woody biomass, wood chips cultivated in a short-rotation plantation near the power plant are considered for co-firing in this work.

The effects on the power generation process of co-firing poplar wood chips with coal in a large-scale steam power plant were analysed. Thereby, co-firing rates of up to 50 % of the fuel heat input were considered. As the wood chips' moisture content right after harvesting is too high for co-firing utilisation, drying the wood chips is essential. Therefore, as well as looking at the effects of co-firing on the boiler and the overall power generation process, several drying processes were considered in order to find the most favourable scenario for drying and co-firing poplar wood chips with coal.

Three main scenarios, for which indirect steam-tube dryers and direct rotary dryers are suitable technologies to efficiently dry large quantities of poplar wood chips, were analysed regarding their technical limitations and impacts on the power generation process. The drying scenario most efficient in reducing CO_2 emissions was then identified by calculating and comparing the total CO_2 emissions resulting from power generation, drying and transportation of wood chips to the power plant site. To determine the scenario most efficient in using the energy input, an overall energy utilisation efficiency, which takes the energy input for drying into consideration as well as for power generation, was defined.

In Scenario 1, an indirect steam-tube dryer is integrated into the power plant's water-steam cycle. Steam for drying is either extracted from the IP/LP crossover pipe (Scenario 1_a) or both the IP/LP crossover pipe and the LP turbine (Scenario 1_b). Wet wood chips are transported to the power plant and are dried prior to co-firing.

In Scenario 2, the poplar wood chips are dried prior to transportation by a stand-alone direct rotary dryer. In two variations of Scenario 2, the drying heat demand can be covered by either a wet wood chips furnace (Scenario 2_a) or an oil burner (Scenario 2_b).

Dieses Werk ist copyrightgeschützt und darf in keiner Form vervielfältigt werden noch an Dritte weitergegeben werden.
Es gilt nur für den persönlichen Gebrauch.

In Scenario 3, a direct rotary dryer is integrated into the power plant's flue gas track. Again, wet wood chips are transported to the power plant and dried on-site prior to co-firing.

Wood differs from coal most significantly in its higher fuel oxygen and moisture content, which results in a lower calorific value. When co-firing wood with coal, a relatively higher wood mass flow is necessary to maintain the total fuel heat input. The change in fuel composition causes a higher flue gas mass flow and a lower flame temperature. This results in a reduced and slightly shifted heat transfer in the boiler. More heat is transferred through the convective heating surfaces, but significantly less heat is transferred by radiation compared to firing coal only. The total steam heat output declines with an increasing co-firing rate, even though the fuel heat input remains constant. Nevertheless, the general influence of co-firing is fairly small. Key process parameters change by less than 1 % of their original value.

In direct co-firing, the overall power generation process is further affected by the electrical power demand of the biomass hammer mill. A decline in the coal mill's electrical power demand is far outweighed by the hammer mills' increasing electrical power demand as co-firing rates rise. Compared to firing coal only, the total auxiliary power demand is increased by 70 % for direct co-firing of poplar wood chips at a rate of 50 %. As the hammer mill's electrical power demand largely depends on the biomass moisture content, drying the poplar wood chips to a fuel moisture content of 10 % is indispensable.

Drying and co-firing in Scenarios 1_a and 1_b are possible without technical limitations for all the co-firing rates considered. However, power generation is greatly impacted by the required extraction of drying steam. It is possible to reduce the occurring efficiency impacts by further process heat integration, yet the benefits in overall efficiency improvement are small and would have to balance extra investment and maintenance efforts. As partially drying steam of a lower quality is used in Scenario 1_b, impacts on power generation are slightly lower than in Scenario 1_a.

The drying process in Scenario 2 represents a simple, proven technology that does not further affect the power generation process. This main advantage of decentralised drying allows each process to be operated regardless of the other's availability. Thereby, no technical issues limit the realisable co-firing rate. Nevertheless, the required thermal and electrical energy demand is considerable and needs to be provided at what may be a remote location. Therefore, investments in a suitable electricity grid connection could be necessary. Fuel supply will be

Dieses Werk ist copyrightgeschützt und darf in keiner Form vervielfältigt werden noch an Dritte weitergegeben werden.
Es gilt nur für den persönlichen Gebrauch.

cheapest when wet wood chips are used as in Scenario 2_a. Also, supplying fuel for an oil burner will not present a technical limit.

Even though the resulting efficiency loss in Scenario 3 is less than in Scenario 1_a or 1_b, this integrated scenario is not suitable for drying and co-firing poplar wood chips with coal. The resulting decline of flue gas temperatures would cause a high risk of corrosion for several process elements. An integrated rotary dryer can be operated only for very low co-firing rates without risking damage to technical compounds.

Overall, Scenario 2_a proved to be the most effective in reducing CO_2 emissions when co-firing dried poplar wood chips with coal in a pulverized fuel fired boiler. If wet wood chips are used to provide the required drying gas, the total resulting CO_2 emissions can be reduced by more than 46 % when half of the power plant's fuel heat input is substituted by biomass.

On the other hand, Scenario 1_b proved to be most effective in overall energy utilisation, due to the benefits of integrated drying. As additional thermal energy input is required for drying, which is not used for power generation, the drying Scenarios 2_a and 2_b are clearly less efficient in regard to the overall energy utilisation than the integrated scenarios.

Considering technical realisation and operation, the decentralised scenarios offer several advantages over the integrated scenarios. Pointing out one scenario as clearly most favourable in all approaches is therefore not possible. The decentralised scenarios can be most favourable when the main focus is reduction of CO_2 emissions and there are few challenges in operation. Whereas the integrated scenarios are most favourable when the priority is an efficient energy utilisation. However, if the co-firing rate is defined in a way that includes the fuel heat input for drying and not only the fuel heat input in the boiler, integrating the drying process would be more beneficial in both energy efficiency and reduction of CO_2 emissions.

Even though problems of slagging and fouling in co-firing, which are caused by alkali metals in biomass fuels, cannot be altered by drying, the fuel quality of locally grown biomasses can be improved. Freshly cut wood does not have to be stored for several months to achieve a reduction in fuel moisture content; drying to a moisture content lower than what could be achieved by natural drying also reduces the energy demand for grinding.

Confirming current experiences, it can be concluded that co-firing woody biomass at high rates is possible without any major thermodynamic impairments. An effective and emission-saving process chain for drying and co-firing cultivated biomass fuels

Dieses Werk ist copyrightgeschützt und darf in keiner Form vervielfältigt werden noch an Dritte weitergegeben werden.
Es gilt nur für den persönlichen Gebrauch.

can be achieved without facing severe technical obstacles. However, appropriate fuel supply and storage logistics would be necessary to handle the considerable wood chip mass flow. Whether the necessary operation and investment costs will allow biomass co-firing to be economically feasible still largely depends on fuel prices and in most cases depends on subsidies.

Dieses Werk ist copyrightgeschützt und darf in keiner Form vervielfältigt werden noch an Dritte weitergegeben werden.
Es gilt nur für den persönlichen Gebrauch.

REFERENCES

[1] UMWELTBUNDESAMT: *Strom- und Wärmeversorgung in Zahlen*. http://-www.umweltbundesamt.de/themen/klima-energie/energieversorgung/strom-waermeversorgung-in-zahlen. Version: May 2015

[2] KALTSCHMITT, M.; HARTMANN, H.; HOFBAUER, H.: *Energie aus Biomasse*. 2. edition. Springer-Verlag, 2009

[3] *Gesetz für den Ausbau erneuerbarer Energien*. 2014

[4] VAN LOO, S.; KOPPEJAN, J.: *The Handbook of Biomass Combustion and Co-Firing*. Earthscan, 2008

[5] SIEGLE, V.; FÖRTSCH, D.; HEIN, D. R. G.; KALTSCHMITT, M.; MAIER, H.; SONTOW, J.; REINICKE, B.; SPLIETHOFF, H.: Untersuchung zur Umrüstung eines Steinkohlekraftwerkes für die Mitverbrennung von Biomasse. In: *VDI Berichte* (1997), S. 121–137

[6] MILES: Chariton Valley Biomass Project Iowa Switchgrass Cofiring Update. In: 2nd World Conference and Technology Exhibition on Biomass for Energy and Industry and Climate Protection (Veranst.): *2nd World Conference and Technology Exhibition on Biomass for Energy and Industry and Climate Protection*. Rome, Italy, 2004

[7] SMAJEVIC, I.; KAZAGIC, A.; HODZIC, N.: *Co-firing Tests of Bosnian Coal with Woody Biomass and Natural Gas in Laboratory and on 110 MWel Power Station*. March 2012. – IEA 2012 Workshop "Cofiring biomass with coal" Copenhagen

[8] BARTOLOMÉ, C.; GIL, A.: *Co-firing comparison of two energy crops with coal in a pulverized fuel combustion pilot plant*. 2nd WORKSHOP Cofiring biomass with coal, March 2012

[9] BECKMANN, M.; POHL, M.; PIEPER, C.; BÖHME, R.; BERNHARD, D.; GEBAUER, K.: Nutzung alternativer Brennstoffe in Kraftwerken. IN: *Chemie Ingenieur Technik* 83 (2011), November, S. 1864–1879

[10] SAMI, M.; ANNAMALAI, K.; WOOLDRIDGE, M.: Co-firing of coal and biomass fuel blends. In: *Progress in Energy and Combustion Science* 27 (2001), pp. 171-214

[11] MELIN, G.: Current use of biomass for energy in Sweden and forecast for the coming years. Oslo, 2009

Dieses Werk ist copyrightgeschützt und darf in keiner Form vervielfältigt werden noch an Dritte weitergegeben werden.
Es gilt nur für den persönlichen Gebrauch.

[12] KALT, G.: Biomass streams in Austria: Drawing a complete picture of biogenicmaterial flows within the national economy. In: *Resources, Conservation and Recycling* 95 (2015), S. 100–111

[13] KALT, G.; BAUMANN, M.; HÖHER, M.; KRANZL, L.; LAUK, C.; LEXER, M.; SCHAUMBERGER, A.; SCHAUMBERGER, J.; SCHIPFER, F.; SCHRIEFL, E.: Transformation path to a low-carbon bioeconomy in Austria. In: *23rd European Biomass Conference and Exihbition*. Vienna, 2015

[14] HOGAN, M.; OTTERSTEDT, J.; MORIN, R.; WILDE, J.: *Biomass for heat and power – opportunity and economics*. 2010

[15] THE CITY OF COPENHAGEN TECHNICAL AND ENVIRONMENTAL ADMINISTRATION: *CPH 2025 climate plan*. WWW.KK.DK/cLIMAte. Version: 2012

[16] GLEJE, F.: Use of biomass in the Amager Power Station. Denmark, 2014

[17] HOFOR: Værket. http://www.hofor.dk/amagervaerket/vaerket/. Version: July 2015

[18] HENDERSON, C.: Cofiring of biomass in coal-fired power plants – European experience. In: *IEA Clean Coal Centre*. 2015

[19] IDEA: *DONG Energy to convert final unit at Avedøre plant to biomass*. http://-www.districtenergy.org/blog/2015/04/01/dong-energy-to-convert-final-unit-at-aved%C3%B8re-plant-to-biomass/. Version: July 2015

[20] DONG ENERGY: *Facts about Avedøre Power Station*. http://www.avedore-windfarm.com/en/about-aved%C3%B8re/aved%C3%B8re-power-plant. Version: July 2015

[21] SANDER, B.: Full-scale investigations on co-firing of straw. In: Elsam Engineering A/S: IEA Workshop. Denmark, 2004

[22] AL-MANSOUR, F.; ZUWALA, J.: An evaluation of biomass co-firing in Europe. In: *Biomass and Bioenergie* 34 (2010), S. 620–629

[23] *Recent developments in biomass co-firing in large coal-fired utility boilers*. Doosan Babcock Energy, 3 2012

[24] CREMERS, M.F.G.: *Technical status of biomass co-firing*. 2009. – IEA Bioenergy Task 32: Deliverable 4

[25] VERHOEST, C.; RYCKMANS, Y.: Industrial Wood Pellets - Report. 2012

Dieses Werk ist copyrightgeschützt und darf in keiner Form vervielfältigt werden noch an Dritte weitergegeben werden.
Es gilt nur für den persönlichen Gebrauch.

[26] Boie, Werner: *Vom Brennstoff zum Rauchgas. Feuerungstechnisches Rechnen mit Brennstoffgrößen und seine Vereinfachnung mit Mitteln der Statistik*. Leipzig : Teubner Verlag, 1957

[27] Riley, J. T.: *Routine Coal and Coke Analysis: Collection, Interpretation, and Use of Analytical Data*, 2007. – Book

[28] Vassilev, S. J.; Vassileva, C. G.; Vassilev, V. S.: Advantages and disadvantages of composition and properties of biomass in comparison with coal: An overview. In: *Fuel* (2015)

[29] Vassilev, S. V.; Baxter, D.; Andersen, L. K.; Vassileva, C. G.: An overview of the composition and application of biomass ash. Part 1. Phase–mineral and chemical composition and classification. In: *Fuel* 105 (2013), S. 40–76

[30] Díaz-Ramírez, M.; Frandsen, F. J.; Glarborg, P.; Sebastián, F.; Royo, J.: Partitioning of K, Cl, S and P during combustion of poplar and brassica energy crops. In: *Fuel* 134 (2014), S. 209–219

[31] Lay, V.F.; Kirk, C.A.; Higginson, R.L.; Hogg, S.C.; Davis, C.: Characterisation, analysis and comparison of multiple biomass fuels used in co-firing trials. In: *23rd European Conference and Exhibition*. Vienna, 2015

[32] Wu, H.; Bashir, M. S.; Jensen, P. A.; Sander, B.; Glarborg, P.: Impact of coal fly ash addition on ash transformation and deposition in a full-scale wood suspension-firing boiler. In: *Fuel* 113 (2013), S. 632–643

[33] Damoe, A. J.; Wu, H.; Frandsen, F. J.; Glarborg, P.; Sander, B.: Impact of Coal Fly Ash Addition on Combustion Aerosols (PM2.5) from Full-Scale Suspension-Firing of Pulverized Wood. In: *Energy & Fuels* 28 (2014), S. 3217–3223

[34] Staal, J.: *DONG Energy Power plans and experience in Biomass*. Geertruidenberg, Nederlands, November 2011

[35] Colechin, M.; Malmgren, A.: *Best Practice Brochure: Co-Firing of Biomass (Main Report)*. May 2005. – Report No. COAL R287 DTI/Pub URN 05/1160

[36] Spliethoff, H.; Hein, K.R.G.: Effect of co-combustion of biomass on emissions in pulverized fuel furnaces. In: *Fuel Processing Technology* 54 (1998), S. 189–205

[37] Munir, S.; Nimmo, W.; Gibbs, B.M.: The effect of air staged, co-combustion of pulverised coal and biomass blends on NOx emissions and combustion efficiency. In: *Fuel* 90 (2011), S. 126–135

Dieses Werk ist copyrightgeschützt und darf in keiner Form vervielfältigt werden noch an Dritte weitergegeben werden.
Es gilt nur für den persönlichen Gebrauch.

[38] MAGELLI, F.; BOUCHER, K.; BI, H. T.; MELIN, S.; BONOLI, A.: An environmental impact assessment of exported wood pellets from Canada to Europe. In: *Biomass and Bioenergy* 33 (2009), S. 434–441

[39] PROSKURINA, S.; HEINIMÖ, J.; MIKKILÄ, M.; VAKKILAINEN, E.: The wood pellet business in Russia with the role of North-West Russian regions: Present trends and future challenges. In: *Renewable and Sustainable Energy Reviews* 51 (2015), S. 730–740

[40] PÖYRY: Global pellet market outlook to 2020. In: *Bioenergy insight* 2 (2011), S. 55/56

[41] EUROPEANCOMISSION: *Directive 2009/28/EC on the promotion of the use of energy from renewable sources and amending and subsequently repealing Directives 2001/77/EC and 2003/30/EC*

[42] Scarlat, N.; Dallemand, J.-F.; Monforti-Ferrario, F.; Banja, M.; Motola, V.: RENEWABLE ENERGY POLICY FRAMEWORK AND BIOENERGY CONTRIBUTION IN THE EUROPEAN UNION – AN OVERVIEW FROM NATIONAL RENEWABLE ENERGY ACTION PLANS AND PROGRESS REPORTS. In: *Renewable and Sustainable Energy Reviews* 51 (2015), S. 969–985

[43] KRÖLL, K.: *Trockungstechnik - Trockner und Trocknungsverfahren*. Vol. 2. Berlin Heidelberg New York : Springer-Verlag, 1978

[44] MUJUMDAR, A. S.; MUJUMDAR, A. S. (Hrsg.): *Handbook of Industrial Drying*. Boca Raton, US : Taylor & Francis Group, 2006

[45] WEGER, J.; VÁVROVÁ, K.; BUBENÍK, J.: Twenty-One Years of Experience with Short Rotation Coppice in the Czech Republic - Conclusions from Practice and Research. In: *23rd European Biomass Conferrence and Exhibition*. Vienna, 2015

[46] C.A.R.M.E.N.E.V.: *Kurzumtriebsplantagen - Energieholz aus der Flur*. http://-www.carmen-ev.de/biogene-festbrennstoffe/brennstoffe/kurzumtriebsplantagen. Version: October 2015

[47] TECHNOLOGIE- UND FÖRDERZENTRUM - KOMPETENZZENTRUM FÜR NACHWACHSENDE ROHSTOFFE (Hrsg.): *Qualitätshackschnitzel nach DIN EN ISO 17225-4*. Schulgasse 18, D - 94315 Straubing, July 2014

[48] MASON, P.; DARVELL, L.I.; JONES, J.M.; WILLIAMS, A.; POURKASHANIAN, M.: On the relationship between particle size and burn-out. In: *5th IEA CCC Workshop on Cofiring Biomass*. Drax, UK, 2015

Dieses Werk ist copyrightgeschützt und darf in keiner Form vervielfältigt werden noch an Dritte weitergegeben werden.
Es gilt nur für den persönlichen Gebrauch.

[49] EVERTS, B.; DISTLER, T.; KATHER, A.: Integration of a drying process in a large-scale pulverized coal-fired power plant for the co-firing of lacal available biomasses at high rates. In: *22rd European Conference and Exhibition*. Hamburg, 2014

[50] FAGERNAES, L.: Formation and behaviour of organic compounds in biomass dryers. In: *Bioresource Technology* 46 (1993), S. 71–76

[51] BADOS, R.; ESTEBAN, L. S.; R.ESCALADA; EDOR, C.; JUAN, R.; CARRASCO, E.: Design, construction and first results of a prototype hybrid-solar biomass dryer. In: *22nd European Biomass Conference and Exhibition*. Hamburg, 2014

[52] RIELA: *Der neue RIELA Bandtrockner*. http://www.riela.de/html/produkte/-bandtrockner.html. Version: October 2015

[53] R.O., KATRES spol. s. (Hrsg.): *Belt drying kiln for sawdust and woodchips – type LTD*. http://www.katres.cz/en/products/belt-drying-kiln-for-sawdust-and-wood-chips/. Version: October 2015

[54] CANADIAN BIOMASS: *Drying Tecnology*. http://-www.canadianbiomassmagazine.ca/dryers/drying-technology-2027. Version: October 2010

[55] FAGERNAES, L.; BRAMMER, J.; WILEN, C.; LAUER, M.; F.VERHOEFF: Drying of biomass for second generation synfuel production. In: *Biomass and Bioenergy* 34 (2010), S. 1267–1277

[56] BÜTTNER, GESELLSCHAFT FÜR TROCKNUNGS- UND UMWELTTECHNIK MBH: *Trocknungsanlagen für die Holzindustrie*. Krefeld, Germany, 2014

[57] ASUE - ARBEITSGEMEINSCHAFT FÜR SPARSAMEN UND UMWELTFREUNDLICHEN ENERGIEVERBRAUCH E.V.: *Direkte Trocknung mit Abgasen aus KWK-Anlagen*

[58] KRÖLL, K.; KAST, W.: *Trocknungstechnik - Trocknen und Trockner in der Produktion*. Berlin, Heidelberk, New York : Springer Verlag, 1989

[59] KONIDIS, J.: *Design of Direct Heated Rotary Dryers / The Department of Mechanical Engineering*. Concordia University, 1984

[60] FEECO_INTERNATIONAL: *Rotary Dryer Handbook*. Green Bay, WI, USA : online,

[61] STEAG ENERGY SERVICES GMBH SYSTEM TECHNOLOGIES: *EBSILON Professional for engineering and designing energy and power plant systems*. https://www.steag-systemtechnologies.com/ebsilon_professional+M52087573ab0.html. Version: 2015

Dieses Werk ist copyrightgeschützt und darf in keiner Form vervielfältigt werden noch an Dritte weitergegeben werden.
Es gilt nur für den persönlichen Gebrauch.

[62] EVERTS, B.; DISTLER, T.; KATHER, A.: Co-firing of local available biomass - decentralised drying vs. integrated on-site drying. In: *23rd European Biomass Conference and Exhibiton*. Vienna, 2015

[63] DISTLER, T.; EVERTS, B.; KATHER, A.: Integration of a torrefaction process in a large-scale pulverized coal-fired power plant for the reduction of energy requirement for biomass milling at higher co-firing rats. In: *22nd European Biomass Conference & Exhibition*. Hamburg, 2014

[64] TEMMERMAN, M.; JENSEN, P. D.; HÉBERT, J.: Von Rittinger theory adapted to wood chip and pellet milling, in a laboratory scale hammermill. In: *Biomass and Bioenergy* 56 (2013), S. 70–81

[65] DUNLAP, F.: *The Specific Heat of Wood / U.S. Department of Agriculture*. 1912

[66] FORTUIN, G.: *Anwendung mathematischer Modelle zur Beschreibung der technischen Konvektionstrocknung von Schnittholz*, Universität Hamburg, Fachbereich Biologie, Diss., 2003

[67] PONNDORF_ANLAGENBAU_GMBH: *Personal Communication*. http://-www.ponndorf-gmbh.de/index.php/de/produkte

[68] BÜTTNER ENERGIE- UND TROCKNUNGSTECHNIK GMBH, KREFELD: *Büttner Energie- und Trocknungstechnik GmbH, Krefeld*

[69] FAULKNER, W. B.; SHAW, B. W.: Efficiency and pressure drop of cyclones across a range of inlet velocities. In: *Applied Engineering in Agriculture* 22 (2006), S. 155–161

[70] VERHOFF, F.H.; BANCHERO, J.T.: Predicting Dew Points of Flue Gases. In: *Chemical Enineering Progress* 70 (1974), Nr. 8, S. 71–72

[71] IVE MBH, ECO TRANSIT WORLD: *EcoTransIT – Ecological Transport Information Tool for Worldwide Transports*. http://www.ecotransit.org/index.de.html. Version: 2014. – commissioned by: EcoTransIT World Initiative

[72] OEXMANN, J.: *Post-Combustion CO2 Capture: Energetic Evaluation of Chemical Absorption Processes in Coal-Fired Steam Power Plants*, TU Hamburg-Harburg, Diss., 2011

Dieses Werk ist copyrightgeschützt und darf in keiner Form vervielfältigt werden noch an Dritte weitergegeben werden.
Es gilt nur für den persönlichen Gebrauch.

Dieses Werk ist copyrightgeschützt und darf in keiner Form vervielfältigt werden noch an Dritte weitergegeben werden.
Es gilt nur für den persönlichen Gebrauch.

Lebenslauf

Persönliche Daten

Name:	Everts
Vorname:	Birte
Geburtstag:	22.04.1987
Geburtsort:	Hamburg

Schulischer Werdegang

09/1993 – 07/1997	Grundschule, Hittfeld/Otter
09/1997 – 07/2006	Gymnasium, Tostedt

Studium

10/2006 – 02/2012	Studium des Maschinenbaus in der Vertiefung Energietechnik Technische Universität Hamburg-Harburg Abschluss: Diplom-Ingenieurin

Beruflicher Werdegang

03/2012 – 07/2016	Wissenschaftliche Mitarbeiterin Technische Universität Hamburg-Harburg Institut für Energietechnik

Dieses Werk ist copyrightgeschützt und darf in keiner Form vervielfältigt werden noch an Dritte weitergegeben werden.
Es gilt nur für den persönlichen Gebrauch.

Dieses Werk ist copyrightgeschützt und darf in keiner Form vervielfältigt werden noch an Dritte weitergegeben werden.
Es gilt nur für den persönlichen Gebrauch.

Dieses Werk ist copyrightgeschützt und darf in keiner Form vervielfältigt werden noch an Dritte weitergegeben werden.
Es gilt nur für den persönlichen Gebrauch.